Forschungszentrum Karlsruhe
in der Helmholtz-Gemeinschaft

Wissenschaftliche Berichte
FZKA 6566

Improvement of the SCDAP/RELAP5 Code with Respect to FZK Experimental Facilities

W. Hering, Ch. Homann
Institut für Reaktorsicherheit

Juni 2007

Forschungszentrum Karlsruhe
in der Helmholtz-Gemeinschaft

Wissenschaftliche Berichte
FZKA 6566

Improvement of the SCDAP/RELAP5 Code with Respect to FZK Experimental Facilities

W. Hering, Ch. Homann

Institut für Reaktorsicherheit

Forschungszentrum Karlsruhe GmbH, Karlsruhe

2007

Forschungszentrum Karlsruhe GmbH
Postfach 3640, 76021 Karlsruhe

Mitglied der Hermann von Helmholtz-Gemeinschaft
Deutscher Forschungszentren (HGF)

ISSN 0947-8620

urn:nbn:de:0005-065660

Abstract

The USNRC severe core damage code SCDAP/RELAP5 mod 3.2 was extended to simulate adequately integral out-of-pile facilities at Forschungszentrum Karlsruhe (FZK). The original model for the CORA electrical heater rod was extended to allow a complete analysis of the whole test section. In addition, in the axial heat conduction module the axial boundary conditions were improved, and the radiation across annular gaps is now taken into account. Furthermore, to allow a fine simulation of reflood conditions, the number of axial zones has been increased to 36, allowing a fine mesh of ~ 0.05 m. A new approach of clad failure estimation is included, based on FZK separate effect tests, but not fully tested.

Together with error corrections, the code is now a reliable basis to support considerably the experiments in the QUENCH facility with pre-test calculations and post-test analyses as demonstrated by several calculations. In addition, more reliable calculations of accident scenarios and related accident management measures are possible for existing and future commercial power plants.

Verbesserung des Programms SCDAP/RELAP5 für FZK Versuchsanlagen

Kurzfassung

Das Kernschmelzcodesystem SCDAP/RELAP5 mod 3.2 der USNRC wurde erweitert, um integrale out-of-pile Versuchsanlagen im Forschungszentrum Karlsruhe adäquat simulieren zu können. Das Heizstabmodell für die CORA Anlage wurde derart ergänzt, dass die gesamte Teststrecke analysiert werden kann. Beim Wärmeleitmodell wurden die Randbedingungen für die axialen Enden der Heizstäbe verbessert und der Strahlungstransport über radiale Spalte berücksichtigt. Für verlässliche Reflood-Rechnungen wurde die Anzahl der axialen Zonen auf 36 erweitert, so dass jetzt Zonenlängen von 0.05 m möglich sind. Ein neuer Ansatz zur Berechnung des Hüllrohrversagens, basierend auf FZK Einzeleffekt-Experimenten, wurde eingebaut, ist aber noch nicht vollständig getestet.

In Verbindung mit einigen Fehlerkorrekturen kann das Codesystem nun zur Unterstützung der Experimente in der QUENCH-Anlage durch Vorausrechnungen und Versuchsanalysen herangezogen werden. Dies wird anhand verschiedener Experimentanalysen gezeigt. Ebenso sind nun verlässlichere Unfallanalysen unter Berücksichtigung von Störfallmaßnahmen für existierende und zukünftige kommerzielle Anlagen möglich.

Table of contents

List of Figures

List of Tables

List of Abbreviations

AIC	Absorber rods with an alloy of silver (Ag), indium (In), and cadmium (Cd)
ASTEC	Accident Source Term Evaluation Code
BIC	Bundle Interpretation Circle of PHEBUS FPT
BOC	Begin Of Cycle
CORA	Complex Out-of-Pile Rod bundle Assembly Out-of-pile severe fuel damage tests performed at FZK, 1984-1992
CSARP	Cooperative Severe Accident Research Program, USNRC
EOC	End Of Cycle
FP	Fission Product
FPT1	Fission Product Test 1
FZK	Forschungszentrum Karlsruhe, http://www.fzk.de/
HS	RELAP5 Heat Structure
HTS	High Temperature Shield
ICARE	Interprétation des Cœurs Accidentés pour les Réacteurs à Eau (interpretation of water reactor cores during an accident)
IMF	Institut für Materialforschung, http://www.fzk.de/fzk/idcplg?IdcService=FZK&node=0739&document=ID_011142
INEEL	Idaho National Engineering and Environmental Laboratory, USA
IRS	Institut für Reaktorsicherheit, http://www.fzk.de/fzk/idcplg?IdcService=FZK&node=0739&document=ID_002109
ISP	International Standard Problem of OECD/NEA
LOCA	Loss Of Coolant Accident
LOFT	Loss Of Fluid Test (Idaho National Engineering Laboratory, Idaho Falls, USA)
LWR	Light Water Reactor
MRS	Melt Relocation Scheme
NEA	Nuclear Energy Agency of the OECD
OECD	Organization for Economic Cooperation and Development
PCT	Peak Core Temperature
PSF	Programm Nukleare Sicherheitsforschung, FZK, http://www.fzk.de/fzk/idcplg?IdcService=FZK&node=0738&document=ID_001788
PWR	Pressurized Water Reactor
QUENCH	Research programme at FZK to investigate material behaviour during LWR reflood conditions
RELAP5	old: Reactor Excursions and Leak Analysis Program, presently: Reactor Leak and Analysis Program, for LWR transients and SBLOCA
SARNET	Severe Accident Research NETwork
SBLOCA	Small break LOCA
SCB	SARNET Code Benchmark
SCD	Severe Core Damage
SCDAP	Severe Core Damage Analysis Package, (USNRC code, developed at INEEL), http://www.nrc.gov/what-we-do/regulatory/research/comp-codes.html#sac

SCDAP/RELAP5: Coupled SCDAP and RELAP5 code to simulate reactor conditions up to SFD conditions

SFD Severe Fuel Damage

TSD Test Sequence Diagram

TMI-2 Three Mile Island Unit 2, Mitigated SFD accident, http://www.libraries.psu.edu/tmi/

USNRC United States Nuclear Regulatory Commission, Rockville, MD

(Remark: URL-Addresses valid November 2006)

1 INTRODUCTION

At the Institute of Reactor Safety (IRS) of the Forschungszentrum Karlsruhe (FZK), the USNRC severe core damage code package SCDAP/RELAP5 (S/R5) /1/ was used for investigations of the safety issues of Light Water Reactor (LWR) plants, especially of the European Pressurized Water Reactor (EPR). To apply the code to full plant conditions it has to be validated against various integral tests. However, integral tests can only partially simulate the in-core behaviour. Besides, they may have some peculiarities that are not prototypic for reactors, but important for the test facility. Similarly, for one or another reason, the test conduct may be different from the sequence of events in a reactor. For code assessment, effects that are based on the features of the facility and of the given test conduct must therefore be taken into account, but must be distinguished from reactor specific physical phenomena and processes. Especially in out-of-pile tests, as considered in this report, the simulation of the decay heat has to be considered carefully. Firstly, electrical heating leads to a different axial power profile than nuclear heating and in addition, it has a positive feedback for metallic heaters because local resistivity and hence local power release increase with temperature.

The first calculations with the original code system /1/ for CORA tests revealed that the deviations between experimental data and code predictions cannot be understood at a first glance and are not due to a single reason. Therefore, they have to be investigated carefully in detail. In this context, improved models have been developed /3/ for the S/R5 code versions mod3.1 /1/ and mod 3.2 /2/ to allow adequate simulations of CORA tests /5/. This work has been extended for the QUENCH facility at FZK /6/. From the analyses of the French facility PHEBUS /7/ at CEA Cadarache, some improvements for the SCDAP shroud model /8/ are added to handle gas-filled gaps with radiative heat transport and to model local closure during temperature transients /7/.

Besides, code improvements were performed to overcome code deficiencies or unphysical assumptions. With respect to reactor applications, the original RELAP restart capability was extended with respect to SCDAP variables. This allows modifying critical model parameters such as ZrO_2 failure temperature, clad in-side oxidation extension, as well as the mode of oxidation limitation /8/, /9/.

In the present report, these extensions are presented. As a start, a brief overview of special properties of the out-of-pile facilities CORA, QUENCH, and the in-pile facility PHEBUS are given in section 1. In section 3, actual nodalisation schemes for these facilities are discussed. The present state of code extensions is presented in section 4. To support code validation, integral experiment analysis procedures are discussed in section 5 supporting interpretation and comparison of different CORA, QUENCH, and PHEBUS FPT experiments and results of code calculations.

2 FZK OUT-OF-PILE FACILITIES

2.1 NIELS Facility

At FZK, several electrically heated out-of-pile test facilities were erected since 1984 to investigate the behaviour of fuel rod segments and bundles under severe core damage conditions. First, the NIELS facility /4/ allowed to heat-up electrically a 0.3 m long single rod as well as a 9-rod bundle in an argon and steam atmosphere was used to investigate principally fuel rod behaviour under beyond design basis conditions. The tests dealt mostly with the phenomenology of the bundle degradation up to the melting temperature of α-Zr(O). From these tests only temperature histories are available as well as the results of the destructive post-test investigations /10/.

2.2 CORA Facility

As a further step and partially engaged by the TMI-2 accident, the CORA facility (Figure 2.1) was designed to study the main processes occurring during a course of a severe fuel damage accident (SFD) under more realistic conditions and to allow the termination of the tests by flooding the test section with steam or water. Moreover, the fuel rod bundle could be observed by on-line optical inspection with several video systems along the test section. The instrumentation also allowed tracking the hydrogen source term. The facility is described in detail in /3/ and /21/. A detailed description of a typical CORA experiment can be found in /12/, /13/, /15/. The general scheme of the out-of-pile test section is given in Figure 2.1. In the meanwhile, the CORA facility has been dismantled due to enhanced safety requirements. An overview of the tests is given in Table 2.1 together with the available literature. In this table, "#" indicates the test number.

The bundle is composed of electrically heated (simulator), unheated (fuel) and of absorber (control) rods. In Table 2.1, S, F, and C give their respective number. The bundle configurations may be different in the tests (Table 2.1), but the dimensions and materials for components outside the shroud insulation are the same. The heated and unheated rods are mounted at the upper bundle flange and kept in place laterally by three grid spacers. To cool the copper electrodes water pools are used at both ends of the simulators. The quench cylinder, filled with water for bundle flooding, is situated below the test section and can be raised over the bundle up the upper end of the heated zone, i.e. up to z = 1.0 m. To allow the quench cylinder lifting, the fluid composed of argon and steam has to enter the bundle from the side at the lower end of the heated zone (steam inlet).

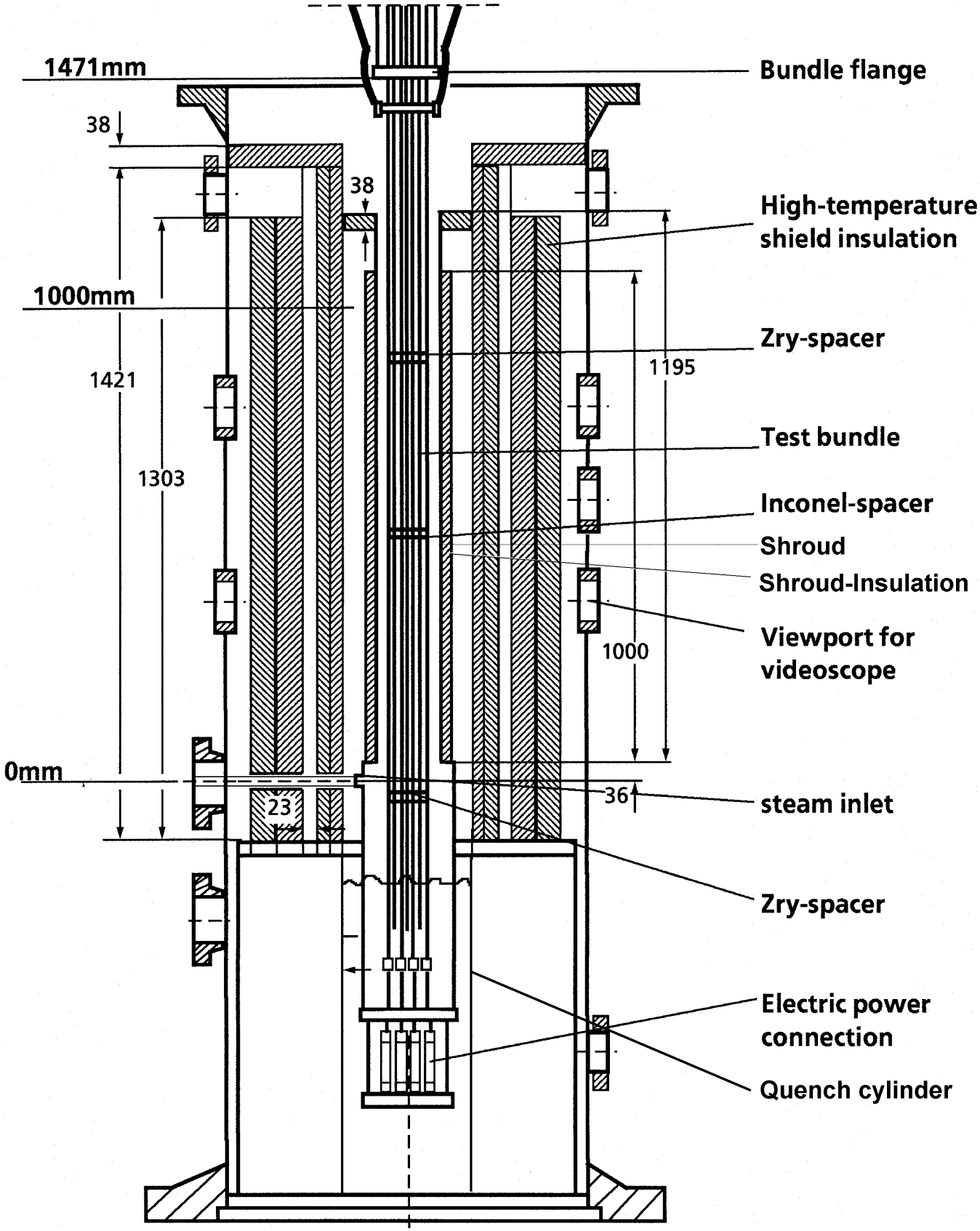

Figure 2.1 Schematics of the test section of the CORA facility at FZK including upper and lower fuel rod bundle connectors, high temperature shield (HTS), and containment.

Table 2.1 Bundle configuration, test conditions, and integral test results for all CORA PWR, BWR, and VVER (bottom) tests (state of test documentation 1999).

PWR Experiments:								
#	**Bundle: S, F, C**	**Initial Heat-up [K/s]**	**Cool-down**	**P_{sys} / P_{rod} [MPa]**	**Pre-oxidation [µm]**	**H_2-mass [g]**	**Test sequence**	**End state: material and ZrO_2 profiles**
2	16 9 0	~ 1	Ar	0.22 / 0.9	no	no data	/3/	/11/, /12/
3	16 9 0	‘’	‘’	0.22 / 0.5	‘’	‘’	/3/	/11/, /12/
5	16 8 1	‘’	‘’	0.22 / 0.5	‘’	‘’	/3/	/12/
12	16 7 2	‘’	water	0.22 / 0.4	‘’	‘’	/3/, /16/	/12/, /13/
15	16 7 2	‘’	Ar	0.22 / 6.0	‘’	180	/3/	
9	16 7 2	‘’	‘’	1.00 / 0.5	‘’	159	/23/	
7	32 20 5	‘’	‘’	0.22 / 0.5	‘’	114	/18/	
13	16 7 2	‘’	water	0.22 / 0.5	‘’	110+100	/15/, /20/	/13/, /14/, /19/
29	16 7 2	‘’	Ar	0.22 / 0.5	10	225	/28/	/37/
30	16 7 2	0,3	‘’	0.22 / 0.5	no	194	/29/	
10	16 7 2	~1	‘’	0.22 / 0.5	‘’	180	/25/	/37/
BWR Experiments:								
#	**Bundle: S, F, C**	**Initial Heat-up [K/s]**	**Cool Down**	**P_{sys} / P_{rod} [MPa]**	**Pre-oxidation [µm]**	**H_2-mass [g]**	**Test sequence**	**End state: material and ZrO_2 profiles**
16	12 6 11	~1	Ar	0.22 / 0.5	no	~167	/22/	/13/
17	12 6 11	~1	water	0.22 / 0.5	‘’	32+118	/22/	/13/
18	28 20 11	~1	Ar	0.22 / 0.5	‘’	106	/26/	
31	12 6 11	0.3	Ar	0.22 / 0.5	‘’	205	/30/	/37/
28	12 6 11	~1	Ar	0.22 / 0.3	55	104	/27/	/37/
33	12 6 11	< 0.3	Ar	0.22 / 0.5	‘’	84	/31/	/37/
VVER Experiments:								
#	**Bundle: S, F, C**	**Initial Heat-up [K/s]**	**Cool Down**	**P_{sys} / P_{rod} [MPa]**	**Pre-oxidation [µm]**	**H_2-mass [g]**	**Test sequence**	**End state: material and ZrO_2 profiles**
W1	13 6 0	~1	Ar	0.22 / 0.5	no	96	/34/	/37/
W2	13 5 1	~1	Ar	0.22 / 0.5	‘’	75	/35/	/37/

The CORA shroud, a Zircaloy liner with ~ 20 mm thick fibre insulation at its outer surface surrounds the bundle. This fibre insulation extends only up to 1.0 m; above this elevation, in the upper electrode zone, the shroud is not insulated to prevent the electrodes, made of molybdenum and copper, from melting. For optical on-line inspection, the shroud has several observation holes that, however, allow the fluid to penetrate into the annular gap outside of the shroud.

Separated by this annular gap, the high temperature shield (HTS), composed of several layers of fibre insulation made of zirconia and alumina oxides, reduces radial heat losses. In the off-gas system above the test section, devices to condense steam and to measure the fluid components are located. CORA tests terminated by flooding with water (quenching) from the bottom show an unexpected increase of the hydrogen source term. Two reflood tests were performed for PWR configuration, CORA-12 /16/ and CORA-13 /19/ and one for BWR environment CORA-17 /13/.

2.3 QUENCH Facility

To investigate this phenomenon, the QUENCH facility has been designed and built at FZK, based on the experiences gathered in the CORA programme /5/. The central part of the experimental set-up /43/ is the test bundle, shown on the left side of Figure 2.3. Situated inside the containment it consists of 20 electrically heated rod simulators (heater rod) and an unheated rod (fuel rod or control rod) in the centre. The simulator construction is similar to that used in the CORA experiments. The simulator is ~ 2.2 m long with a heated zone of 1 m length. In this heated zone, the simulator consists of a 6 mm thick tungsten electrode, surrounded by ZrO_2 pellets with an outer diameter of 9.2 mm. At the bottom and top end of the heated length, the tungsten heater is connected to a molybdenum electrode of 8.6 mm diameter and a length of 0.3 m and 0.576 m, respectively. The molybdenum electrodes (Figure 2.3 left) are connected to copper electrodes of the same diameter and a length of 0.39 m, and 0.19 m, respectively, cooled by water. The cladding is made of Zry-4 with a thickness of 0.725 mm and an outer diameter of 10.75 mm, such leaving a gap of 0.05 mm between the pellets and the cladding. The inner 9 simulators can be heated independently of the outer 12 ones.

Four Zry instrumentation tubes or massive rods with an outer diameter of 6 mm are placed at the bundle corners (Figure 2.3) to achieve similar hydraulic conditions in the sub-channel near the shroud as in the bundle. Furthermore, they can be used for additional instrumentation. One corner rod may be withdrawn during the test to measure the actual oxidation profile. Axially the fuel rods, simulators and instrumentation tubes are fixed by an Inconel grid spacer at z = -200 mm and three Zry grid spacers at axial levels of 50 mm, 550 mm and 1050 mm, respectively. The Inconel spacer is used to reduce the effect of the inlet nozzle on the fluid in the test section.

The bundle is enclosed in a Zry shroud with an inner diameter of 40 mm and a thickness of 2.38 mm. The material oxidizes like the rods and so simulates the effect of surrounding rods, which would be present in a larger bundle. To insulate the bundle it is surrounded by ~ 3.8 cm of ZrO_2 fibre material and enclosed in an Inconel tube with an outer diameter of 80 mm and a thickness of 3 mm, the inner cooling jacket.

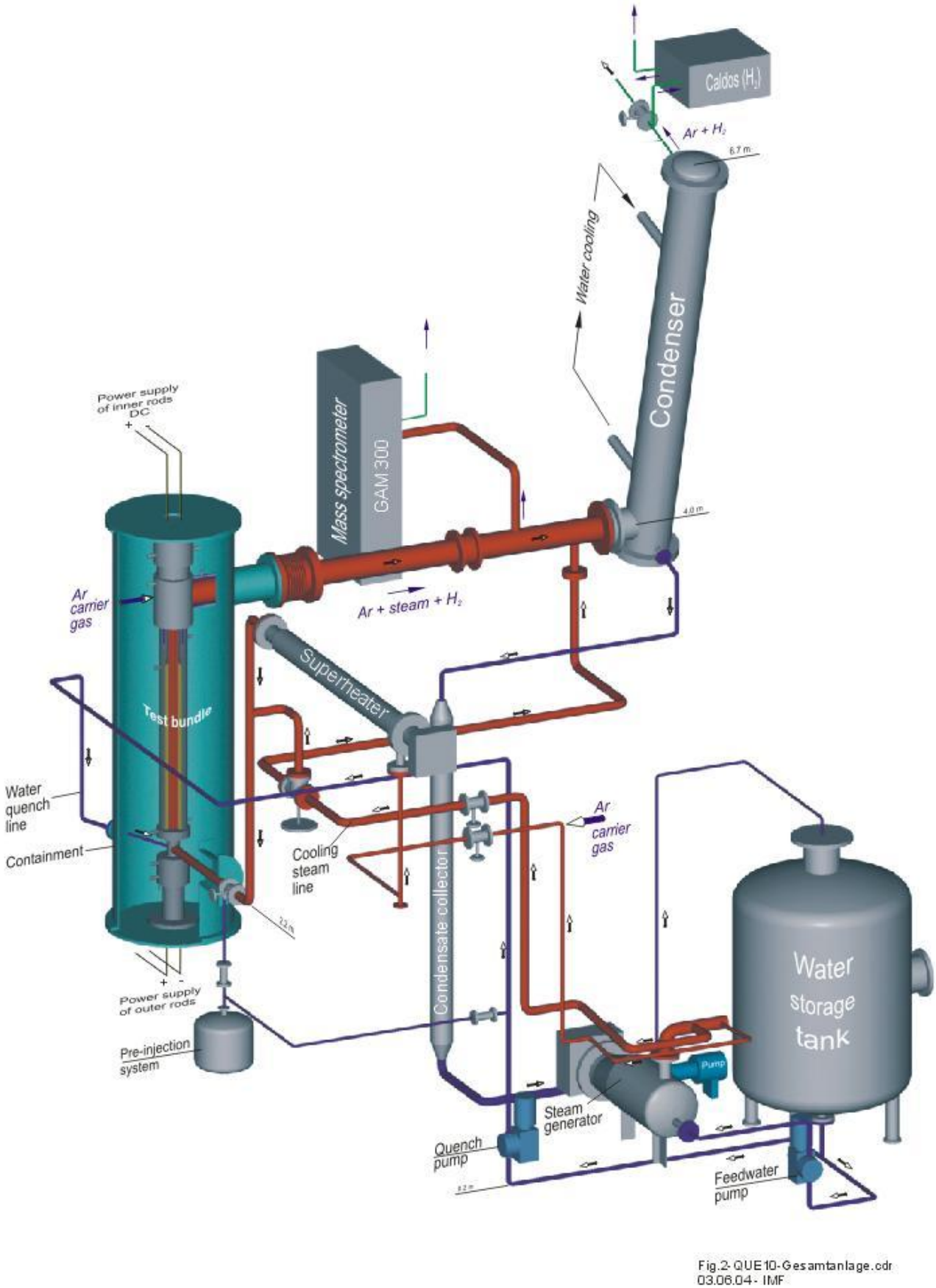

Figure 2.2 Overview of the complete QUENCH facility including thermal-hydraulic parts as well as measurement devices.

Starting with test QUENCH-04 (Table 2.2) the unheated fuel rod is equipped with additional thermocouples placed on the inner clad surface, to allow precise measurement of the cladding temperatures during reflood (Figure 2.3 right). The unheated fuel rod is instrumented by two centre thermocouples to give information about the central temperatures.

For radial heat removal, the bundle is cooled by a counter-current argon flow and a counter-current water flow in the upper electrode zone, respectively. Both flows are just outside the inner cooling jacket (Figure 2.3). The flow channel has a width of 6.7 mm. It is bounded outwardly by another Inconel tube, the outer cooling jacket, with a thickness of 2 mm. The containment consists of steel cylinder with a thickness of 5 mm and an inner radius of 400 mm. The off-gas line (Figure 2.2 centre) consists of a co-axial double tube with an inner gas flow pipe and a water-cooled annulus. In this section, the mass spectrometer pipe is attached.

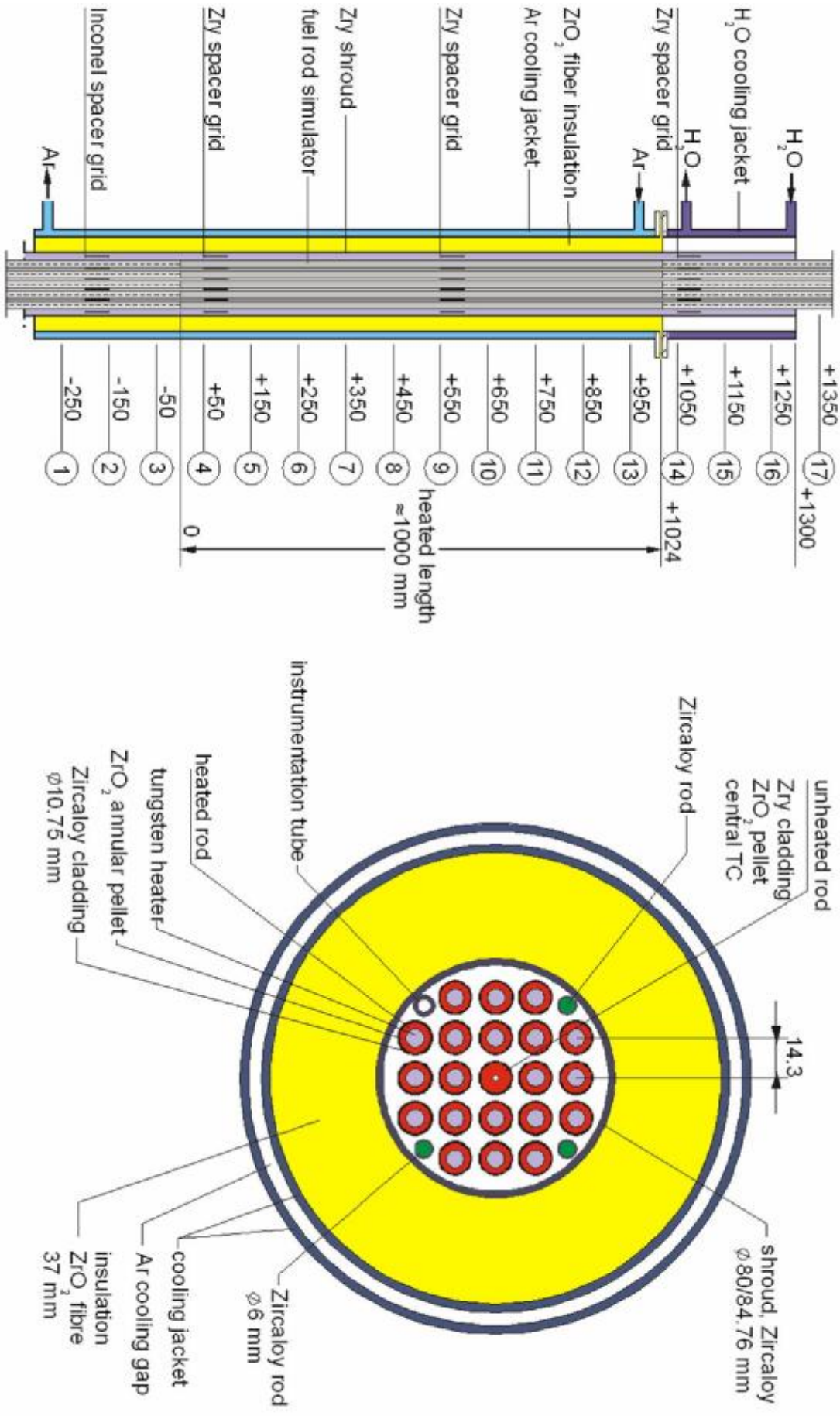

Figure 2.3 Axial and radial scheme of the QUENCH facility with instrumentation levels.

Table 2.2 QUENCH test matrix (April 2007)

QUENCH-01 Feb 26, 98	**water**	**52**	**1830**	**312**	**580**	**36/3**	COBE Project: partial fragmentation of pre-oxidized cladding
QUENCH-02 Jul 7, 98	**water**	**47**	**2470**	na	completely oxidized	**20/140**	COBE Project: no additional pre-oxidation; quenching from high temperatures
QUENCH-03 Jan 20, 99	**water**	**40**	**2450**	na	completely oxidized	**18/120**	delayed flooding; 240 s after temperature escalation has started
QUENCH-04 Jun 30, 99	**steam**	**50**	**2110**	**82**	**≈ 170**	**10/2**	cool-down behavior of slightly pre-oxidized cladding by injected cold steam
QUENCH-05 Mar 29, 2000	**steam**	**48**	**2020**	**160**	**≈ 400**	**25/2**	cool-down behavior of pre-oxidized cladding by injected cold steam
QUENCH-06 Dec 13, 2000	**water**	**42**	**2060**	**207**	**≈ 660**	**32/4**	OECD-ISP, prediction of H_2 source term by different code systems
QUENCH-07 Jul 25, 2001	**steam**	**15**	**2100**	**230**	completely oxidized	**66/120**	COLOSS Project: impact of B_4C absorber rod failure on H_2, CO, CO_2 and CH_4 generation
QUENCH-08 Jul 24, 2003	**steam**	**15**	**2070**	**274**	completely oxidized	**46/38**	Reference test to QU-07 without absorber rod
QUENCH-09 Jul 3, 2002	**steam**	**49**	**2150**	na	completely oxidized	**60/400**	COLOSS Project: impact of B_4C absorber rod failure on H_2, CO, CO_2 and CH_4 generation in steam-starved conditions
QUENCH-10 Jul 21, 2004	**water**	**50**	**2180**	**514**	completely oxidized	**48/5**	LACOMERA-QUENCH-01: air ingress during spent fuel storage container accident
QUENCH-11 Dec 8, 2005	**water**	**18**	**2040**	**170**	completely oxidized	**9/132**	LACOMERA-QUENCH-02: boil-off test with subsequent flooding
QUENCH-12 Sep27, 2006	**water**	**47**	**2100**	tbd	tbd	**34/24**	ISTC-1648.2: physico-chemical behavior of VVER type cladding (Zr1%Nb) during flooding
QUENCH-13 2007	**water**						test with AgInCd absorber rod
QUENCH-14 2008	**water**						test with M5 cladding

3 FACILITY MODELS FOR S/R5 CALCULATIONS

3.1 CORA

A typical nodalisation scheme for PWR reflood tests in the CORA facility /21/ derived from the S/R5 mod3.2 assessment manual /38/ is shown in Figure 3.1. It includes only the heated zone (1.0 m, Figure 2.1) with ten axial nodes plus upper and lower plena. In radial direction one channel is used for the bundle (21 ... 30) and two radial rings for the gap between shroud insulation and HTS. The inner ring in the gap simulates the volume filled by the rising quench cylinder whereas the outer part is not flooded. Three cross flow junctions (226, 227, and 228) simulate the windows in the shroud. Since S/R5 mod 3.1 /1/ only allowed one SCDAP shroud component, the HTS had to be simulated as a RELAP heat structure. Consequently, no radiative heat transfer could be simulated between the CORA shroud outer surface and the HTS inner surface.

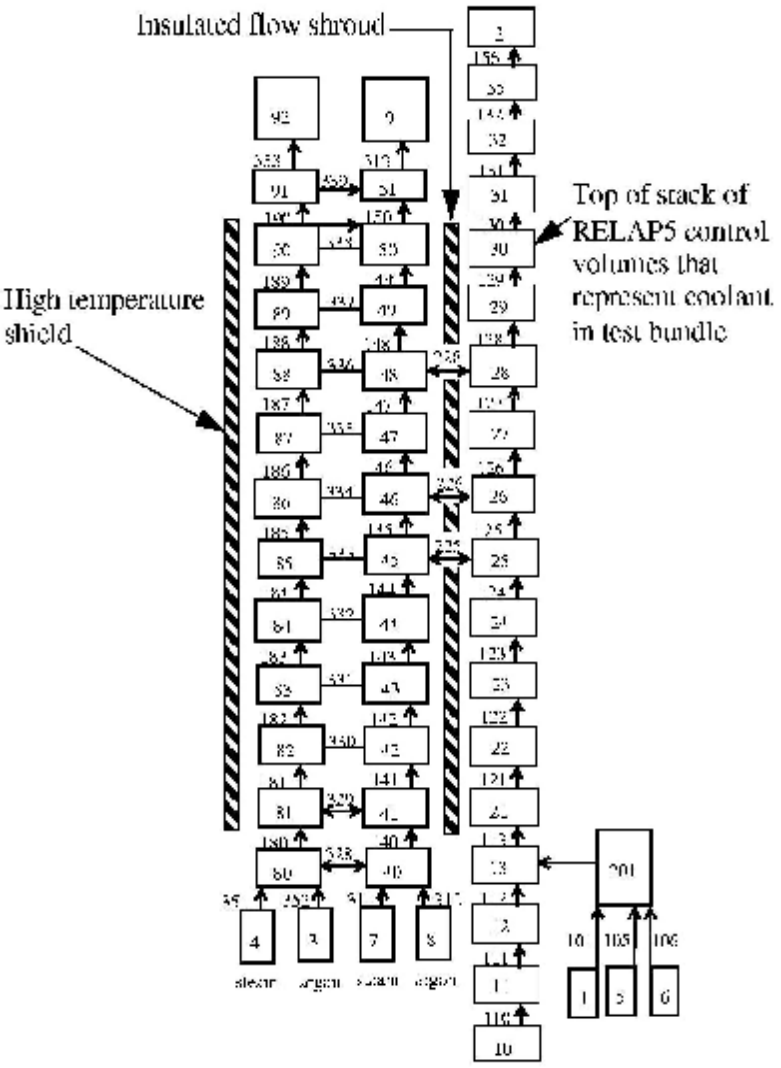

Figure 3.1 Standard CORA two channel nodalisation

However, the rod temperature at the end of the heated zone, determining the axial heat conduction, is not sufficiently well known from experimental data. Besides, electrical power input in the electrode zones is not negligible. The same holds true for the hydrogen production, especially during reflood.

During the quench phase in the reflood tests, the quench water level rises from the lower to the upper electrode zone. The complete reflood phase could not be simulated correctly, using the nodalisation shown in Figure 3.1 /21/. Based on experiences with SCDAP /3/ and taking into account the requirements of the QUENCH facility (section 3.2), the description of the facility was extended as follows:

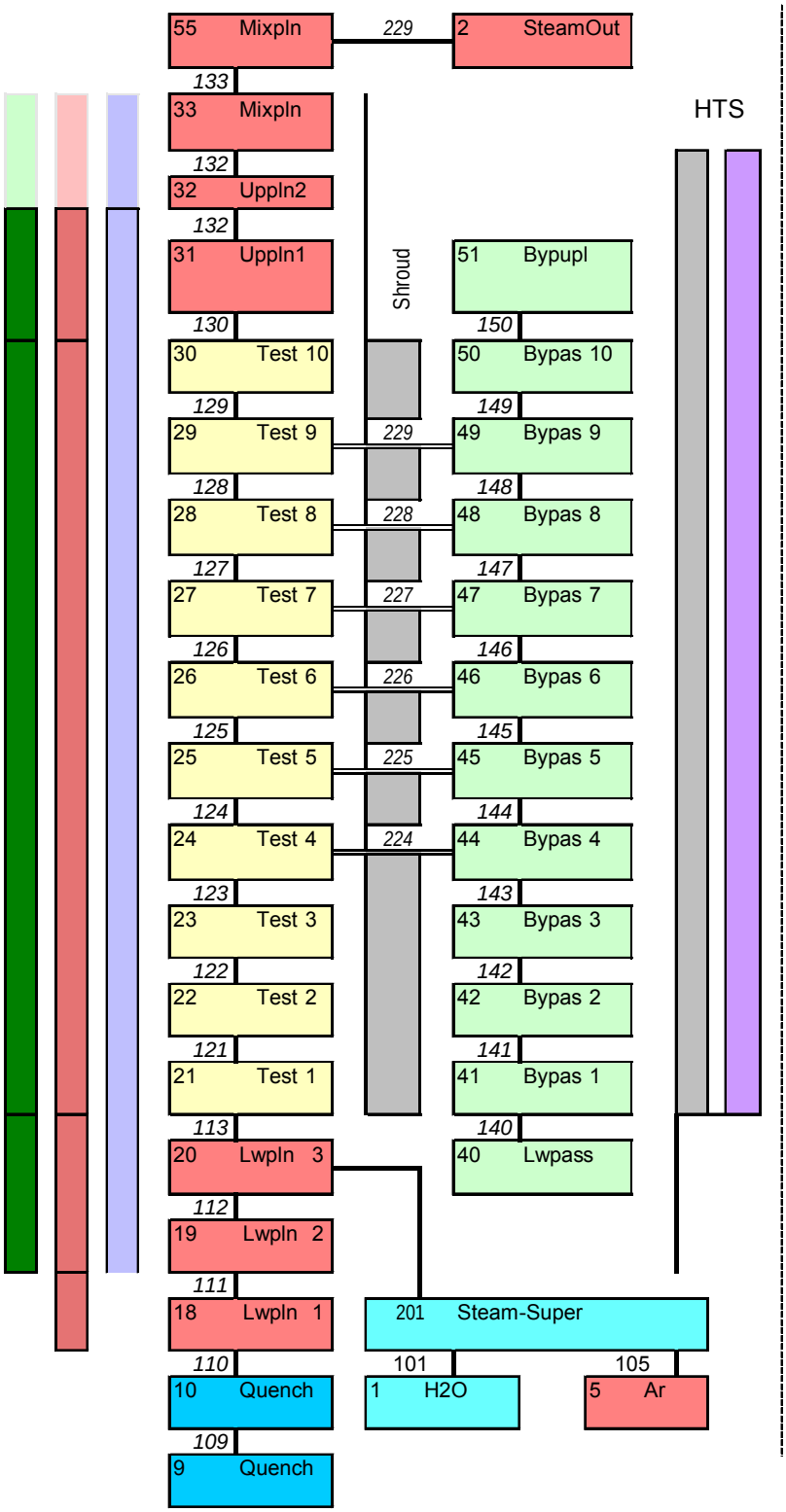

Figure 3.2 Improved model for CORA-7 including axial extensions to top and bottom electrode zones

1. Simulated test section extends up to the water pools at the axial ends of the heated rods.
2. HTS simulated as SCDAP component to model radiation between outer shroud surface and the inner surface of the HTS (S/R5 mod 3.2).
3. Taking credit from the gap radiation and closure model, developed for the PHEBUS FP facility /8/, the absence of the shroud insulation in the upper electrode zone could be considered, too.

To achieve this purpose, code improvements have to be performed (section 4) which may be incorporated in the S/R5 mod3.3.

For the reflood simulation, the original nodalisation of the bypass was kept as mentioned above to simulate the partitioning due to the rising cylinder /39/ by interrupting the cross flows between bundle and gap at pre-defined times according to the axial position of the quench cylinder. Except for the lateral fluid inlet, all other out-of-pile peculiarities can be simulated with S/R5 mod 3.2 including radiative heat transport across gas-filled gaps and the closure of gap due to thermal expansion /8/. The latter feature is important for PHEBUS tests.

3.2 QUENCH

For the pre-design calculations, developed for optimization of the facility and safety considerations, a detailed facility model was created /41/, /42/. It fuses together the test section and containment modelled by FZK with the off-gas system modelled by AEAT /41/. The detailed model of the off-gas pipe was used mainly for analysis of structure heat-up.

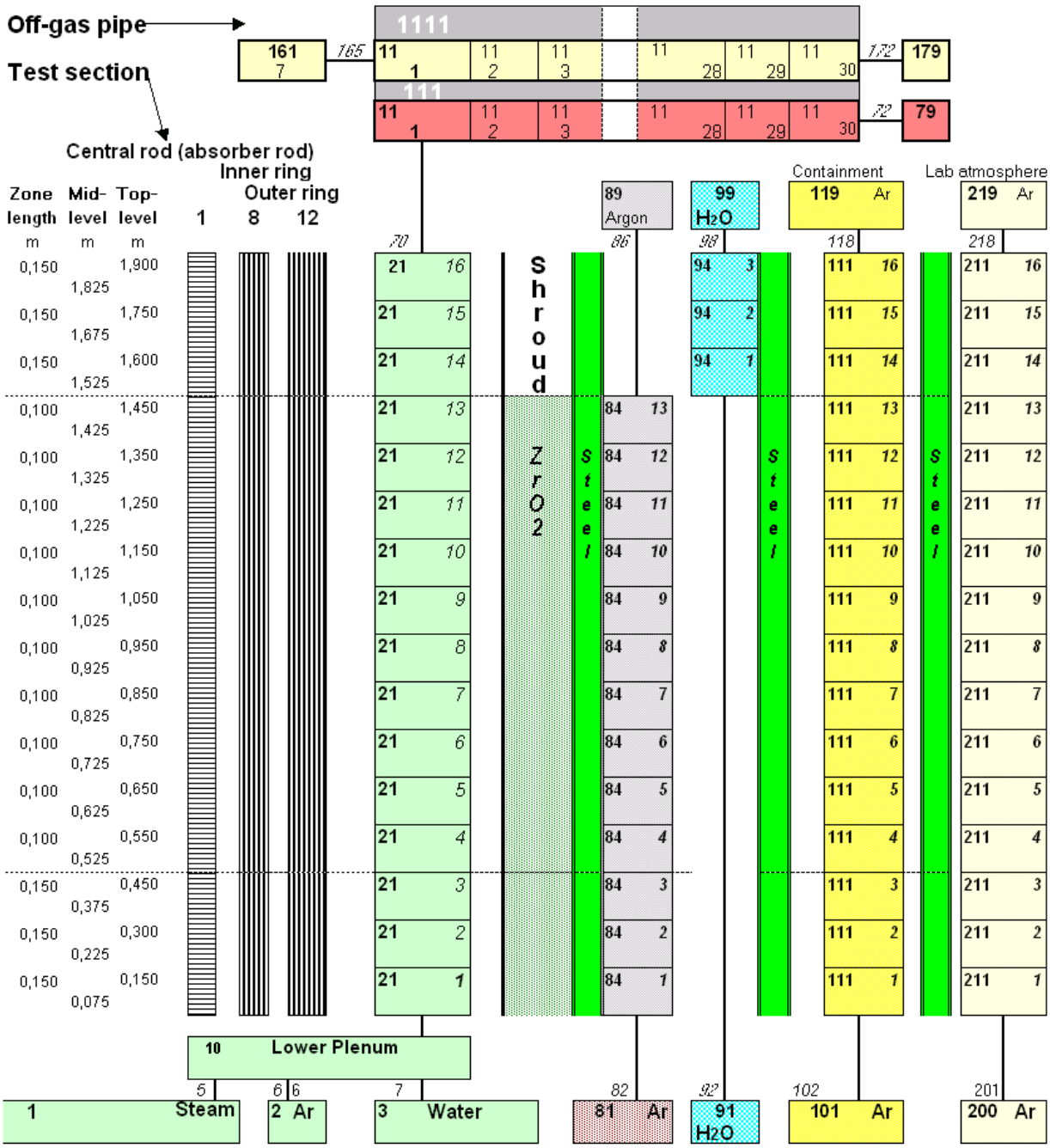

Figure 3.3 Detailed nodalisation for the QUENCH facility used for pre-test calculations and post-test analyses including simulation of all cavities up to the laboratory atmosphere (right side).

All solid structures in the bundle region from the central rod to the containment are included and treated as SCDAP components so that two-dimensional heat conduction within the structures and radiation between adjacent structures are taken into account. The central rod, the inner and outer ring of heated rods, and the corner rods (not included in Figure 3.3) are treated as separate SCDAP components. The shroud component includes the Zircaloy shroud, the fibre insulation with the gap in the upper electrode zone and the inner cooling jacket made of steel. It takes credit from the gap model developed for PHEBUS FP test to simulate radiative heat transfer across gaps filled with non-condensable gases. The containment and laboratory atmospheres are modelled to be stagnant. No radial boundary condition is required except for the temperature outside the containment in the laboratory (Figure 3.3). The solid structures of the off-gas pipe are treated as RELAP structures to reduce computing times.

The material properties (heat conductivity and capacity) of the shroud insulation had to be adjusted to take into account its cylindrical shape, because in S/R5 only slab geometry can be considered as a shroud component. A further adjustment of the thermal conductivity of the insulation material had to be made to achieve a better agreement between measured and calculated temperatures outside the insulation material for test QUENCH-01. The adjusted values have been left unchanged hereafter.

For parameter studies and model development, a simpler version, the “bundle model”, was extracted from the detailed model to speed up the calculation, maintaining the axial discretisation of the detailed model. Only one representative simulator is considered for all 20 heated rods and only one counter-current cooling flow is modelled for the whole length of the bundle. All parts of the facility outside the outer cooling channel are neglected. To obtain the same total heat transfer as in the detailed model the cross section of the cooling flow area was modified locally.

3.3 PHEBUS FP

Similar to the simulation of out-of-pile tests, the in-pile experiments in the French PHEBUS reactor at Cadarache research centre were used for code validation. Figure 3.4 shows the nodalization scheme. The stiffeners are modelled as SCDAP components, but not included in the figure. Input decks for the experiments FPT0 and FPT1 were optimized to run on a IBMRISC 6000 Power 3 node within ~ 3h using the nearly implicit scheme as long as possible. This allows testing of early and late phase core degradation models in a near reactor environment.

The lower and upper zones of the bundle are 0.05 m high to account for the thermocouple locations. Furthermore, a fine discretisation model with 22 nodes is available.

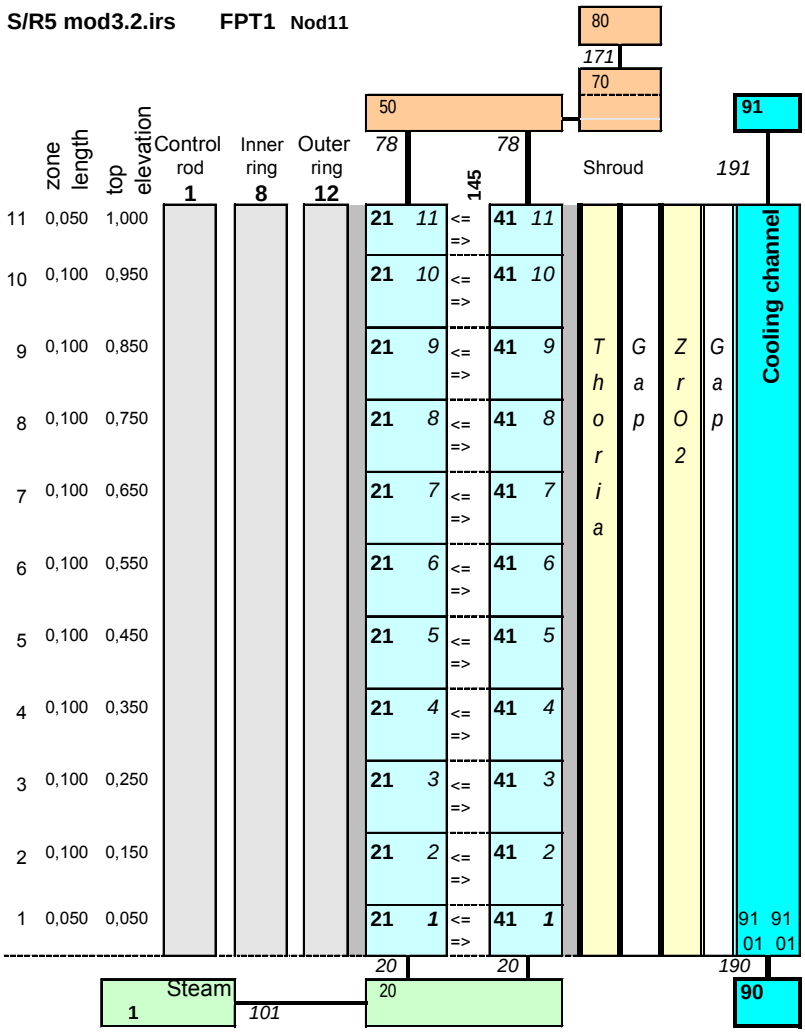

Figure 3.4 Simplified fast running PHEBUS input model

3.4 Extension of Number of Axial Nodes

At the quench front, the temperature in fuel rods or structural elements varies strongly with elevation due to strong changes of the heat transfer coefficients for the various heat transfer regimes from liquid water to pure steam. In RELAP5 /48/, a special feature called “mesh-refinement” is implemented to handle reflood conditions more realistically by increasing the number of axial meshes below and above the quench front and solving the heat conduction equation in two dimensions. The user can specify the number of subdivisions of each RELAP5 heat structure individually to control the accuracy.

For SCDAP heat conduction is always treated two-dimensionally, but no mesh refining is implemented. For typical reflood conditions, it was found that for axial zone lengths below 3” (0.075m) no significant differences in the results were predicted /49/. In the current CORA, QUENCH, and PHEBUS FP analyses, the typical zone length is 0.10 m, an appropriate value for severe accident analyses, in which no steep axial temperature gradients have to be analyzed.

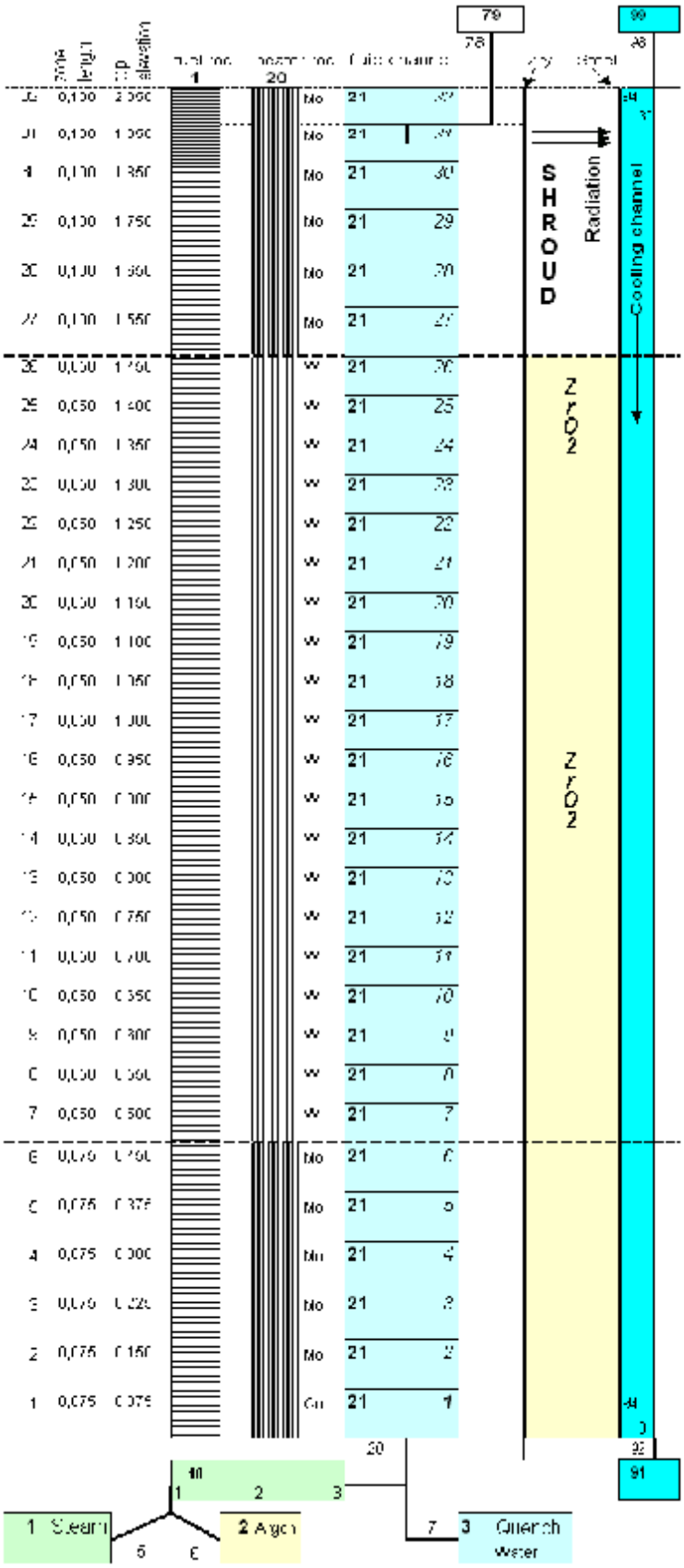

Figure 3.5 Refined axial nodalisation scheme with 32 meshes for fast post-test analyses.

In the original version, a refinement of the axial zones was limited by the code restriction to a maximum of 20 axial zones. During work for further axial refinement, several code errors were removed, associated with wrongly dimensioned multidimensional arrays in the conduction module.

With the new S/R5 capabilities, a refined model of the facilities was developed (“fine axial discretisation”), where the initial axial subdivisions of the three bundle zones (“coarse axial discretisation”) were doubled, as shown in Figure 3.5 for the simplified QUENCH bundle model. This procedure leads to rather a fine mesh length of 0.075 m in the lower electrode zone and of 0.05 m in the heated section so that the requirements mentioned in /49/ are fulfilled. In this way, the heater rod model includes 20 tungsten nodes in the heated zone plus 5 molybdenum nodes and one copper node at the lower electrode zone and 6 molybdenum nodes for the upper electrode zone. In the upper electrode zone, the fluid now leaves the bundle at 1.9 m, one zone below the upper end as indicated in Figure 3.5.

As for the coarse axial discretisation of the simplified bundle

model, a fluid channel with either argon or water exists outside the outer cooling jacket. To ensure realistic radial boundary conditions, the fluid cross sections are modified to meet the temperatures and thus the radial heat flux calculated with the complete facility model. In addition, an axial temperature profile can be imposed to meet experimental boundary conditions. Further code improvement also includes the capability to extend the fine 0.05 m mesh into the lower electrode zone.

With the finer axial mesh, a better representation of the facility peculiarities (Figure 2.2) can be achieved. However, due to the reduction of the zone length, the time step has to be reduced, too, because of the Courant limitation so that for fast computation the nearly implicit solution has to be used to keep the computation time sufficiently limited.

4 CODE IMPROVEMENTS

The code improvements can be split into three groups - the adaptation to the QUENCH facility, the error correction and/or improvement of physical models, and extensions to enhance the code efficiency.

4.1 Adaptation to the QUENCH Facility and Test Conduct

During the analyses of the commissioning tests /43/, the improvement of the S/R5 input deck required a more detailed representation of the power history to consider power response tests with multiple power levels. This could not be realized with the original version, because it was restricted to power histories up to 20 intervals. With an increased value of 36 in the header file scddat.H, the commissioning tests as well as tests with a long pre-oxidation phase such as QUENCH-01 could be simulated successfully. Pre-oxidation phases require a fine-tuning of the electric power input to avoid undesirable temperature excursions.

4.2 Electrical Heater Rod Model

This model is used for FZK out-of-pile test facilities, where the bundle is heated electrically with tungsten heater rods. The original INEEL model has some shortcomings to represent the geometry and the correct materials and can therefore not handle correctly QUENCH type heater rods. The FZK electric heater model (routine wolfht) computes the local heat release in the heated zone (tungsten) as well as in the electrode zones (molybdenum, copper) of the heater rod. The model includes the geometry change of the metallic conductors from tungsten to molybdenum as well as the physical properties of these materials /3/.

As listed in the Appendix, the material database has been extended by data for specific resistance (fnres), thermal expansion (fnexp), and surface emissivity (fneps) for radiation coupling used in the shroud model for PHEBUS FP tests (s. Section 4.4.4). The data for heat capacity, density, heat conductivity for molybdenum and copper were also included in the existing subroutines (fncp, fnro, fnk).

Material property data, required for the heater rod materials, such as electric conductivity, thermal conductivity, thermal expansion, and emissivity are now included in the MATPRO library as listed in the Appendix. The specific resitivities are expressed as follows:

$$r_W(T) = -2.61*10^{-2} + 2.63*10^{-4}*T + 2.20*10^{-8}*T^2 \quad (4.1)$$

$$r_{Mo}(T) = 2.249*10^{-2} + 5.36*10^{-5}*T + 1.38*10^{-7}*T^2 - 2.22*10^{-11}*T^3 \quad (4.2)$$

$$r_{Cu}(T) = -7.89*10^{-3} + 9.90*10^{-5}*T - 5.49*10^{-8}*T^2 + 3.16*10^{-11}*T^3 \quad (4.3)$$

with temperature T in K and specific resisitvity in Ω mm^2/m. Resistivity increases with temperature, and since for a given electrical current local release of electrical power is proportional to local resistance, local electrical power input increases with temperature. This is a positive feedback. Since the total electrical power input is prescribed in calculations, overestimated temperature and local electrical power release imply underestimation elsewhere with all its consequences. Therefore, such effects are not restricted to a small region, but lead to global errors. This makes calculations for electrically heated bundles more difficult than for nuclear heating. The problem aggravates errors for heat release due to exothermal reactions like oxidation that in turn overestimate temperature further.

Thermal expansion of the conductors is considered reducing the resistance increase with temperature according to Eqn. (4.4).

$$R_{(W,Mo,Cu)}(T) = r_{(W,Mo,Cu)}(T) * \frac{dz}{A_{wire} * (1. + b(T))} \tag{4.4}$$

with A_{wire} nodal cross section area (mm²),

δz nodal length (m),

T rod temperature (K),

$r_{(W,Mo,Cu)}(T)$ the specific resistance of the materials (Ω mm²/m), and

β(T) thermal expansion coefficient

In the QUENCH facility, electric power is deduced from measured electric current I and voltage U. Voltage is measured outside the bundle. For this reason, the potential drops across wires, conducting metal blocks and related contact resistances, especially of the sliding contacts at the ends of the fuel rod simulators, are included in the measurement. The electric power, released outside the bundle, has therefore to be taken into account explicitly, when measured current and voltage are used to determine the power release into the bundle. This is presently done by assuming a resistance R_{static} in series with the resistance of the electrodes and the tungsten heater. It represents the resistance that is outside the bundle but still within the domain of voltage measurement. The total heater rod resistance amounts to:

$$R_{(simulator)}(T) = R_{static} + \sum_{i=1}^{N} R_{(M,Wo,Cu)} \tag{4.5}$$

Presently, R_{static} has the same constant value for all fuel rod simulators and independent e.g. of temperature. For the heater rods of the CORA facility, a value 1.6 mΩ is used and for the QUENCH facility R_{static} = 4 mΩ ± 5%. When the computational domain does not include the whole rod length, the experimental value has to be changed to account for that part of the rods that is outside the computational domain.

It is not clear up to now, whether this approach is reasonable. Detailed measurements during the QUENCH test seem to be very difficult or even impossible. More information might, however, be deduced from measured bundle temperatures during the test. In the following, a proposal for a better approach is outlined.

The actual circuit consists of n parallel fuel rod simulators with n = 8 for the inner circuit and n = 12 for the outer circuit (Figure 4.1 shows the case of two parallel rods, i.e. n = 2). Each fuel rod simulator should be represented by a resistance R_1, representing the tungsten heater and the electrodes, and a resistance R_2 for everything else related to each rod, i.e. above all the sliding contacts. The resistance that is common for all n fuel rod simulators in the circuit, i.e. for the common metal blocks, the wires and the related contact resistances, is given by R_0.

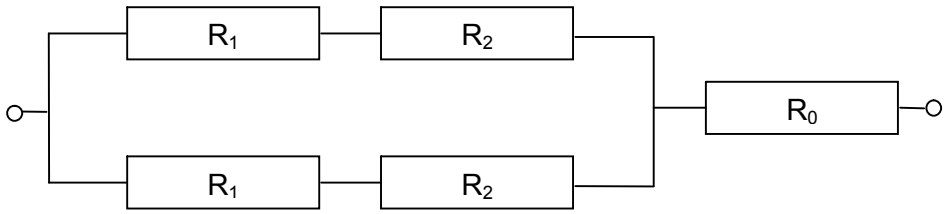

Figure 4.1 Electrical circuit between the voltage measurement points

The total resistance of this arrangement is

$$R_{total} = (R_1 + R_2)/n + R_o \qquad (4.6)$$

Since no information is available for a single rod in the parallel circuit, it is assumed that R_2 is the same for all 20 fuel rod simulators and that R_o is the same for both circuits. R_{total} can be derived from measured electric current and voltage as $R_{total} = U/I$ and holds for both circuits according to the above assumption about rod behaviour. R_1 can be derived from material property data for every applied electrical power according to the measured axial temperature profile; R_0 and R_2 can be determined from measured electric current and voltage from the respective equations for both circuits. To reduce uncertainty due to non-equilibrium conditions, only steady state conditions should be chosen. If experimental accuracy is good enough, this concept might give a better representation than the present one. For time reasons, this has, however, not been done.

4.2.1 INPUT modifications

The user can choose between two versions of subroutine wolfhe, controlled by card 40000100 and card 40cc0300. On card 40000100, the new word 5 has following meaning:

Original ORNL model: <0 (no electrode zones at all)
FZK model for CORA: 2 (first and last zone uses copper electrode)
FZK model for QUENCH: 3 (only lowest zone uses copper electrode)

The type of the heat rod composition is printed to the output file during input processing:

QUENCH: FZK-model: 3
CORA: FZK-model: 2

QUENCH

```
* number of zone 2D ht.  CORA  QUENCH/CORA
40000100  32      1      5     3
*Radius of tungsten       electrodes  # of nodes
40cc0300   0.003    4.0e-3    0.0043       3          ** 16 axial zones
40cc0300   0.003    4.0e-3    0.0043       6          ** 32 axial zones
```

CORA

```
* number of zone 2D ht.  CORA  QUENCH/CORA
40000100  32      1      5     2
*Radius of tungsten       electrodes  # of nodes
40cc0300   0.003    1.6e-3    0.0043       3          ** 16 axial zones
```

If an input deck contains simulators, additional information appears in the output and in the auxiliary file (stdio), showing the axial temperature and power profile. In this way, the axial power redistribution can be plotted easily, since the nodal power unuc is not available for minor edits. An example of the output is added in the appendix (section 8.5).

4.2.2 Fuel-Rod State Model

In the advanced fuel rod state model, the variations of the material layers are tracked during transient, considering the non-reactor specific internal composition of the CORA and QUENCH heater rods. This includes the annular dimension of the fuel pellets as well as the gap between tungsten and annular pellet.

4.2.2.1 Prototypic Pellets (CORA)

In CORA, fresh fuel pellets made of depleted uranium were used for unheated and heated rods. In the original SCDAP version, these fresh fuel pellets were handled as cracked fuel (imat=7), filling the gap completely. This is an approach feasible for in-pile tests under reactor conditions but not for FZK type out-of-pile tests.

The code is now forced to use the material UO_2 (imat=6, fresh fuel pellets) and a thin gap between pellet and cladding. Actually, radiation is not considered, but the user can adapt the heat conduction data to account for that contribution, because the material in the gap is defined by the user, indicated by index imatr3=9 (gas atmospere). Direct radiation Q_{12} between two bodies 1 and 2 at temperatures T_1 and T_2 can be accounted for as

$$Q_{12} = \sigma A_2 F_{12} (T_1^4 - T_2^4) \quad (4.7)$$

where F_{12} is the view factor. This is equivalent to

$$Q_{12} = \sigma A_2 F_{12} (T_1^2 + T_2^2) (T_1 + T_2) (T_1 - T_2) \quad (4.8)$$

Setting Δx the distance between the two bodies, we can define an effective thermal conductivity λ_{eff} that satisfies

$$\lambda_{eff} \Delta x = \sigma F_{12} (T_1^2 + T_2^2) (T_1 + T_2) \quad (4.9)$$

so that as a first approximation radiation can formally be modelled like heat conduction. A crucial point is, however, that the effective heat conductivity depends on the temperature of both bodies, and at least, when tables are used, additional assumptions have to be made. To account for realistic radial heat fluxes, especially during steam cool down prior to quenching, a simple radiation model (section 4.4.4) as used for the shroud component is implemented (see appendix).

Also the geometry of the tungsten heater was not considered for heat transport, but modelled by UO_2. Therefore, the UO_2 mass was overestimated. Since UO_2 and tungsten have different heat conductivity and heat capacity, the reality is not well represented. Especially in case of strong temperature gradients, the code overpredicts the temperature i. e. at the upper end of the heated zone. The new model also includes thermal expansion and the growth of the gap between tungsten heater and UO_2 pellet.

4.2.2.2 Simulant Materials (QUENCH)

To simulate the QUENCH facility, pellet material property data were adapted to ZrO_2 as given in Figure 4.2, using built in MATPRO material data for high temperature ZrO_2 (imatr3=5) or as a user defined table (imatr3=12), including data delivered by the manufacturer. The data differ slightly from those used in the MATPRO library (imatr3=5). ZrO_2 melting, melt relocation and material interactions with the Zry cladding, as occurred in tests QUENCH-02 and QUENCH-03, cannot be modeled correctly with the actual code version. When respective code improvements are envisaged, it should be kept in mind that the models only refer to such out-of pile tests because of the non-reactor specific pellet (ZrO_2) material.

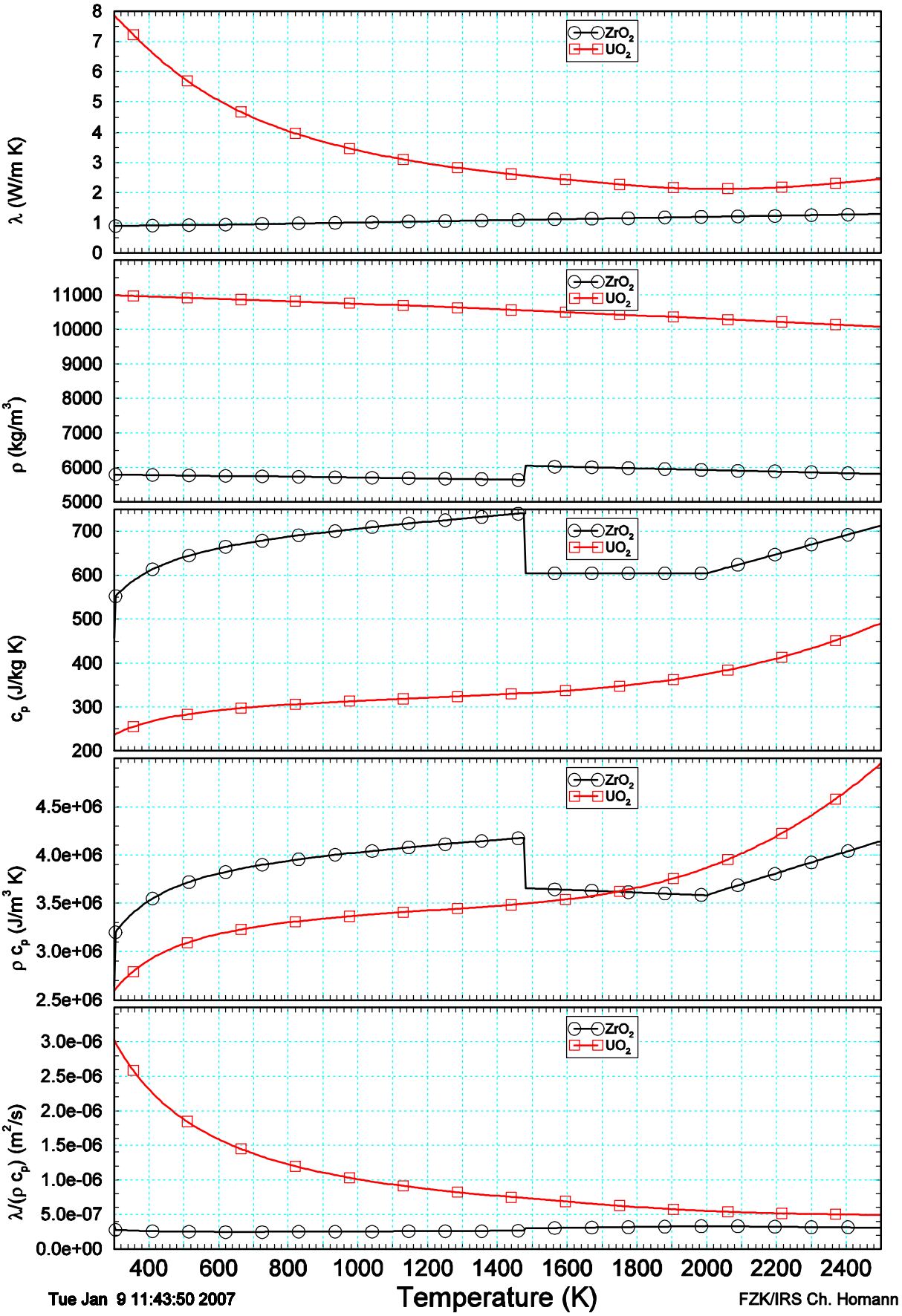

Figure 4.2 Comparison of pellet material properties of ZrO_2 pellets, used in QUENCH and prototypic UO_2 pellets, used for CORA, and thermal diffusivity (bottom) in the relevant temperature range.

4.3 Status of Control Rod Models

In the existing Western PWRs, Ag-In-Cd control rods are used and in BWRs B_4C control rod blades with Zircaloy canisters. For completeness, we mention that in the French reactors a third type is used, a kind of compound control rod, composed of B_4C in the lower part and Ag-In-Cd in the upper part.

A review of SCDAP component models revealed that several models are available:

1. The original LWR model could handle Ag-In-Cd and B_4C materials originally. During code development, the B_4C part was deactivated, the damage models were developed for PWR conditions solely. As a consequence, no oxidation of any absorber species is included, because liquid Ag-In-Cd is assumed to relocate into colder parts of the bundle.

2. For BWRs, two models are available:

   - A detailed control rod – blade-box component developed at ORNL, which incorporates a chemical package, based on SOLGASMIX approach. However, released gases are not tracked in the non-condensable field of RELAP5. (This component did not work in PWR environment, code failed after initialization)
   - A simplified “BWR” model, which handles only the B_4C – SS system. This model was tested for QUENCH-07 and the LOOP reactor scenario /61/. In a first attempt, the code failed, when radiative heat transfer was calculated. The reason for code failure, the non-existing surface material index, was corrected, and the code continued until control rod failure.

3. The N-reactor B_4C-rod with steel cladding, but without Zircaloy guide tube. Steel and B_4C oxidation are modeled, but the model could not be activated in a PWR environment.

To simulate the cylindrical B_4C control rod as used in QUENCH-07 and QUENCH-09, not to mention the French compound rod, no existing model is adequate. A complete model has to address properly the following issues:

- Material properties and configuration (pellets, powder)
- Dissolution of B_4C by liquid SS-Zr mixture below melting temperature of SS.
- Control rod cladding failure: SS breach
- Interaction of metallic Zry with SS-B_4C
- Determine the degree of the protective character of ZrO_2
- B_4C oxidation and release of H_2 (later CO, CO_2) after ZrO_2 failure including limited access of steam through breach
- Relocation of melt composed of Zr, SS, evaporation/loss of B_2O_3

For reactor applications, however, it has to be assessed, whether the benefit of an exhaustive model is worth the effort for its development and qualification. When only heat-up of the core is of interest, such detail is probably not necessary; for release of fission products, e.g., some more efforts may be advisable.

As in the original programme version, control rod components can only be specified in the input, when at least one simulator or fuel rod component is specified.

4.4 Extension of physical models

4.4.1 Material Property Data

Originally, only Zircaloy or ZrO_2 surfaces are taken into account in S/R5. Even when the user inputs another material, ZrO_2 replaced it internally, based on the assumption that a protective oxide layer is built on a Zircaloy shroud. However, experimental facilities use other material such as alumina or thoria oxide as shroud materials. As part of code improvements, this logic was corrected for the shroud component, and the material properties were derived from the data bank.

4.4.2 Heat Transfer in Post-CHF Regime

S/R5 mod 3.2 is based on the RELAP5 mod 3.2 code version which includes improvements developed at Paul Scherrer Institute at Würenlingen, Switzerland /25/. Furthermore, the improved FZK-CHEN-correlation /45/ was implemented to improve the capability to determine the heat transfer prior to the quench front.

Tests with S/R5 made differences in heat transfer coefficients between RELAP heat structures (HS) and SCDAP components obvious. As a first assumption it was supposed that the mesh refinement, activated in the HS, might lead to the different values, but a closer look revealed that the conditions for the call of the heat transfer subroutine were different and led to the observed different values. Currently, a simplified approach is used. It takes credit from a “virtual” HS in the fluid channel and uses that heat transfer for the SCDAP components. Due to man power restrictions and lacking actual demand, a final solution of this problem has to be postponed.

4.4.3 Improvements for 2-D Heat Conduction

In our efforts to model FZK out-of-pile test facilities, we found that in the original S/R5 version the first and last axial nodes of the simulator had fixed temperatures for the whole transient as indicated by the card 40cc0250 and 40cc0251. So these zones do not participate in the convective heat transfer to the fluid. This may lead to large errors at the upper boundary, because the temperatue gradient to the hot zone is large. In the QUENCH facility, where the fluid inlet is at the bottom, this shortcoming also causes problems at the lower boundary. Therefore, we defined the prescribed boundary

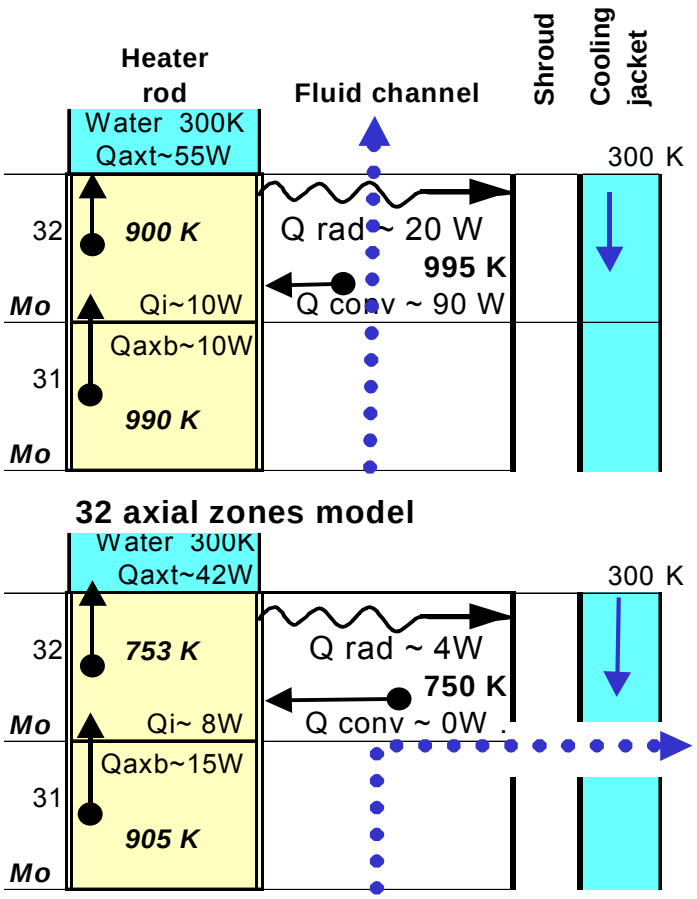

Figure 4.3 Brief power balance at upper axial end of heater rod.

temperature to exist at the axial ends of the end zones and calculated the nodal temperature as a function of 2-D heat conduction, convective heat transfer and radiation. This allows to make assumptions about the temperature response of the copper electrodes and to compute a realistic energy balance for the whole length of the heater rods.

When extending the axial nodalisation to 36 nodes (section 3.4) it was found that two-dimensional arrays for the intermediate variables a, b, c, d were missaligned so that data were overwritten. Original array dimensions were based on radial discretisation, perhaps due to historical reasons, because initially the number of radial zones was larger (32) than that of axial nodes (10).

To demonstrate the importance of our code improvements, a brief heat balance is given for the top electrode zone of the heater rod in case of purely axial fluid flow conditions (top of Figure 4.3). The heat input for node 32, composed of the internal heat source (Qi), the axial heat conduction from zone 31 (Qaxb), and the convective heat input from the fluid (Qconv) amounts to 110 W. The Zircaloy oxidation is not considered. The heat sinks are composed of axial heat conduction (Qaxt) to the water-cooled ends of the heater rod and the radiation to the shroud (Qrad). In total, ~ 30 W is available to heat up this axial zone. In the QUENCH facility, the hot fluid leaves the vertical test section at ~ 0.1 m below the upper end into the horizontal part of the off-gas pipe. In Figure 4.3 bottom, the power balance is shown for this case, indicated by the bent dotted arrow. The convective heat-up vanished and together with the reduced radiative heat losses the rough power balance sums up to ~ -20 W. This indicates that the axial heat conduction efficiently cools the upper two nodes of the heater rod.

4.4.4 Radiative Heat Transfer in Annular Gaps

S/R5 can only calculate radiation heat transfer between SCDAP components or between RELAP heat structures. Both models use view factors, emissivities, coefficients

and surface temperatures to determine the heat flux in the enclosure. Since the emissivity is a material property, its has been added to the material data base (section 4.4.4).

4.4.4.1 Heater Rods (simulator)

In original S/R5, there are two different treatments to simulate the gap between pellet and cladding. As known from power reactors, the annular gap is closed after some months so that the pellet is extended to the cladding inner surface with a reduced density. In this case, no gap is simulated. For ballooned fuel rod sections, a gap is formed in which radiative heat transfer is calculated as additional artificial heat conduction.

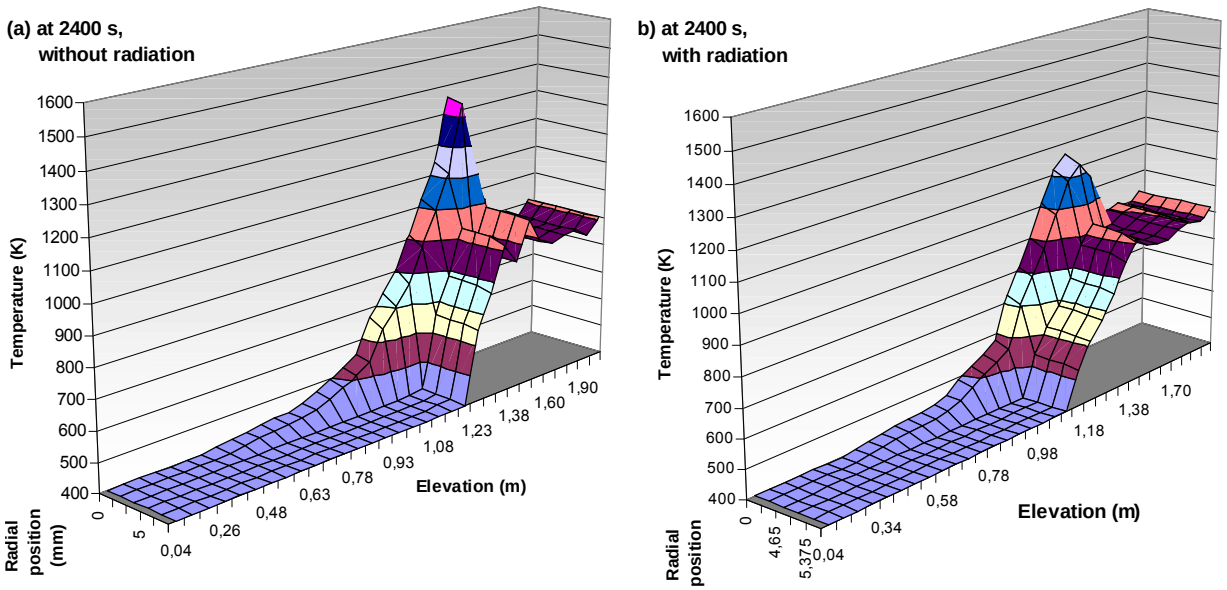

Figure 4.4 Radial temperature profile calculated for QUENCH-02 at 2400 s without (a) and (b) with radiation across the gap between pellets and cladding.

For FZK out-of-pile facilities, however, no pellet growth is observed so that a gap exists up to clad melting and failure. Under normal heat-up conditions, the radial heat flux is rather small so that this deviation might be accepted. Under reflood conditions, however, the temperature gradient to the fluid is very large so that an error in the gap conductance becomes remarkable as can be demonstrated from Figure 4.4. In the left side of this figure, the 2-D temperature field of a heater rod is shown for QUENCH-02 at 2400 s, i.e. during cool-down, without taking into account radiation between pellet and cladding. Three axial zones can be distinguished: up to ~ 0.8 m, the bundle has been

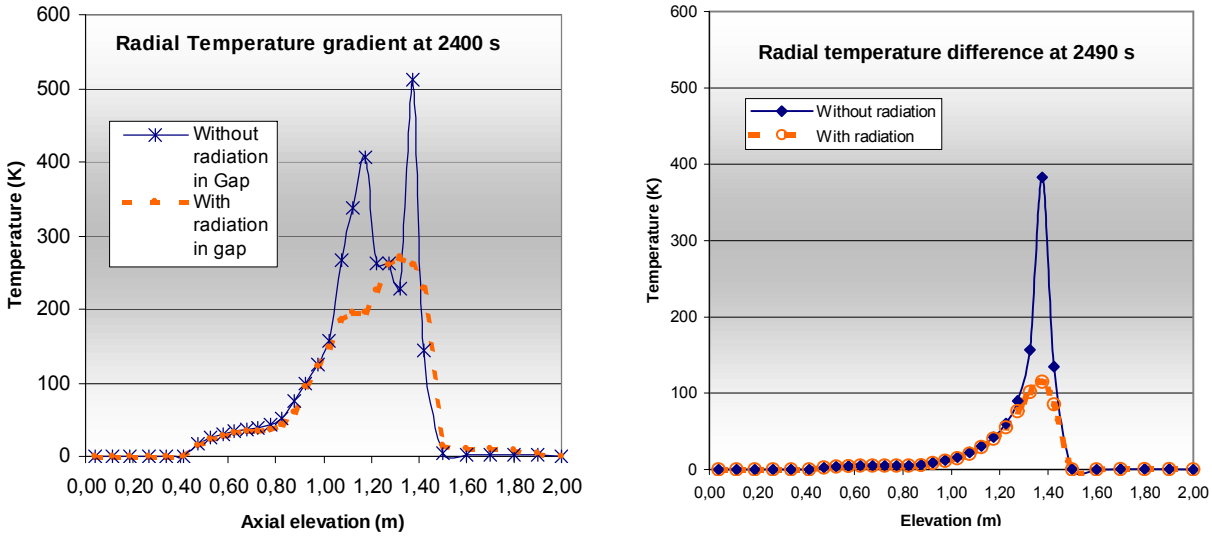

Figure 4.5 Radial temperature difference versus axial elevation for 2400 s (left) and at the end of the calculation at 2490 s (right).

cooled down completely at that time, the hot zone, where only the cladding has been quenched, and the upper electrode zone above 1.2 m with a flat temperature profile at a high level; it is cooled by steam.

The right side of Figure 4.4 shows the same case, but radiation between pellet and cladding is taken into account. Detailed investigation shows that the contribution of radiation to heat removal from the rod starts at ~ 30 % below 1000 K and increases up to 80 % at 2150 K. Especially in the hot zone, the radial temperature difference is reduced, as can be seen in Figure 4.5. Since the axial power distribution is strongly affected by the axial centerline temperature, this code feature increases the capability of S/R5 to simulate QUENCH and CORA tests realistically.

4.4.4.2 Shroud

Within the shroud component, S/R5 only calculates solid state 2-D heat conduction in a slab geometry (x-z), no gap can be considered. For test facilities, such gaps may exist, and at high temperatures, radiative heat transfer is much more efficient than pure heat conduction, especially if an insulating non-condensable gas such as argon is used as filling gas.

For the French PHEBUS facility, used for the PHEBUS FP program, only one single shroud has to be modelled, and the gaps are allowed to close due to thermal expansion. The relevant code improvements have been documented in /8/. As a first step, the material has to be identified in the model, as imatr3=10, normally used for fiber insulation, and is set to imatr3=9 for further gap handling. In the CORA facility, a gap exists in the high temperature shield HTS. Such a gap exists also in the shroud of the CORA and the QUENCH facility in the upper electrode zone, because the fiber

insulation ends at ~ 1.0 m to avoid overheating of the upper electrode zone. The PHEBUS model has therefore been extended for the two German facilities.

In a first attempt, the heat transport due to radiation has been simulated by an effective heat conductivity as outlined in section 4.2.2.1. This approximation is used for temperatures above 1000 K and, for this reason, acts mainly in the region of the gap only and not below. However, as stated in that section, the effective heat conductivity depends on the temperature of both bodies and is therefore only valid for given boundary temperatures. Normally, there is no strong need to simulate this heat flux better, because it is outside the test section, but due to the heat conduction inside the upper electrode zone, two effects become important:

1. For metallic electrical heaters, local resistivity and hence local power release increase with temperature. Therefore, the electrical power, released in the bundle, is wrong, when heat removal in the upper electrode zone is not modelled correctly. This positive feedback of electrical heaters is known since long, and played a role for analysis e.g. of CORA-7.
2. During reflood, Zry in the upper electrode zone oxidizes significantly and acts as an additional local heat source, discussed e.g. for CORA-13 (ISP-31).

To clarify this item, the radiative heat transfer was activated for CORA, assuming an annular gap with a gap width of 0.019 m, the thickness of the fiber insulation, extending from 1.0 m to 1.30 m axial elevation. At the outer surface a „virtual“ layer of fiber material had to be assumed to define clear boundary conditions. In reality, however, such a radiation shield did not exist, the Zircaloy shroud could radiate directly to the inner HTS surface. To overcome this deficiency and in order to consider the steam absorption, the emissivity of this „virtual“ layer was reduced from 1.0 (ideal) to 0.4.

In the QUENCH facility such a gap is shown in Figure 2.3 and Figure 4.3. The inner surface is the Zircaloy tube of the shroud, the outer surface is the inner cooling jacket; the filling gas is pure argon. The outer surface is kept at room temperature by water, whereas the inner surface of the shroud may be heated up to more than 2000 K. No virtual layer of fiber material needs to be input. In addition, the MATPRO library is enlarged for emissivities of metallic Zircaloy surfaces, used in the new model. It is of course only valid as long as the shroud is intact, i.e. normally up to the initiation of the quench or cool-down phase. In the appendix (Table 8.3), the output of the model is explained. It may be used to check the correct modeling.

4.4.5 Local Clad Failure Criteria

In a bundle or nuclear reactor, failure of the ZrO_2 layer initiates melt relocation and stops clad oxidation at the breach location, but may initiate double sided oxidation of the clad in the surrounding. In the existing severe accident code systems such as MELCOR, S/R5, MAAP, ICARE2, and KESS, failure of the ZrO_2 layer is based on a

simple user defined temperature level and an oxide layer thickness criteria. In some codes, a detailed mechanistic model is available to calculate ZrO_2 failure based on a local stress-strain correlation. So far, two facts hinder the use of such a sophisticated approach: the lack of adequate material data for the complex compound system (several metal and oxide layers) and the lack of a fine axial, radial, and, more important, azimuthal temperature resolution. Following the sophisticated approach, the mesh density has to be increased by several orders of magnitude (to reach e.g. axially 50 meshes per meter, radially 12 meshes per layer, and azimuthally 8 for each rod) compared to presently used meshes, which are based on the idea of a representative rod. Moreover, the validation of such an approach seems to be a Sisyphus task, since each rod in a small bundle experiences a different environment and thus a different heat-up history.

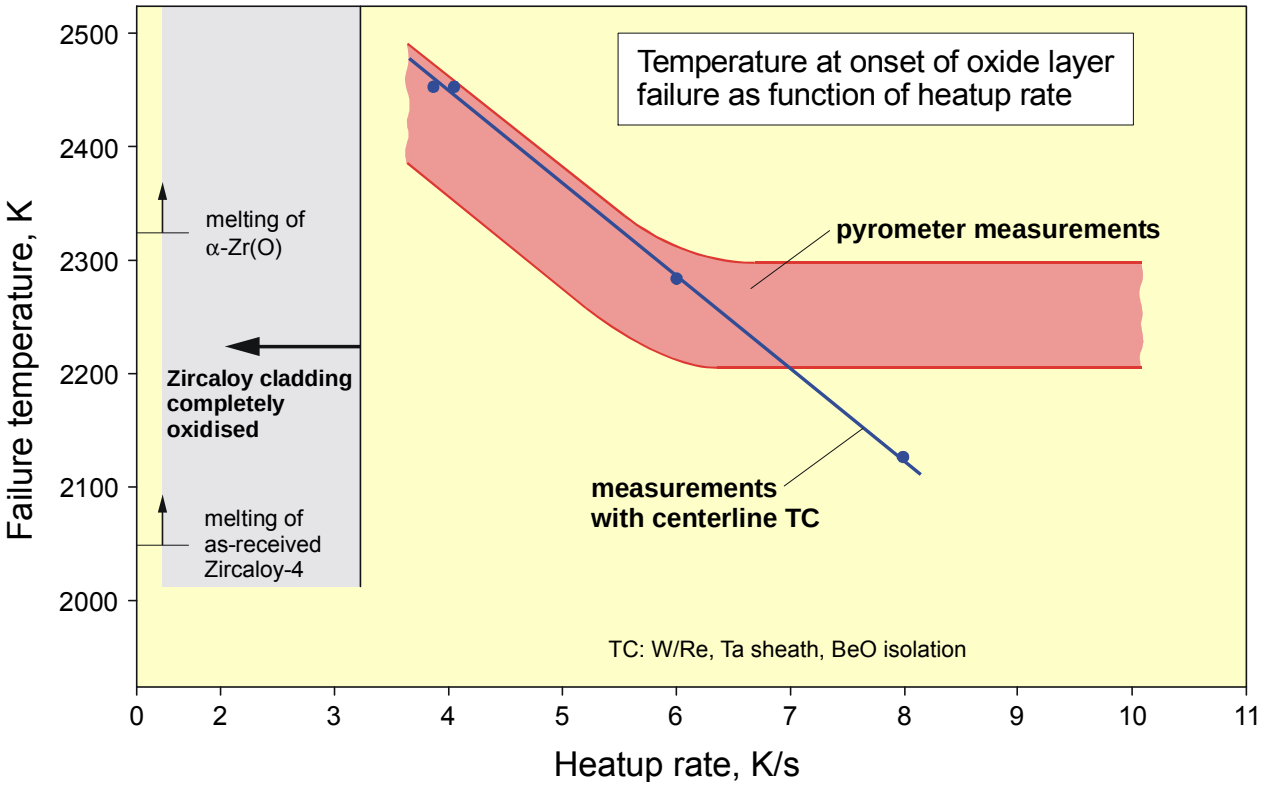

Figure 4.6 Measured dependency between average effective heat-up rate and detected failure temperature in the single rod QUENCH rig.

Because of these difficulties, most code users accept the inherent uncertainty and use the two parameters to control the further sequence of their simulation. The parameters can be optimized using various integral effects, but the extrapolation for reactor applications is still difficult. Firstly, these two parameters are valid for the whole bundle or core; the latter may extend up to 4.2 m height and several meters in diameter. Secondly, various core loading strategies imply axial and radial decay heat profiles and thirdly, boil-down velocity varies axially. All these effects cause differences in local heat-up rates and make the choice of global values for the parameters difficult. Therefore,

different cladding failure criteria were often used for validation calculations and reactor applications to take into account the different lateral environments.

In a first approach for an improvement, it was tried to take into account the heat-up rates. It will be shown that in this way the failure temperature is no longer a global value for the whole bundle but that it may vary from mesh to mesh. At FZK/IMF /51/, separate effect tests in an oven have been performed under steam-argon atmosphere for various heat-up rates, initiated above 1473 K. A quasi-linear relation was found (Figure 4.6) for local heat-up rates between 3.5 and 8 K/s. Below a heat-up rate of 3.5 K/s, the cladding becomes completely oxidized and may remain intact up to 2950 K as indicated in Figure 4.6; above 8 K/s the ZrO_2 layer of the cladding fails just above melting of metallic Zry (2033 K). According to the experimental data shown in Figure 4.6, failure temperature can be described by:

$$T_{ZrO2\,fail} \sim -82.0 * \frac{dT}{dt} + 2787 \tag{4.10}$$

where temperatures are measured in Kelvin and time in seconds. Since in real environments, no such stable conditions can be assumed, the main problem is to transfer the knowledge obtained under constant heat-up rates into the varying heat-up rates in integral test or reactor conditions. A direct transfer of the results leads to unexpected high failure temperatures around 2700 K, because heat-up is non-linear under real conditions due to the temperature dependency of the oxidation in any case and due to the electrical heating in case of out-of-pile experiments. In any case, the heat-up rate above 1473 K seems to be important for the clad failure temperature.

In contrast to furnace situations, no such stable conditions can be assumed in real environments. In electrically heated bundles, heat-up rates vary due to the positive feedback, and they vary in both integral out-of-pile tests and reactor conditions due to the temperature dependency of heat release by oxidation. For this reason, direct transfer of the results, obtained from the above SETs, may lead to unexpectedly high failure temperatures around 2700 K. In any case, the time and the heat-up rate above about 1400 K seem to be important for the clad failure temperature.

A closer inspection of the results shows that the large heat-up rates as stated above are only found above 1700 K, when the exothermal energy exceeds the decay heat level. A reasonable compromise is to consider the heat-up rate only above a given minimum temperature T_0, set to 1400 K, reached at time t_0 so that pre-oxidation phases or slow boil down phases, which lead to very stable oxide layers, are taken into account, too. Consequently, the heat-up rate in Eqn. (4.10) should be replaced by an effective heat-up rate averaged starting at T_0 = 1400 K

$$\frac{dT}{dt}_{eff} = \dot{T} = \frac{T - T_0}{t - t_0} \tag{4.11}$$

This procedure gives heat-up rates below 4 K/s. In the model, the applicability range is restricted to the interval between 2250 K, the melting temperature of α-Zr(O), and 2500 K, as indicated in Figure 4.6. Between both temperatures, a linear approach is chosen:

$$T_{YrO2\,fail} \sim 2500 - 138 * \dot{T} \qquad (4.12)$$

to replace Eqn. (4.10). In Eqn.(4.12), temperatures are measured in Kelvin and time in seconds. The different values, compared to Eqn. (4.10), account for the non-linear heat-up in integral bundle experiments and in a reactor environment. For a further validation of this approach, experimental data are still not available.

4.5 Standardized Oxidation Correlation

As an outcome of the 5th European Framework Program COLOSS, a set of standardized oxidation correlations was defined /52/. An analysis revealed (see Figure 4.7 to Figure 4.9) that the S/R5 correlation in the low temperature section (CATHCART) is nearly identical with the proposed one, but in the high temperature section, URBANIC, gives higher oxidation rates. The code includes now either CATHCART or LEISTIKOW at low temperature and PRATER/COURTRIGHT for high temperatures.

Between both regimes, an interpolation section was advised in /52/, taking into account cubic and tetragonal ZrO_2 structures. First validation results were performed for PHEBUS FPT1 as shown in section 5.3. Also reactor analyses were performed to identify the influence of the modification (The modified code sections are listed in the appendix.)

During implementation of the new oxidation correlations, a typing error was detected in the original coding, which had led to a slight over-prediction of the hydrogen release at high temperatures by the Urbanic-Heidrick mass gain correlation. In a next step, the simulation of steam-starved conditions has to be addressed to evaluate conditions in QUENCH-09 and PHEBUS FPT3. In QUENCH-09, the steam starved conditions led to reduction of the protective oxide layer, prior to reflood phase /54/.

Before further validation, work on the new high temperature oxidation correlation is made, further programme changes are necessary to take into account the reduction of Zr oxidation after comsumption of primary β-Zr /62/. Otherwise, premature temperature escalations may be calculated erroneously /61/.

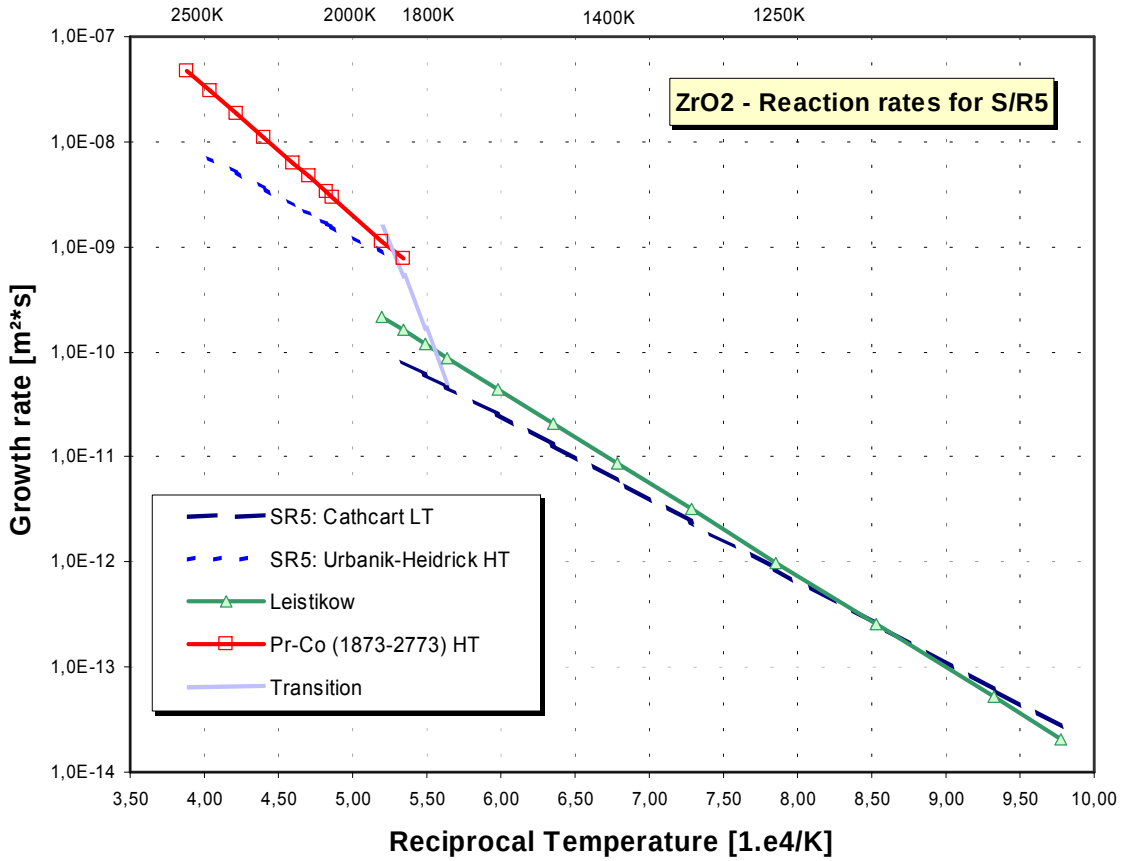

Figure 4.7 Correlations of the growth rate of the ZrO_2 layer

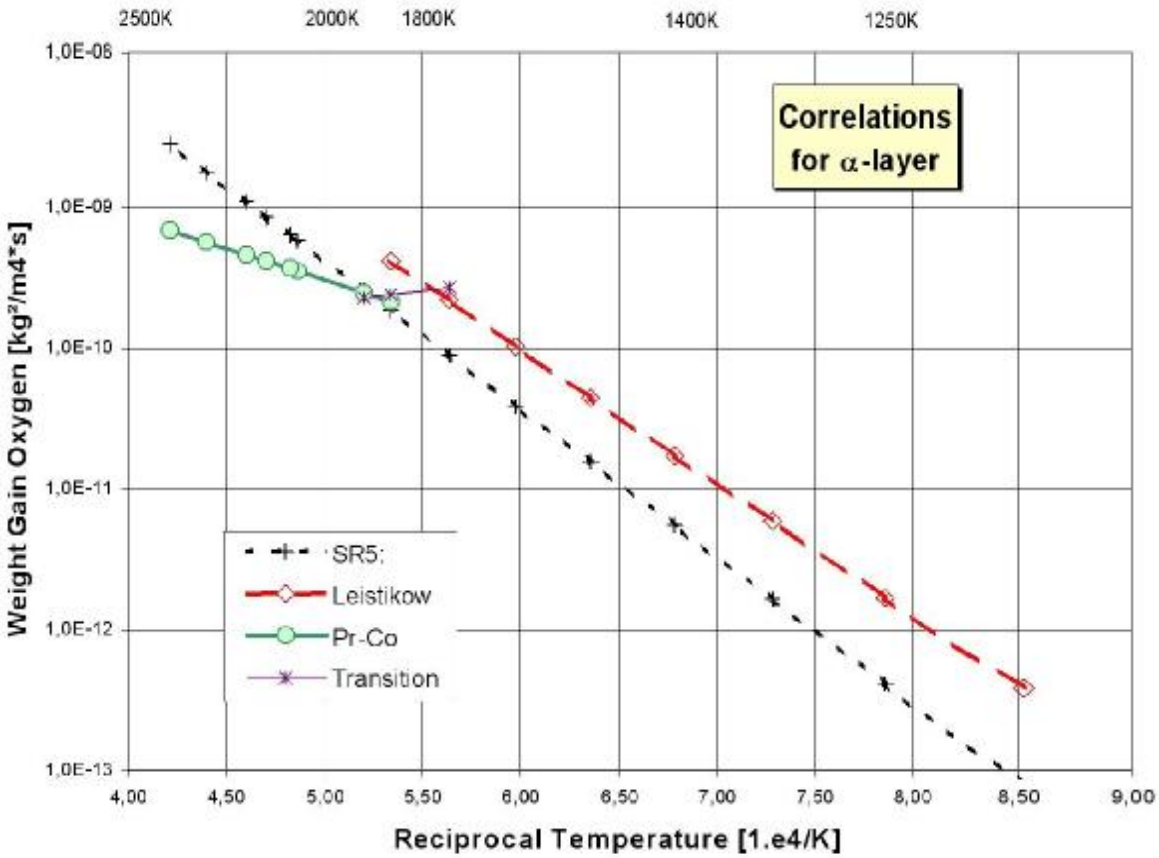

Figure 4.8 Correlations for the α-Zr(O) growth rate

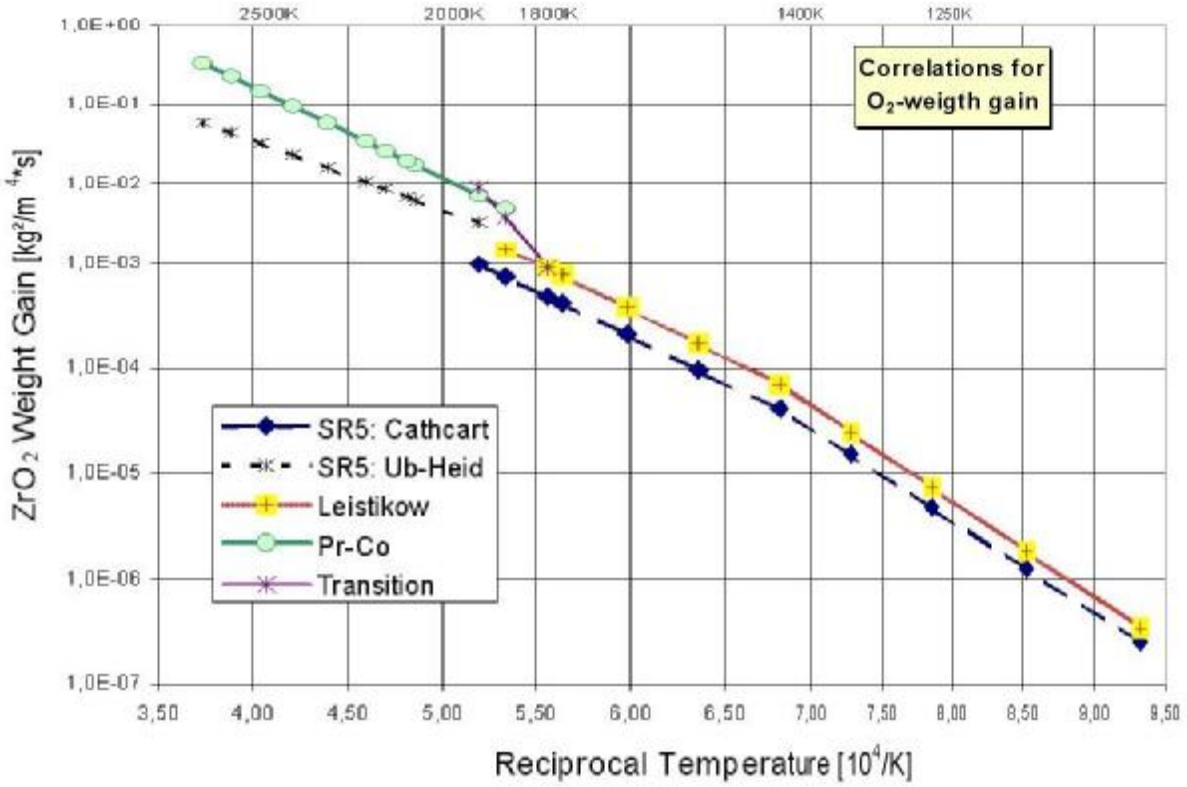

Figure 4.9 Correlations for the ZrO_2 weight gain rate

4.6 Late Phase Core Degradation

So far, the transition to debris and subsequent pool formation is oriented at a number of temperature levels that are more or less based on the various physico-chemical material behaviour. Therefore, the fuel rods composed of UO_2 pellets in a ZrO_2 hull, are considered to fail and to collapse at 2830 K, the solidus temperature of their eutectics. Then, a partially liquefied debris is formed, which is transferred subsequently into a molten pool due to insufficient decay heat removal. The failure temperature originates from the pseudo binary phase diagram of UO_2-ZrO_2.

In the PHEBUS FPT experiments 1, 2, and 4, no high temperature ceramic melting was observed; relocation, leading to the formation of a molten pool, occurred around 2600 K. Such a behaviour was not seen in the test PHEBUS FPT0 with fresh fuel pellets, indicating a certain influence of the fuel burn-up. Since the experimental data are considered to be reliable, we deduce that an unknown mechanism triggers the rod collapse significantly (300 K) below the eutectic melting temperature. The measured solidus temperatures of irradiated mixtures are slightly below the values for fresh fuel (Figure 4.10). Several important mechanisms are discussed in literature as /55/:

1. Material separation:
   Influence of material separation occurring during early temperature escalation.
   In this case, the Zircaloy cladding oxidized completely before any significant fuel dissolution by molten Zircaloy, and in the late degradation phase, thermal stresses

may induce the relocation, i.e. the ceramic material relocates as a solid body, partially within the ZrO_2 hull.

2. Locally liquefied debris:
   During the temperature escalation, the pellet dissolution by molten Zircaloy starts, however, after the melt relocation as rivulets, a part of metallic melt remains at higher bundle position, and the dissolution process continues (the temperature remains always below 2800K). It is assumed, that "molten pools" (bridges, blockages) are formed between the rods during the oxidation phase and finally the materials relocate as a ceramic melt.
3. Influence of structure materials:
   Metallic atoms (from absorber rod) may reduce the melting point of fuel forming new phases. However, post-test examination, performed by JRC/ITU on the solidified ceramic mixture samples, taken from the molten pool, shows that the melting point is at 2750 K, i.e. slightly below the melting point of a pure UO_2–ZrO_2 mixture (2800 K) Figure 4.10).

All these hypotheses do not consider any influence of fuel burn-up. However, the boundary conditions of the PHEBUS tests are quite common, except for the differences in the burn-up. Taking into account the pellet, the porosity of which is increased and hence the strength is reduced with increasing burn-up, the issue 1, separation of UO_2 and ZrO_2, is favored, allowing fuel particles to relocate within the ZrO_2 hull. In low-pressure scenarios, the slightly enlarged gap (ballooning) may promote this effect.

In the present codes, such early fuel rod collapse is not foreseen, neglecting user defined parameters in MAAP and MELCOR. S/R5 calculates solidus and liquidus temperatures based on the pseudo binary phase diagram mentioned above using the MATPRO library. Consequently the fuel rod can only collapse above that temperature. The same behaviour is seen in ICARE2 calculations.

As a contribution to the PHEBUS bundle interpretation circle (BIC), a particle relocation approach was postulated and implemented in S/R5. It assumes that above a given temperature, which might be burn-up dependent, the fuel pellet stack becomes instable leading to particle relocation forming loose (rubble) debris.

To get a more profound support for this hypothesis, a literature review about the late phase fuel rod degradation and melting temperature was performed, mainly based on the OECD report on in-vessel code validation matrix /56/. However, the existing database is rather scarce, because either high temperature was reached at zero or low burn-up (CORA, FPT0, PBF, LOFT) or the medium burn-up experiments were stopped before high temperatures were reached (ACRR, FLHT). As can be seen in Figure 4.11 for some experiments, two values are published, one based on the PIE results, giving the melting temperature of the mixture and a lower value which was used to analyze the test with different codes.

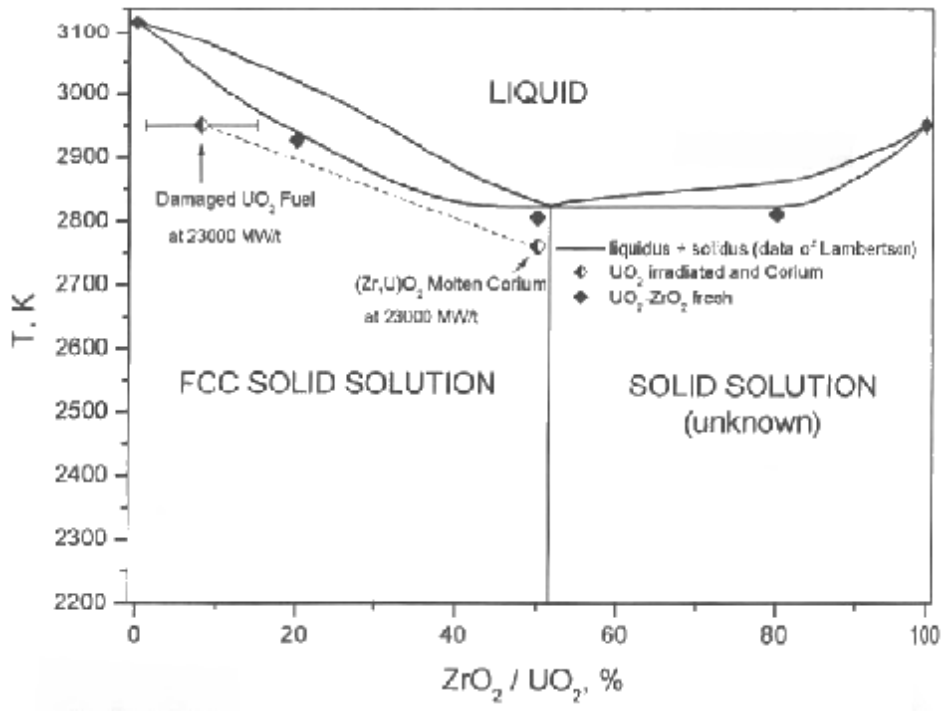

Figure 4.10 Solidus temperature of different species in PHEBUS FPT1 /55/.

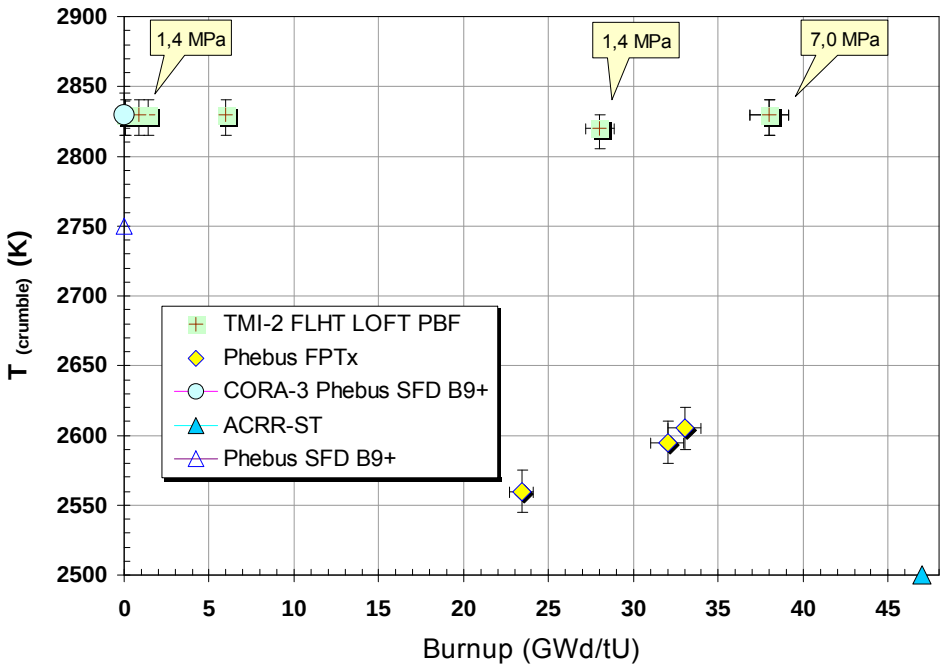

Figure 4.11 Debris/molten pool creation temperature

In the upper half of Figure 4.11, the results of PIE indicating the temperature range of the molten pool and/or debris bed are given and in the lower half the corresponding artificial crumbling temperatures. From physico-chemical considerations, melting temperatures below 2700 K require larger amount of metallic species (Fe,Cr) than found in the samples (< 3%).

Taking into account environmental boundary conditions and the various bundle configuration as given in /56/, some differences were found. The experiments in the United States were performed at higher system pressure and the mass fraction of absorber melt seems to be somewhat lower. In all cases the pressure difference across the clad vanishes after clad failure even at least after ZrO_2 layer failure, which occurred in nearly all cases below 2500 K. What remained is that spray area of absorber melts may have been increased due to the low system pressure, but it is restricted to the direct vicinity of the absorber rod and is inhibited by thin ZrO_2 layers.

Due to the high system pressure, the gap between clad and pellet is closed, preventing relocation of liquid metal. As a consequence, fuel dissolution takes place immediately after melting temperature of metallic Zry is reached, or at least, that of α-Zr(O). As a consequence, an indirect effect of the accident scenario cannot be excluded.

4.7 Further Error Corrections

Besides essential code improvements, some minor errors were found and some corrections implemented into the code. A brief overview including the coarse location as well as the status of error correction is given in Table 8.2 in the appendix.

Table 4.1 List of affected SCDAP and RELAP subroutines

Subroutine	**Topic**	**Status**
wolfht	FZK sophisticated model for CORA and QUENCH heater rods	new
expmat / fnexp	SCDAP database for expansion coefficients, required for gap closure model	new
epsmat / fneps	SCDAP database for surface emissivity coefficients, required for gap closure model	new
cora / scddat	Header file modified to handle extensions properly	mod
effht	Material properties and heater rod (with annular gap), fuel rod, and shroud (with slab gap)	mod
heatc2	2-D heat conduction optimized for CORA / QUENCH	corr
fstate	Heat and fuel rod material sequences for CORA / QUENCH	mod
rfuel / rusrmt	Input file handling updated	mod
matdat	Extended database: data storage	mod
fnk / fnro / fncp	Extended database: data base as polynomial functions	mod
fnres	SCDAP database for electric resistivities	new
rshrod / slabc	Extension of shroud model to handle prescribed conditions at outer surface	mod
pstdnb	FZK/Chen transition boiling heat transfer correlation	mod
scdad4	Determine heat-up rate and clad failure temperature	mod
state	Extension of plot variable list (extvol)	mod
iradht	Allow non-cylindrical geometry for radiation coupling (view factor)	mod
coxwth	Extension to standardized oxidation correlations	mod
coxthk	Extension to standardized oxidation correlations	mod

Remarks:
new: Subroutine is new in S/R5
mod: modified/updated to increase capability
corr: error correction (i.e. wrong data dimensions)

5 CODE ASSESSMENT

Code assessment can be done by code to data or code-to-code comparison /57/. Code to date comparison also requires the knowledge of the reliability of the experimental data, used to validate the code calculations. For CORA, this work has been finished except for the reflood phase. Here the enormous measured hydrogen production rate as well as the total amount of released hydrogen has to be checked more carefully. Since the facility has been dismantled, only the existing data as well as code calculations can be used to investigate this phase.

Another difficulty arises, because collecting and publishing of experimental data is often only focused on special questions and therefore only based on a selection of the whole amount of data. For code validation, however, the whole bandwidth of time- and space-resolved data to global behaviour, the interplay of different processes are of interest, as well as phenomena that can only be observed in integral tests and not in separate effects tests such as long distance material movements. Furthermore, the experimental findings, e.g. about material composition, may be known in much depth, but only at a few local positions. In such a case, it is impossible to decide whether the experimental findings are representative for the given conditions, because the material composition may vary locally in the test. Therefore, they cannot be used reliably to assess the more global data of the codes.

To support code validation, two tools to analyze experimental data of integral tests were developed at FZK /3/, /15/. They allow to localize effects that can only be detected indirectly e.g. by gas analyses or inner rod pressure measurement. The first one is the melt relocation scheme (MRS) as discussed for CORA-7 (Figure 5.1), the second one the test sequence diagram (TSD), which is given in Figure 5.2 for CORA-13 (ISP-31) and for PHEBUS FPT1. Apart from this, some examples of our code assessment work are presented in the following for the three integral test facilities, considered in this report.

5.1 CORA

5.1.1 CORA-7

A detailed description of the post-test bundle state is found in /18/. In the following, only a short description of those events is given that are necessary to demonstrate the MRS. The first core degradation event is the rupture of the fuel rod claddings due to over-pressurization between 4038 s and 4100 s. In this time interval, the videos, taken during the test, indicated the first material relocation phenomena in the upper half of the bundle. In the lower half, below the central Inconel grid spacer no relocation phenomena were observed. This finding was supported by the post-test inspection where no

fuel rod and control rod damage was found below 0.4 m. This finding is well documented by the videoscope films (Figure 5.1 indicates that below 0.6 m only droplet type relocation could be observed. Droplets are formed by rivulet relocation of low viscous material and can be found always below the relocation front. As can be seen in Figure 5.1, massive melt relocation only occurs between 0.6 m and 0.8 m. The subsequent melt relocation into the lower half was stopped by power shutdown at 4180 s. In sum, the MRS gives the possibility to distinguish between melt of absorber material and of fuel rods.

The droplet mass is rather small so that the thermal energy transported can be neglected henceforth, leading to a rather cold and intact lower half of the test section. Single droplets after 4200 s indicate that the oxidation process is still ongoing since the CORA test facility can store large amounts of steam.

Due to the early test termination and hence relatively low degree of destruction, the local and global influence of the five control rods should be observable. For modeling purposes, the thickness of traces of absorber/steel/zirconium melt relocation on the oxidized cladding surface is important, because it reduces the mass of relocated absorber melt at its final position. Furthermore, the transport mechanisms from absorber alloy into the degraded fuel rods should be investigated.

5.1.2 CORA-13

CORA-13, (ISP-31) is a good example for a well documented test /13/, /19/, /21/, that shows all significant SFD phenomena up to the high temperature quench of a partially degraded fuel rod bundle. Starting with CORA-2, test sequence diagrams as shown in Figure 5.2 were established to identify the temporal and local conditions in the bundle during the test. In the CORA program, optical videoscopes allowed on-line visual inspection of the axial and, to a minor extent, lateral bundle degradation at several elevations. In CORA-13, the shroud was closed except for three small observation windows so that the fluid conditions were rather properly defined and facilitated calculations. The test objectives comprise bundle heat-up, oxidation, degradation with blockage formation, and test termination by fast reflood at high temperatures.

As most other CORA tests, CORA-13 consisted of four phases: up to 3000 s the pre-heat phase, used to precondition the facility, the initial heat-up phase (up to ~ 4000 s) followed by the transient escalation phase, which ends at 4800 s with the shut down of electrical power, and the quench phase, which terminated the experiment. In the test sequence diagram (TSD, Figure 5.2) the latter three phases are represented. It is divided into three sections, please note that the time axis in Figure 5.2 is magnified for the reflood phase.

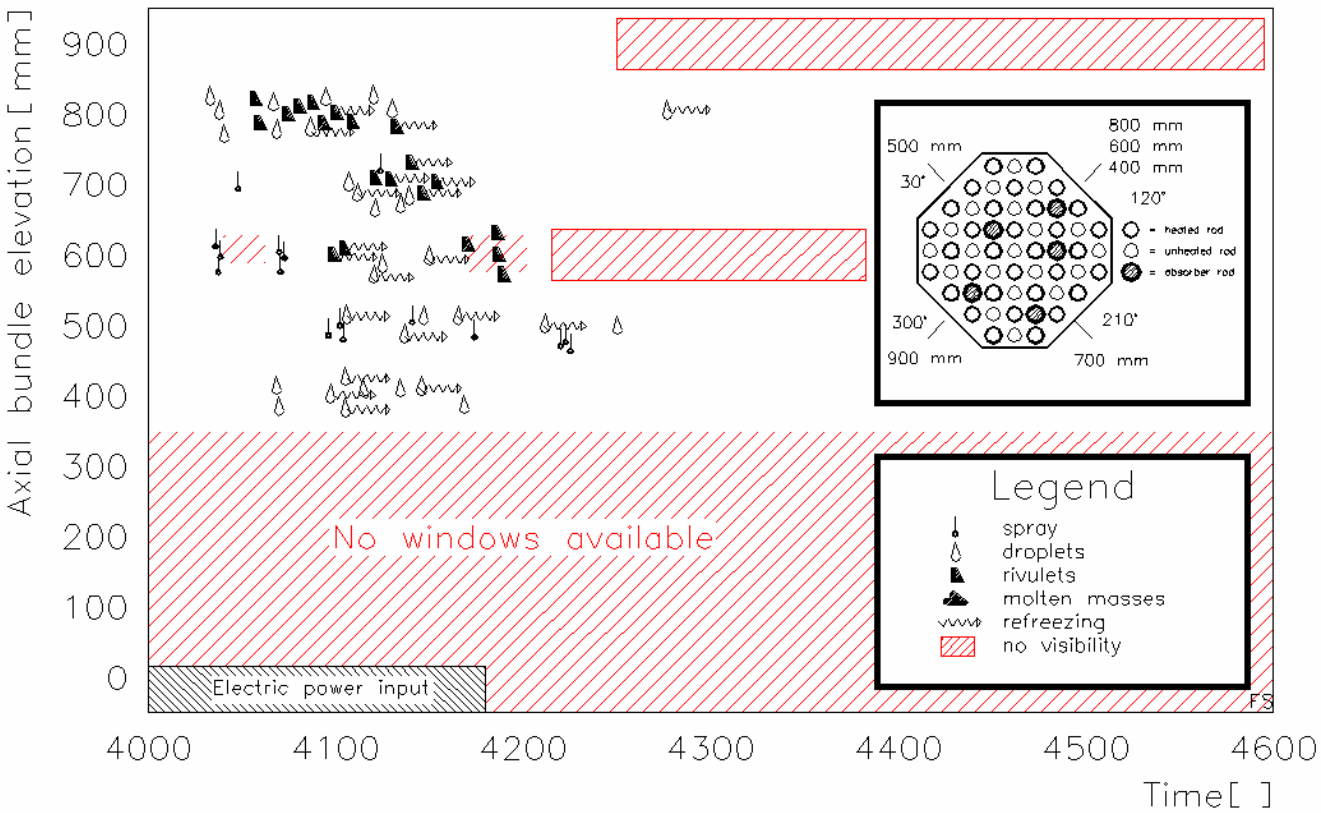

Figure 5.1 Melt relocation depicted from video information /44/ in the upper half of the CORA-7 bundle. In the lower half, the Zircaloy shroud closed the observation windows.

- The upper section comprises the isotherms, indicating the times at which the given temperature is reached at a given elevation. These times are derived from reliable thermocouple readings.
  Also global findings from off-gas monitoring can be added, taking into account the necessary temperature level. In the CORA tests, the outcome of the videoscope analyses were added too, together with the sound diagnostics of microphone mounted at the water filled quench cylinder. So each melt droplet or rivulet could be detected by the sound of the evaporating water.
- In the center section, power and inlet mass flow rates are given together with the measurements of the mass spectrometer in the off-gas system. The experimental data are supported by analytical test analyses to define properly the fluid conditions at the bundle entrance.
- In the lower section, some explanations indicate significant events, changing the bundle degradation.
- Axial profiles may be added right of the existing diagrams e.g. to characterize the final bundle status.

Main advantage of the TSD compared to axial temperature profiles is in the combination of all available data, allowing to understand the status the bundle at a glance for any time during the test. Also the dynamics become more visible, e.g. rapid heat up

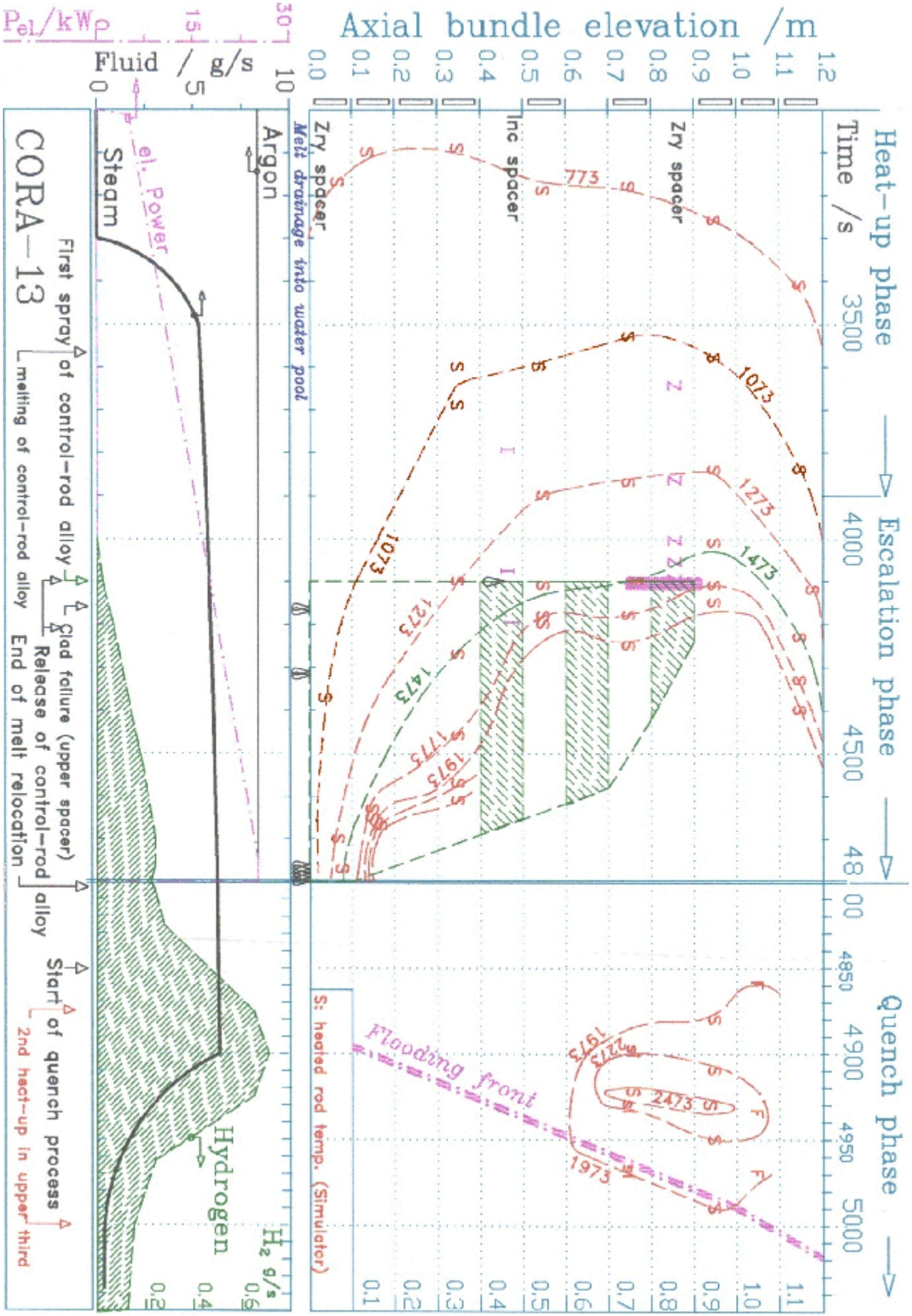

Figure 5.2 Test sequence diagram of CORA-13 (ISP-31)

due to melt relocations as well as axial temperature gradients, visualized by a high isotherm density. In the following the TSD is used to explain observation in experiment CORA-13, starting at 3000 s.

Validation work is finished with FPT1 due to limited man power and the ASTEC validation within SARNET. On can derive from the 1073 K isotherm, which indicates the solidus temperature of the Ag-In-Cd alloy, that the control rod is liquid above 0.1 m at control rod failure indicated at ~ 4100 s. On the basis of the isotherms, the failure location can be located between 0.8 and 0.9 m, allowing to specify the upper limit for released absorber mass to 0.1 – 0.25 kg for both control rods (10-20 % of whole inventory). Parts of the melt relocated down to the water surface in the quench tank, as indicated by the droplets in “Melt drainage into water pool” between the upper and the centre section in Figure 5.2. This phase lasts ~ 150 s, followed by a slower melt relocation up to 4800 s.

This phase ended with massive drainage of melt into the water pool at ~ 4760 s, just before electrical power was shut down. The maximum fuel rod temperatures were ~ 2130 K in the escalation phase and ~ 2570 K in the quench phase. The faster heat-up detected at 0.5 m elevation at 4100 s is explained by some accumulated mass on the remnants of the middle grid spacer, which was already partially liquefied.

Additional information from detailed post-test analyses /19/ indicated that the molten control-rod material reacted with the Zircaloy claddings and tube guides. As can be depicted from Figure 5.2, the time window for interaction is sufficiently long, more than 600 s. After its release, the metallic melt, composed of Ag-In-Fe-Cr, was capable to dissolve UO_2 pellets partly. Only thick ZrO_2 layers on the external cladding surface prevented substantial amount of metallic Zircaloy melt from running off so that it remained in contact with UO_2 on one side and ZrO_2 on the other side and dissolved both materials chemically. Remnants of film flow type melt relocation along the rods were not found during post-test inspections, maybe caused by the high temperatures of the increased bundle damage.

On account of the different solidification temperatures of the melts, stratification developed such that the metallic lumps of melt rich, in absorber material, are super-imposed by metallic and/or ceramic (Zr, U, O) blockages, formed later.

Water quenching of the hot degraded fuel rod bundle caused additional fragmentation, especially of metal rich blockages in the lower half of the bundle, which were still at temperatures above 2273 K.

The detected temperature increase started at an elevation of 0.6 m and extended into in the upper electrode zone; it originated from the strong oxidation of the remaining metallic Zircaloy in the shroud as well as in the fuel rods. The axial position of the water

level during the quench phase is unknown, but we can derive from experimental data that the axial movement of the peak temperature isotherm (2473 K) is much faster than the rise velocity of the quench water cylinder as indicated in Figure 5.2. Now, the velocity of the quench cylinder is an upper limit for the rise velocity of the water level, because the water inventory is reduced due tu evaporation losses. Furthermore, at the start of the quench phase, the water level was ~ 0.02 m below the top of the quench cylinder due to evaporation before the quench phase. In this way, we can derive that the axial movement of the peak temperature isotherm is also much faster than the rise of the water level.

Hydrogen production amounts to 210 g with 52 % of it produced in the transient phase (~1500 s above 1000 K) and 48% in the quench phase (~150 s). During the transient phase, the H_2 production rate rises from 0 to 220 mg/s; it reached 700 mg/s in the quenching phase /13/.

5.2 QUENCH

Bundle tests have been supported since the very start of the QUENCH program to support design and construction of the facility. Much detailed information is contained in the reports of our institution about the various tests. Some examples of our work are given below.

As a side effect, analysis of the experiments with the various facility models revealed that the simulation of the off-gas pipe is important to meet the pressure data more precisely as well as to avoid artificial (numerical) pressure spikes in the test section. This holds especially for water reflood scenarios.

5.2.1 Axial Discretisation

For QUENCH-07, post-test calculations have been performed for 16 and 32 axial nodes /58/. Figure 5.3 shows axial profiles of selected variables at the time when the corner rod Figure 3.3 was withdrawn, i.e. after heat-up of the bundle to about 1700 K and pre-oxidation for nearly 900 s. For the fine axial discretiszation (solid lines), an escalation is calculated just to start, whereas for the coarse discretisation (dashed lines) the escalation is calculated to start about 120 s earlier. For this reason, the peak value of hydrogen production rate is calculated to be one order of magnitude larger for the coarse axial discretisation. Consequently, the calculated oxide layer thickness are very different. They agree quite well for the fine axial discretisation and in this way demonstrate its necessity. As can also be seen from Figure 5.3, the fine axial discretisation generally improves the agreement in the upper electrode zone. The latter effect was also seen for QUENCH-09 /59/.

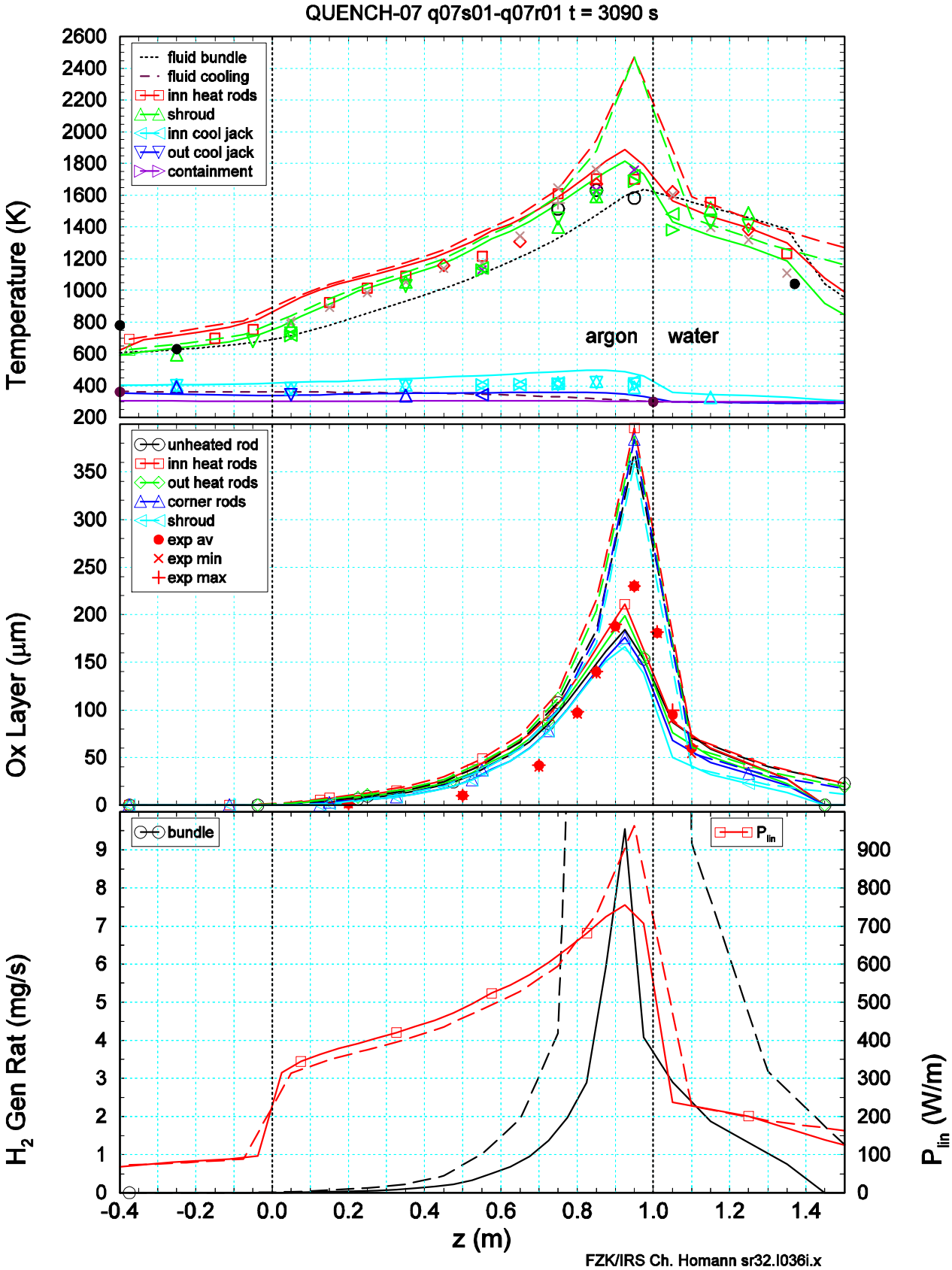

Figure 5.3 Axial profiles of calculated and measured variables for QUENCH-07

The figure shows from top to bottom measured and calculated axial profiles of temperatures, oxide layer thickness, hydrogen production rate, and linear electrical rod power at the time, when a corner rod was withdrawn.

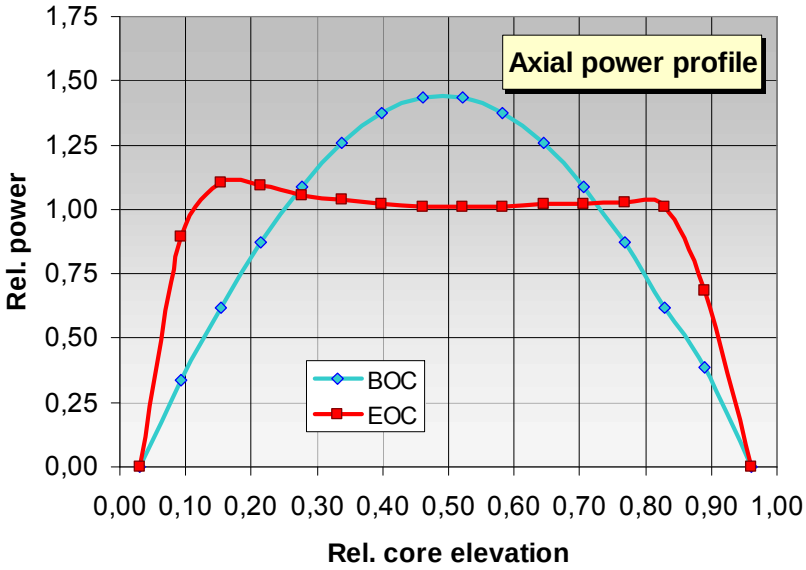

Figure 5.4 Axial power profile in a nuclear power plant (BOC/EOC: begin/end of cycle)

5.2.2 Electrical Heater Rod Model

Figure 5.3 demonstrates also the necessity for a detailed electrical heater model. With increasing temperature, the specific resistance and hence the local release of electrical power increase. At the upper end of the heated zone, the linear rod power is about two times the value of the lower end.

This effect leads to a steeper axial temperature profile than a flat profile like in a nuclear power plant as shown in Figure 5.4. There, the axial power profile, is only dominated by the burn-up rate and not influenced by temperature.

Consequently, the maximum temperature reacts rather sensitively, when the electrical power is changed. The effect is even enhanced, when heat release due to oxidation plays a role. Therefore, much care is necessary to model the test conditions in calculations: e.g., an overestimation of the maximum temperature gives an overestimation of local power release at that position which, in turn, increases temperature further. Since the total power release is prescribed, power input in the other parts of the bundle is too small, so that the whole axial temperature profile is changed.

The axial variation of the linear rod power is even larger in QUENCH-11. In contrast to all previous experiments, the bundle was filled with water up to about the upper end of the heated zone at the start of the test and slowly boiled off. When the collapsed water level was measured to be as low as 195 mm below the heated length, about 1 g/s water was injected to counterbalance evaporation. Figure 5.5 shows time dependent results. Rod power increases with electrical power input. As long as water exists at a given axial elevation, temperature is at saturation value and linear rod power is rather low. Values

increase sensibly after evaporation. Figure 5.6 shows axial profiles for temperature and linear rod power. In early times of the test, profiles are rather flat, because temperature is at or near saturation value in the whole bundle. They rise drastically after evaporation, and the ratio of linear rod power at the upper and the lower end of the heated zone is about 5. This is by far more than in normal QUENCH tests as QUENCH-07, because in QUENCH-11 temperature in the lower electrode region is kept to saturation value. Therefore, temperature at the lower end of the heated zone and the temperature increase in the heated zone are higher.

During the participation in the SARNET Code Benchmark (SCB) on QUENCH-11 /60/, the computational work was dominated by model facility and test effects. Input changes were mainly within experimental accuracy and certainty. This does not only demonstrate the sensitivity of the results, when system parameters are changed, it is also an indication that the code improvements, discussed in this report, are adequate and, at the time being, do not need further work.

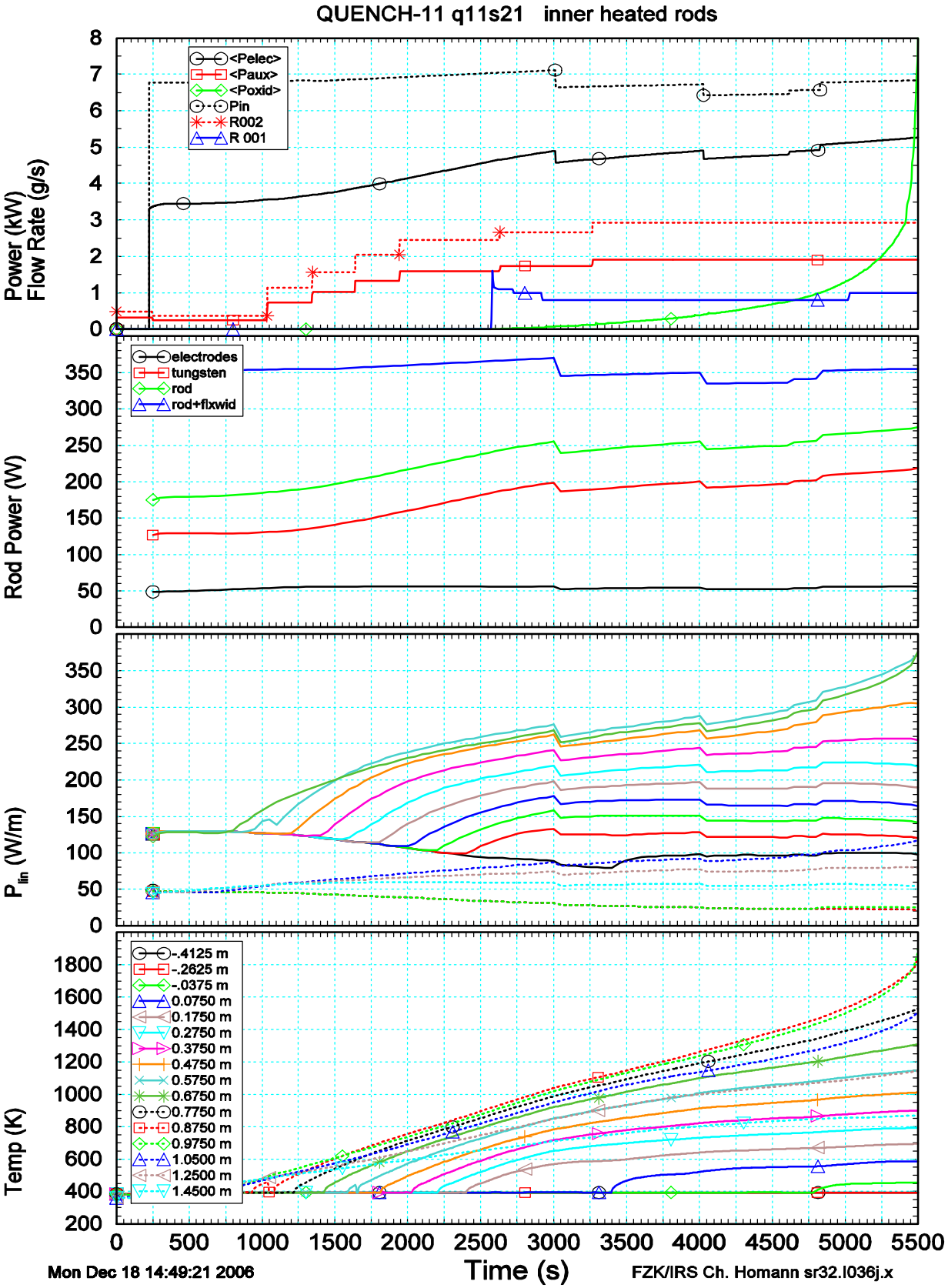

Figure 5.5 Selected variables as a function of time for QUENCH-11

The figure shows from top to bottom electrical bundle and auxiliary power as well as chemical power, released into the bundle, measured electrical bundle and auxiliary power and flow rate R001 (top), electrical power released into any of the inner heated rods and its various parts, and respective linear rod power and clad surface temperature at various axial elevations

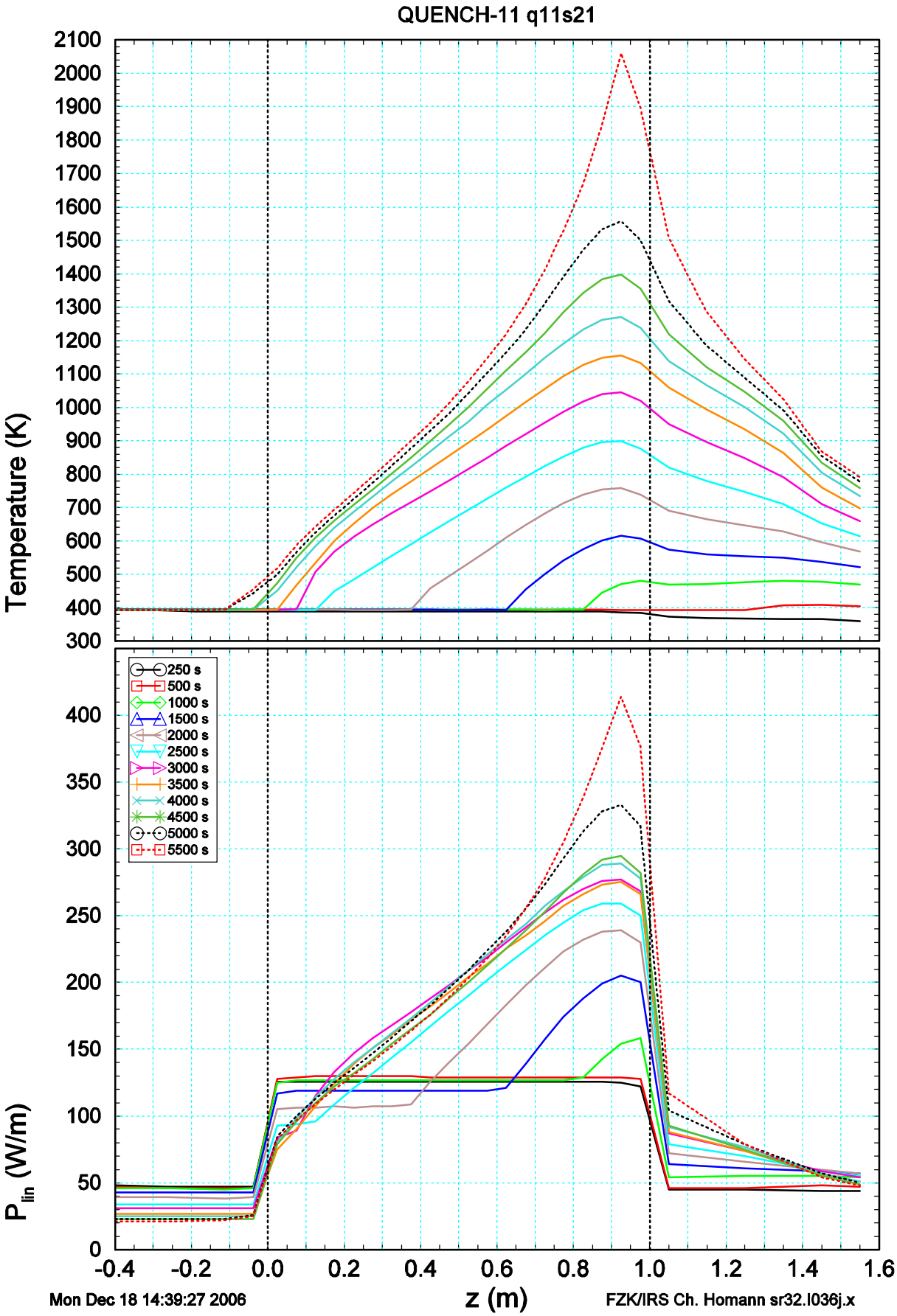

Figure 5.6 Axial profiles for clad surface temperatures and linear rod powers at different times for QUENCH-11

5.3 PHEBUS FPT Experiments

Another source of experimental data for code validation are the in-pile tests in the French PHEBUS FP facility at Cadarache. As a contribution to BIC, post test analyses were performed with S/R5 and ICARE2. The results are documented in /8/ and /9/; here only some aspects related to CORA and QUENCH are mentioned. Meanwhile, validation work is finished with FPT1 due to limited man power.

5.3.1 PHEBUS FPT0

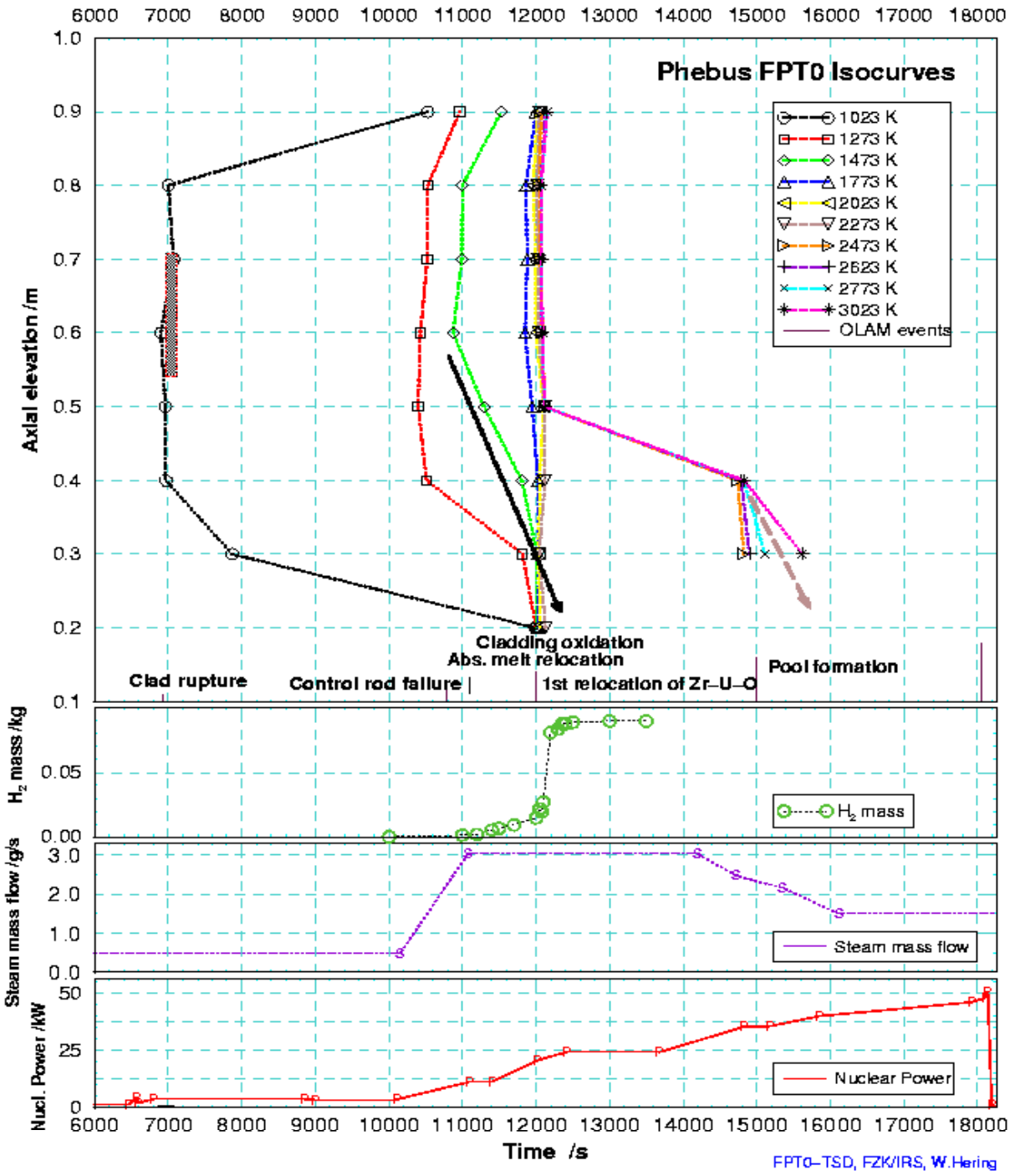

Figure 5.7 Test sequence diagram of PHEBUS FPT0 including OLAM signals

Comparing the test squence diagram of ISP-31 (CORA-13) in Figure 5.2 with one of PHEBUS FPT0 in Figure 5.7, the rather smooth axial temperature variation in the latter becomes obvious. Strong changes are only seen after massive material relocation at high temperatures. Therefore, it is very difficult to identify the axial position of maximum temperature in the bundle, which is important for localisation of clad failure position. The steep increase in the hydrogen release just after 12000 s is caused by a widespread onset of escalation of clad oxidation. This is different to CORA and QUENCH experiments.

5.3.2 FPT1

The test was also used for the OECD International Standard Problem No. 46, ISP-46. ISP-46 consisted of four sections: code degradation, primary circuit, containment, and fission products. For the core degradation phase, some scoping calculations were performed, focused on the standardized oxidation correlations (Figure 5.8) and the improved oxidation correlations (Figure 5.9). The comparison of the temperatures between 400 mm and 700 mm (Figure 5.8) indicates that the peaks are met quite well for both oxidation correlations, but the code calculates an earlier escalation than measured in the experiment.

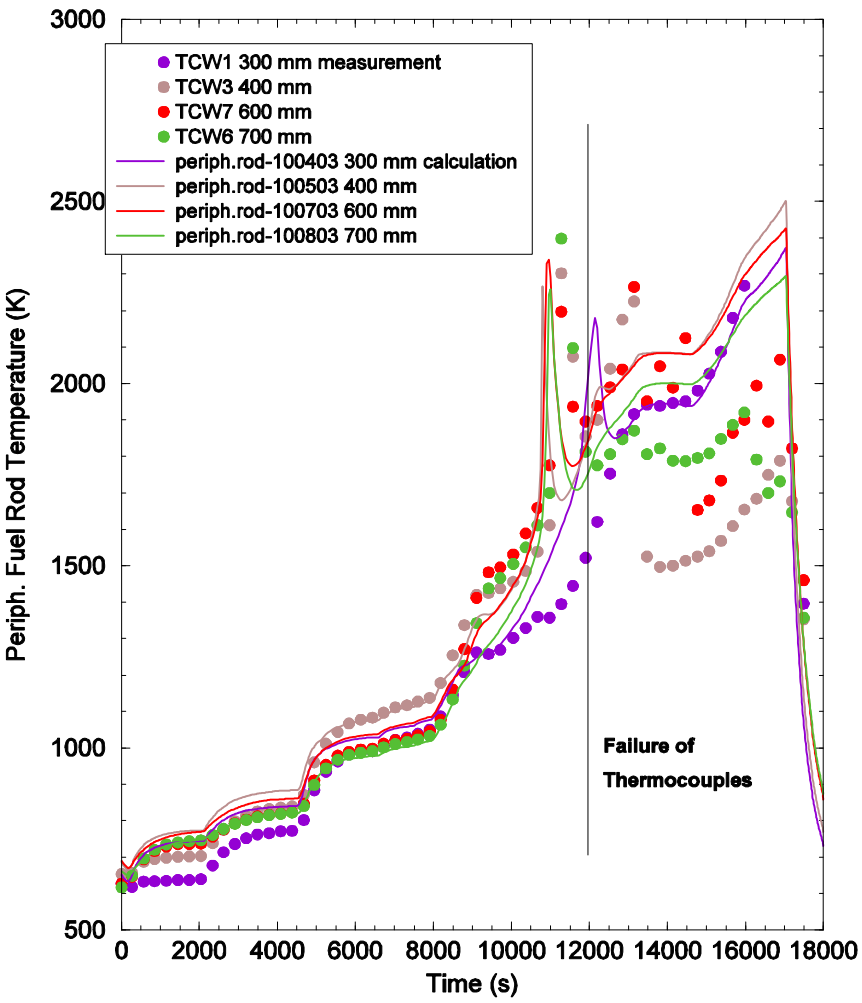

Figure 5.8 Comparison of experimental (symbols) and analytical (lines) results produced by S/R5 for PHEBUS FPT1 (ISP-46)

As a consequence of the improved oxidation correlations, the hydrogen production rate is increased starting ~ 9000 s (Figure 5.9 top), increasing the maximum bundle temperatures faster than observed in the experiment. Nevertheless the total amount of hydrogen release is not influenced significantly. Due to the earlier temperature escalation, the nuclear heat level is

lower so that the maximum temperatures are ~ 150 K lower as in the reference case. The steeper temperature rise is associated with the steeper transition between low temperature and high temperature oxidation correlations. After the oxidation phase, the temperatures level out, and the bundle conditions are dominated by the nuclear power release.

After 16300 s, the influence of the new transition model (section 4.6) for late phase degradation is visible (Figure 5.9 bottom). In a first approach it is assumed that the un-attacked fuel pellets may disintegrate, if a defined (presently user parameter) burn-up level is exceeded and a minimum clad ballooning was calculated in that fuel rod section.

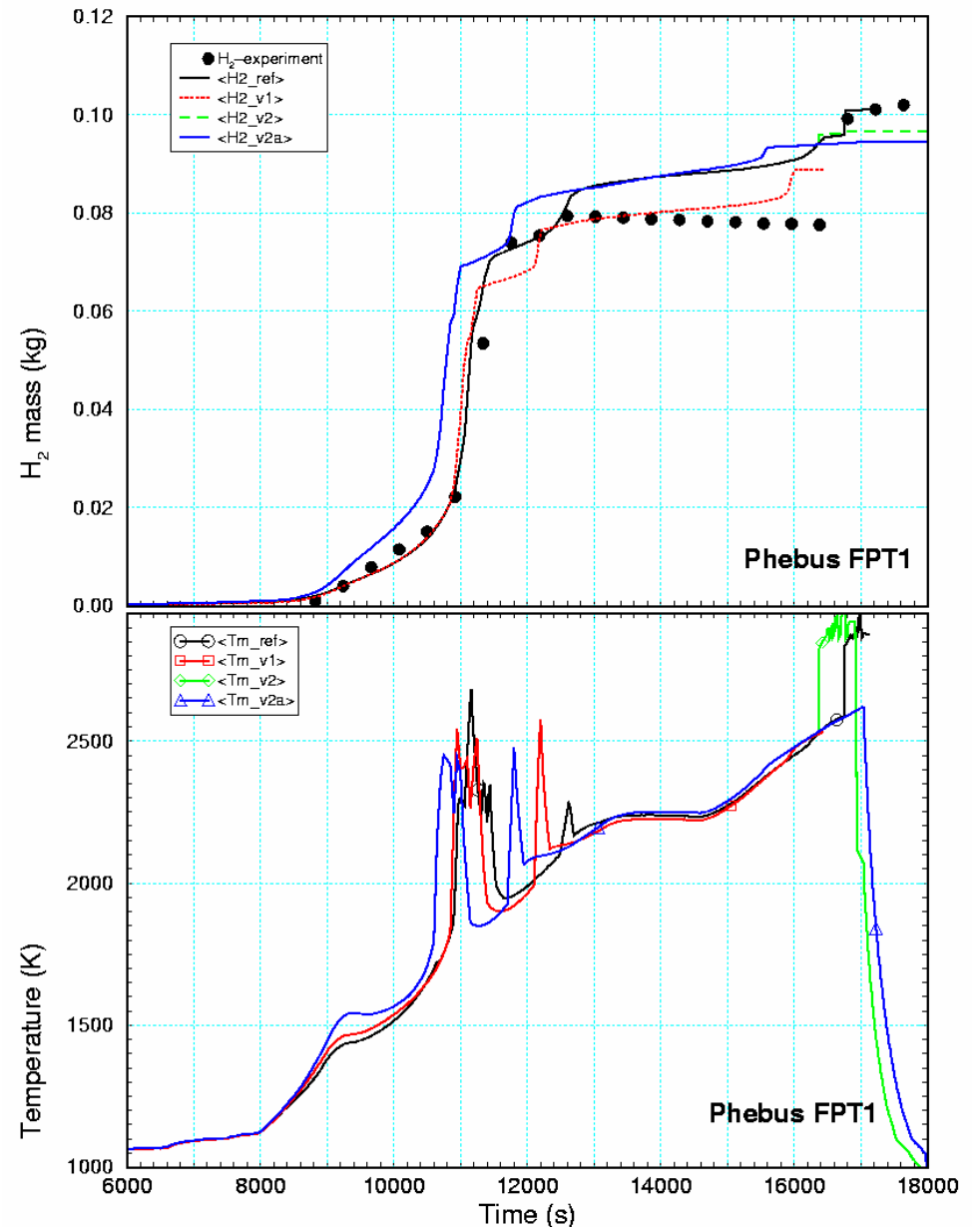

Figure 5.9 Parameter studies for ISP-46 (PHEBUS FPT1) core degradation phase to test new oxidation correlation and late phase transition

6 SUMMARY AND CONCLUSIONS

Application of severe accident codes like SCDAP/RELAP5 relies on verification against in-pile and out-of pile tests. Such work shows that facility specific details have to be modelled. For this purpose, a number of extensions has been made in SCDAP/-RELAP5 to model the CORA, QUENCH, and PHEBUS FP test facilities in a better way than before. They refer to the early core melt phase and lead to a reasonable improvement and hence more reliable results, as can be shown by comparison with the former status.

An important issue is the correct modelling of electrically heater rods, because the axial profile of power release depends sensitively on this item. The feedback of local temperature on electrical power release is a special feature of all electrically heated bundles. A detailed analysis yielded a number of tasks to be solved. Another main topic refers to radiative heat transfer in gaps as they do not only exist in the rods between intact pellets and clad but also in enclosures of rod bundles in experimental facilities. Determination of radial heat transport out of the bundle influences the axial temperature profile in the bundle with all its consequences, not only for electrically heated bundles.

The simulation of the radiation heat transfer in gaps filled with non absorbing fluid, originally developed for PHEBUS applications, is very useful to calculate the radial heat losses in the upper electrode zone of the QUENCH facility, where the fiber insulation is absent. Here, no artificial material properties had to be used to calculate the effective heat flux. Since the gap is rather large (~ 19 mm in the CORA facility and 37 mm in the QUENCH facility) the gap-closure model is not applicable here. The extended code version was used successfully for pre-test and post-test analyses of QUENCH experiments.

Nevertheless, some differences remain which cannot be eliminated by modeling since they influence the RELAP5 code structure, which is essentially one-dimensional. At the moment, the turbulent fluid inlet section, which extends up to 0.3 m in CORA bundle cannot be simulated quite well since no cross-flow heat transfer correlation is available in RELAP5. For the code validation, this only influences the axial electric power profile, shifting the peak virtually to the bottom and thus leading to higher fluid temperatures.

Experiences gained during S/R5 extension and optimization were transferred into the ASTEC validation as part of the **S**evere **A**ccident **R**esearch **Net**work in the 6th Framework program allowing both code-to-data and code-to-code validation.

7 LITERATURE

/1/ M. Allison et al.: SCDAP/RELAP5 mod3.1 Code Manual, Vol. I - IV. NUREG/CR-6150, EGG-2720, Oct. 1993.

/2/ M. Allison et al.: SCDAP/RELAP5 mod3.2 Code Manual, Vol. I - V. NUREG/CR-6150, INEL-96/0422, revision 1, Oct. 1997.

/3/ W. Hering: Modellierung des Experimentes CORA und Interpretation von Versuchsergebnissen mit dem erweiterten Kernschmelzcode SCDAP/MOD1, Diss. Stgt., IKE 2-100, 1993.

/4/ S. Hagen, H. Malauschek, S.O. Peck, K.P. Wallenfels: Temperature Escalation in PWR Fuel Rod Simulator Bundles due to the Zircaloy/steam Reaction Test ESBU-1, Test Results Report, KfK-3508, 1983

/5/ P. Hofmann et al.: Essential Experimental Results of the CORA Test Program on Severe Core Damage Phenomena, Kerntechnik 59(4-5), 1994, pp 197 - 202.

/6/ P. Hofmann, V. Noack, D. Piel, L. Schmidt: Status of the Planned Quench Experiments with Fuel Rod Simulators, First International QUENCH Workshop, Karlsruhe, Oct. 4 - 6, 1995.

/7/ Van der Hardt, A. V. Jones, C. Lecomte: The PHEBUS FP Severe Accident Experimental Program, Nuc. Safety 35(2), 1994, pp. 187 - 205.

/8/ S.O. Smit, W. Hering, W. Sengpiel: Analysis of Fuel Bundle Behaviour in PHEBUS FPT0 with SCDAP/RELAP5, FZKA-5882, 1998.

/9/ S.O. Smit, W. Hering, W. Sengpiel: Investigation of the Phebus FPT0 bundle degradation with SCDAP/RELAP5 Wissenschaftliche Berichte, FZKA-6083 (April 98).

/10/ S. Hagen, H. Kapulla, H. Malauschek, K.P. Wallenfels, B. Buescher: Temperature escalation in PWR fuel rod simulator bundles due to the zircaloy/steam reaction: post test investigations of bundle test ESBU-2A. KfK-3789 (November 86).

/11/ S. Hagen, Interactions in Zircaloy/UO2 fuel rod bundles with Inconel spacers at temperatures above 1200 °C : (post-test results of severe fuel damage experiments CORA-2 and CORA-3), KfK-4378, 1990.

/12/ K. Minato, W. Hering, S. Hagen: Zircaloy Oxidation and Cladding Deformation in PWR-specific CORA Experiments, KfK 4827, 1991.

/13/ W. Hering, K. Minato, F. Nagase: Behaviour of the Zircaloy Cladding in PWR-Specific CORA Experiments, Nuclear Technology, Vol. 102, pp. 100-115, April 1993.

/14/ S. Hagen, P. Hofmann, V. Noack, L. Sepold, G. Schanz, G. Schumacher: Comparison of the Quench Experiments CORA-12, CORA-13, CORA-17, FZKA report 5679, August 1996.

/15/ W. Hering, P. Hofmann: Material Interactions during Severe LWR Accidents; Summary of Separate-effects Results, KfK 5125, February 1994.

/16/ S. Hagen, P. Hofmann, V. Noack, G. Schanz, G. Schumacher, L. Sepold: Result of SFD Experiment CORA-12, KfK report 5054, Feb.1993.

/17/ J. Burbach: Ergebnisse von REM/EDX-Mikrobereichsanalysen des Siedewasserreaktor – Buendelabschmelzexperiments CORA-16, KfK-5282, 1994.

/18/ Hagen, S., Hofmann, P., Noack, V., Sepold, L., Schanz, G., Schumacher, G.: Large bundle PWR test CORA-7 test results. Wissenschaftliche Berichte, FZKA-6030 (April 98), http://bibliothek.fzk.de/zb/abstracts/6030.htm

/19/ S. Hagen, P. Hofmann, V. Noack, G. Schanz, G. Schumacher, L. Sepold: Result of SFD Experiment CORA-13 (OECD International Standard Problem 31), KfK-5054, Feb. 1993.

/20/ Firnhaber, M., Trambauer, K., Hagen, S., Hofmann, P.: OECD/NEA-CSNI international standard problem No. 31. CORA-13 experiment on severe fuel damage. GRS-106 (Juli 93) / KfK5287 (Juli 93), (http://www.nea.fr/html/nsd/docs/1993/csni-r1993-17.pdf)

/21/ W. Hering, P. Hofmann: Material Interactions during Early-Phase Core Melt Progression, Festschrift Energie-Technik-Umwelt, Prof. Dr. Unger, RUB Bochum, May 1994.

/22/ R. Hüper: Sicherheitorientierte LWR-Forschung, Jahresbericht 1988, FZKA-4550 (Juli 1989).

/23/ R. Hüper: Sicherheitorientierte LWR-Forschung, Jahresbericht 1993, FZKA-5327 (Juni 1994).

/24/ K. Hain: Out-of-pile Experimente zur Untersuchung schwerer Kernschäden, KfK-4274, (Juni 1987).

/25/ Hagen, S., Hofmann, P., Noack, V., Sepold, L., Schanz, G., Schumacher, G.: Cold lower end test CORA-10: test results. Wissenschaftliche Berichte, FZKA-5572 (November 97) http://bibliothek.fzk.de/zb/abstracts/5572.htm.

/26/ Hagen, S., Hofmann, P., Noack, V., Sepold, L., Schanz, G., Schumacher, G.: Large bundle BWR test CORA-18: test results. Wissenschaftliche Berichte, FZKA-6031 (April 98) http://bibliothek.fzk.de/zb/abstracts/6031.htm

/27/ Hagen, S., Hofmann, P., Noack, V., Sepold, L., Schanz, G., Schumacher, G.: Pre-oxidized BWR test CORA-28: test results. Wissenschaftliche Berichte, FZKA-5571 (Juni 97) http://bibliothek.fzk.de/zb/abstracts/5571.htm

/28/ Hagen, S., Hofmann, P., Noack, V., Sepold, L., Schanz, G., Schumacher, G.: Pre-oxidized PWR test CORA-29: test results. Wissenschaftliche Berichte, FZKA-5928 (August 97) http://bibliothek.fzk.de/zb/abstracts/5928.htm

/29/ Hagen, S., Hofmann, P., Noack, V., Sepold, L., Schanz, G., Schumacher, G.: Slow heat-up PWR test CORA-30: test results. Wissenschaftliche Berichte, FZKA-5929 (Oktober 97) http://bibliothek.fzk.de/zb/abstracts/5929.htm

/30/ Hagen, S., Hofmann, P., Noack, V., Schanz, G., Schumacher, G., Sepold, L.: BWR slow heatup test CORA-31: test results. KfK-5383 (Dezember 94).

/31/ Hagen, S., Hofmann, P., Noack, V., Schanz, G., Schumacher, G., Sepold, L.: Dry core BWR test CORA-33: test results. KfK-5261 (Dezember 94).

/32/ Hagen, S., Hofmann, P., Noack, V., Sepold, L., Schanz, G., Schumacher, G.: Impact of absorber rod material on bundle degradation seen in CORA experiments. Wissenschaftliche Berichte, FZKA-5680 (Dezember 96) http://bibliothek.fzk.de/zb/abstracts/5680.htm

/33/ Ott, L., Hagen, S.: Interpretation of the results of the CORA-33 dry boiling water reactor test. Nuclear Engineering and Design, 167(1997) p. 287-306.

/34/ Hagen, S., Hofmann, P., Noack, V., Schanz, G., Schumacher, G., Sepold, L.: Behaviour of a VVER fuel element tested under severe accident conditions in the CORA facility: Test results of experiment CORA-W1. KfK-5212 (Januar 94).

/35/ Hagen, S., Hofmann, P., Noack, V., Schanz, G., Schumacher, G., Sepold, L.: Behaviour of a VVER-1000 fuel element with boron carbide/steel absorber tested under severe fuel damage conditions in the CORA facility: Results of experiment CORA-W2. KfK-5363 (Oktober 94).

/36/ Firnhaber, M.: CORA-W2 experiment on severe fuel damage for a Russian type PWR: comparison report ; OECD/NEA/CSNI international standard problem ISP 36, FZKA-5711, OECD/NEA/CSNI/R(95)20, 1996.

/37/ V. Noack, S. Hagen, P. Hofmann, G. Schanz, L. Sepold: Material distribution in Light Water Reactor-type Bundles tested under Severe Accident Conditions, Nuclear Technology, Vol.117, Feb 1997, pp. 158-170.

/38/ The SCDAP/RELAP5 Development Team: SCDAP/RELAP5/MOD 3.2 Code Manual, NUREG/CR-6150, INEL-96/0422, Idaho Fall, Idaho, USA, 1997.

/39/ Ch. Homann, W. Hering, W. Sengpiel, D. Struwe, C. Messainguiral: Analysis of LWR Fuel Rod Bundle Experiments with SCDAP/RELAP5, 1996 RELAP5 International Users Seminar Dallas, TX, USA, March, 17-21 1996.

/40/ Hering, W., Homann, Ch., Sengpiel, W., Struwe, D.: Severe core degradation analysis for an advanced reactor concept using SCDAP/RELAP5. Proc. of the Internat. Topical Meeting on Advanced Reactors Safety, Orlando, Fla., June 1-5, 1997 Vol. 2, S.945-52 La Grange Park, Ill. : American Nuclear Soc., 1997.

/41/ T.J. Haste, C.J. Fry, R.P. Hiles, P. Hofmann, V. Noack, W. Hering, Ch. Homann, Th. Linnemann, M.K. Koch, H. Unger: Design Studies for FZK Degraded Core Bundle Quench Experiments, AEAT-1360, May 1997.

/42/ Ch. Homann, W. Hering, Chr. Messainguiral: Analytical activities for test preparation. 3rd International Quench Workshop, Karlsruhe, December 2-4, 1997.

/43/ P. Hofmann, Ch. Homann, W. Leiling, A. Miassoedov, D. Piel, L. Schmidt, L. Sepold, M. Steinbrück: Results of the QUENCH Commissioning Tests, FZKA Report 6099, August 1998.

/44/ F. Seibert, private communications, 1993.

/45/ E. Elias, V. Sanchez, W. Hering: Development and validation of a transition boiling model for RELAP5/MOD3 reflood simulations, NEDEA 183 177-332 (1998).

/46/ P. Hofmann, W. Hering, C. Homann, W. Leiling, A. Miassoedov, D. Piel, L. Schmidt, L. Sepold, M. Steinbrück, QUENCH-01 Experimental and Calculational Results. FZKA 6100.

/47/ P. Hofmann, C. Homann, W. Leiling, A. Miassoedov, D. Piel, L. Schmidt, L. Sepold, A. Miassoedov: Experimental and Calculational Results of the Experiments QUENCH-02 and QUENCH-03. FZKA 6295.

/48/ RELAP5/MOD3 Code Manual, SCIENTECH Inc., Rockville MD, NUREG/CR-5535 Vol.1-8, June 1999.

/49/ C. Frepoli, L.E. Hochreiter, J. Mahaffy, F.B. Cheung: A noding sensitivuty analyis using COBRA-TF and the effect of spacer grids during core reflood, ICONE-8711, Proceedings of ICONE-8, April 2-6, 2000, Baltimore, MD, USA.

/50/ Barin, I.: Materialdaten on ZrO_2, Thermochemical Data of Pure Substances, VCH Weinheim, 1989.

/51/ A. Miassoedov, private communication 2000.

/52/ Schanz G., Application procedures for the recommended oxidation kinetics correlations and their interpolation, private communication.

/53/ Antony, J., Brockmeier U.: Vergleich der Oxidationsmodelle in den Progammen SCDAP/RELAP5, ATHLET-CD, ICARE2, MELCOR, KESS-III, MAAP und MELPROG, RUB E-32, April 1983.

/54/ Miassoedov A.: QUENCH-07 and QUENCH-09 data reports.

/55/ Toth B.: Minutes of the 19th Meeting of the Phébus FP Bundle Interpretation Circle, Aix-en-Provence, 17. October 2002.

/56/ In-Vessel Core Degradation Code Validation Matrix. Update 1996-1999. NEA/CSNI/R(2000)21, Feb. 2001, http://www.nea.fr/html/nsd/docs/2000/csni-r2000-21.pdf

/57/ W. Hering, Ch. Homann, A. Miassoedov, M. Steinbrück: Specification of the International Standard Problem ISP-45 (QUENCH-06), Nuklear Report 3355, OECD/NEA/CSNI/R(2001)1, January 2001.

/58/ Homann, Ch., Hering, W., Birchley, J., Fernandez Benitez, J.A., Ortega Bernardo, M.: Analytical support for the B_4C control rod test QUENCH-07. Wissenschaftliche Berichte, FZKA-6822 (April 2003) SAM-COLOSS-P055

/59/ Homann, Ch., Hering, W.: Analytical support for the B_4C control rod test QUENCH-09. Wissenschaftliche Berichte, FZKA-6853 (April 2003) SAM-COLOSS-P057

/60/ Homann, Ch., Hering, W.: SARNET Benchmark on QUENCH-11 - Contributions with SCDAP/RELAP5, Internal Report NUKLEAR 3412, Nov. 2006.

/61/ Adroguer, B., Chatelard, P., van Dorsselaere, J.P., Duriez, C., Cocuaud, N., Bellenfant, L., Bottomley, D., Vrtilkova, V., Mueller, K., Hering, W., Homann, C., Krauss, W., Miassoedov, A., Steinbrück, M., Stuckert, J., Hozer, Z., Bandini, G., Birchley, J., Berlepsch, T.von, Buck, M., Benitez, J.A.F., Virtanen, E., Marguet, S., Azarian, G., Plank, H., Veshchunov, M., Zvonarev, Y., Goryachev, A.: Core loss during a severe accident (COLOSS), Nuclear Engineering and Design, 221(2003) pp. 55-76.

/62/ Schanz, G., Adroguer, B., Volckek, K.: Advanced treatment of zircaloy cladding high-temperature oxidation in severe accident code calculations. Part I Experimental database and basic modelling, Nuclear Engineering and Design, 232(2004) pp. 75-84.

8 APPENDIX

8.1 Heater Rod Model for QUENCH

Table 8.1 Heater rod material sequences for QUENCH usage

Material layers iax	imat	irad	imat	irad	imat	irad	imat	irad
1	22	.430E-02	12	.466E-02	1	.538E-02		
2	21	.430E-02	12	.466E-02	1	.538E-02		
3	21	.430E-02	12	.466E-02	1	.538E-02		
4	21	.430E-02	12	.466E-02	1	.538E-02		
5	21	.430E-02	12	.466E-02	1	.538E-02		
6	21	.430E-02	12	.466E-02	1	.538E-02		
7	4	.300E-02	12	.458E-02	9	.466E-02	1	.539E-02
8	4	.300E-02	12	.458E-02	9	.466E-02	1	.539E-02
9	4	.300E-02	12	.458E-02	9	.466E-02	1	.539E-02
10	4	.300E-02	12	.458E-02	9	.466E-02	1	.539E-02
11	4	.300E-02	12	.458E-02	9	.466E-02	1	.539E-02
12	4	.300E-02	12	.458E-02	9	.466E-02	1	.539E-02
13	4	.300E-02	12	.458E-02	9	.466E-02	1	.539E-02
14	4	.300E-02	12	.458E-02	9	.466E-02	1	.539E-02
15	4	.300E-02	12	.458E-02	9	.467E-02	1	.539E-02
16	4	.300E-02	12	.458E-02	9	.467E-02	1	.539E-02
17	4	.300E-02	12	.458E-02	9	.467E-02	1	.539E-02
18	4	.300E-02	12	.458E-02	9	.467E-02	1	.539E-02
19	4	.300E-02	12	.458E-02	9	.467E-02	1	.539E-02
20	4	.300E-02	12	.458E-02	9	.467E-02	1	.539E-02
21	4	.300E-02	12	.458E-02	9	.467E-02	1	.539E-02
22	4	.300E-02	12	.458E-02	9	.467E-02	1	.539E-02
23	4	.300E-02	12	.458E-02	9	.467E-02	1	.539E-02
24	4	.300E-02	12	.458E-02	9	.467E-02	1	.539E-02
25	4	.300E-02	12	.458E-02	9	.467E-02	1	.539E-02
26	4	.300E-02	12	.458E-02	9	.467E-02	1	.539E-02
27	21	.430E-02	12	.467E-02	1	.539E-02		
28	21	.430E-02	12	.467E-02	1	.539E-02		
29	21	.430E-02	12	.466E-02	1	.539E-02		
30	21	.430E-02	12	.466E-02	1	.539E-02		
31	21	.430E-02	12	.466E-02	1	.538E-02		
32	21	.430E-02	12	.466E-02	1	.538E-02		

Material index:

4	tungsten,	12	ZrO_2 QUENCH pellets,
21	molybdenum,	22	copper,
1	Zircaloy,	5	ZrO_2 high temperature oxide
9	Gap /Argon + radiation (FZK-improvement)		

8.2 Shroud Gap Model

S/R5 uses a fixed mesh for 2-D heat conduction calculation in all components including the shroud. Creating a moving mesh would be very difficult and time consuming, slowing down the code unacceptably /9/. Therefore, we decided to simulate the gap deformation by adjusting the thermal conductivity of the gap material in a more physical way. The actual gap heat conduction is calculated considering the actual gap width as well as the radiation and transferring the result into the original mesh.

The radiation heat transfer is calculated from the boundary temperatures of the gap and the emissivities of the adjacent surfaces. The computed heat flux is than transformed into a thermal conductivity to be added to the thermal conductivity of the gap whose gap width corresponds to the thermal expansion of the adjacent material layers.

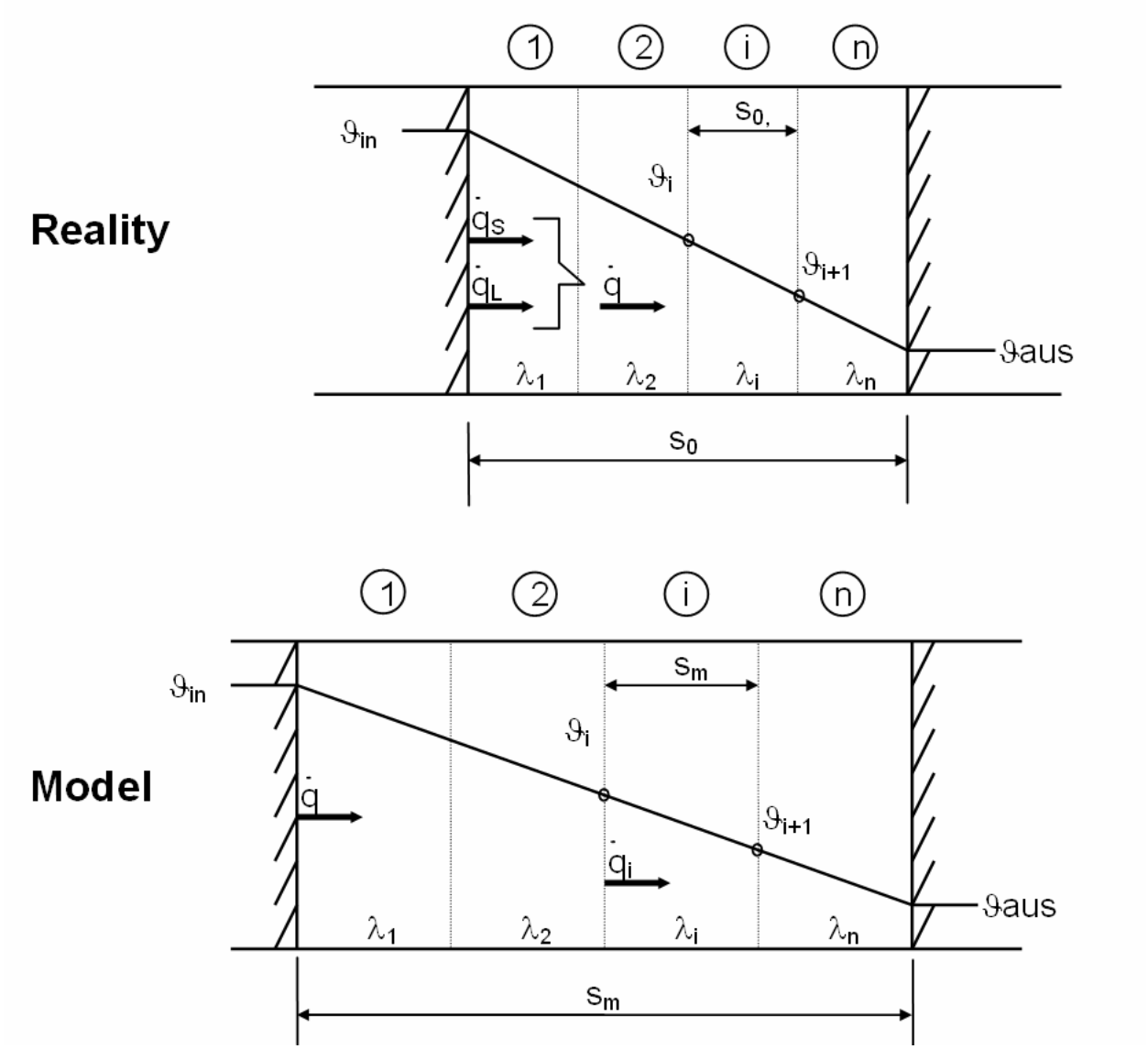

Figure 8.1 Comparison of reality and model of a shroud gap

Since the gap is filled with gas, the heat capacity can be neglected henceforth. The total heat flux across the gap $\dot{q}$ in the real shroud geometry is composed of heat conduction $\dot{q}_L$ and radiation $\dot{q}_S$ (s. Figure 8.1). The shroud is assumed to have a rectangular geometry, leading to a linear temperature curve where the boundary temperatures ϑ_{in} and ϑ_{aus} are equal to these of the real ones due to equal heat transfer $\dot{q}$. Further on, an averaged thermal conductivity across the whole gap is computed independently from temperature variations in the gap. Due to this simplification, a linear temperature curve is achieved across the whole gap. To facilitate further refinements, the general cased is considered in the following as long as possible.

The transformation of thermal expansion effects and radiation heat transfer into thermal conductivity leads to the introduction of a thermal conductivity correction coefficient $\lambda_{cor,i}$ that has to be added to all other thermal conductivity coefficients λ_i. The comparison of reality and model provides the following equations:

For the real geometry shroud:

$$\dot{q} = \left(\frac{1}{\sum_{i=1}^{n} \frac{s_{0,i}}{l_i}} + es \cdot \left[J_{in}^2 + J_{aus}^2 \right] \left[J_{in} + J_{aus} \right] \right) \cdot \left(J_{in} - J_{aus} \right) \tag{A.1}$$

and for the model assumptions

$$\dot{q} = \dot{q}_i = \left(\frac{l_i}{s_{m,i}} + \frac{l_{cor,i}}{s_{m,i}} \right) \cdot \left(J_i - J_{i+1} \right) \tag{A.2}$$

Thus, one gets from Eqn. (A1) and (A2) the following equation for $\lambda_{cor,i}$:

$$l_{cor,i} = \left(\frac{1}{\sum_{i=1}^{n} \frac{s_{0,i}}{l_i}} + es \cdot \left[J_{in}^2 + J_{aus}^2 \right] \left[J_{in} + J_{aus} \right] \right) \cdot \frac{J_{in} - J_{aus}}{J_i - J_{i+1}} \cdot s_{m,i} - l_i \tag{A.3}$$

The assumption of a linear temperature distribution leads to a constant thermal conductivity coefficient λ_i. Therefore, the summation in Eqn. (A3) could be simplified to

$$\sum_{i=1}^{n} \frac{s_{0,i}}{l_i} = \frac{s_0}{l_i} \tag{A.4}$$

Similarly, the linear temperature profile and the same temperatures at the gap boundaries result in an equal temperature gradient, whereby from Eqn. (A3) under consideration of Eqn. (A4) follows:

$$l_{cor,i} = l_i\left(\frac{s_m}{s_0} - 1\right) + s_m \cdot es \cdot \left[J_{in}^2 + J_{aus}^2\right]\left[J_{in} + J_{aus}\right] \quad \text{(A.5)}$$

where the actual gap width in the real shroud is calculated as follows:

$$s_0 = s_m + r_{m,aus} \cdot b \cdot \left(J_{mat,aus}\right) - r_{m,in} \cdot b \cdot \left(J_{mat,in}\right) \quad \text{(A.6)}$$

With this correction factor, one gets the new thermal conductivity coefficient $\lambda_{eff,i}$ for each node of the modelled gap. They are equal for a given elevation, and they equal the conductivity λ_{eff} of the whole gap due to the assumption of a linear temperature profile:

$$l_{eff} = l_{eff,i} = l_i\left(\frac{s_m}{s_0}\right) + s_m \cdot es \cdot \left[J_{in}^2 + J_{aus}^2\right]\left[J_{in} + J_{aus}\right] \quad \text{(A.7)}$$

The relation of the real, actual gap thickness to the initial gap thickness represents the correction factor due to gap closure and the second term is the transformed radiation heat transfer coefficient.

This calculated integral conductivity is increased due to the contributions of the radiation e.g. at ~ 1000 K term the net conductivity is ~ 10 % higher. In case of gap closure, effective conductivity reaches very high values (~ 50 W/(K m) ~ metallic conduction values). Due to the vanishing gap width, the added radiation term is negligible.

The implementation of this model in the code requires some additional assumptions. Firstly, we assume that the outer material of the shroud always has the same temperature and therefore does not expand. Thus, an existing gap (ca. 0.5 mm at $\Delta\vartheta$=700 K) will close very quickly. Secondly, if one there are two or more gaps in the shroud, only the material next to the gaps (without the outermost one) will move according to thermal expansion. If then an outer gap closes, the outer material of the next inner gap cannot move outwards anymore until the outer gap will open again. No elasticity is taken into account for any material.

The necessary program changes are realized in subroutines: effht.f, slabc.f, etc.

8.3 S/R5 Open Problems

The version distributed by INEEL for the QUENCH teams differs slightly with respect to input / output features, however, physical models seems to be implemented correctly. The following table lists the modifications and errors found during validation work.

Table 8.2 List of errors found during application of S/R mod3.2 and their actual status (March 2000).

Description	Affecting	Subroutine	Status
Shroud model not consistent in early and late phase	No melting of shroud, only in late phase, interaction with debris, fuel rod, molten pool?	heatld, slabc	open
Shroud interaction only possible for material #18	PHEBUS FPT 0	heatld	open
Material emissivities (only Zr data available for in-core radiation, no influence of oxide layer thickness)	Radiation coupling, open issue in case of reflood	zoemis	finished
No radiation coupling between upper plenum structures	Reduced heat up of control rod drive guide tubes at low pressure	U*	open
No late phase data on rstplt, i.e. ztpcoh, zbtcoh, ... missing M(pool)	Documentation of late phase results	heatld, rubtrn, ...	open
No concentration of non-condensables, available for all volumes	Programming of EXTDAT proposed by SCIENTECH		in work at FZK
Radiation absorption of steam	increased radiation absorption in case of low pressure	emissiv	still in work
Oxidation limitation and double sided oxidation		oxstat, oxidiz	partially solved
Radiation between pool crust/ debris and environment	To high temperatures in the void region above the pool affecting HR melt-down		open
Slumping mechanisms, PPR, DRP, etc unclear	Behaviour of debris bed below crust of molten pool		open
User defined slumping of UPS structures independent of UPS temperature	Debris formation in lower plenum at T_m < 500 K	ups***	open
Definition of variables shqin and shqout not clear in multi-shroud configurations	Output data	scdad7	open
Prescribe temperature and/or heat transfer coefficients at outer shroud surface	Outer fluid channel not required (QUENCH), experimental data can be used.	slabc rshrod	in work

8.4 Output of the Shroud Gap Model

Table 8.3 Output of FZK gap handling model for QUENCH shroud component.

EFFHT-GAP **Output**	**Description**
GAPS : 1 Comp/Typ/Ax: 3 2 27	Number of gaps in shroud component icomp number (3), type cylindrical (2), axial node number of gap bottom (27)
imat_in : 1 imat_out : 11	Inner layer material index (Zircaloy) outer layer material index (Inconel)
inngs: 1 : 17 inngs: 2 : 10	Inner layer heat conduction index outer layer heat conduction conduction
outngs:1 : 1 outngs: 2 : 2	Gap statistics Gap statistics
Rgap_in : .0424 Rgap_out : .0791	Inner gap radius (m) Outer gap radius (m)
Rmat_in : .0412 Rmat_out : .0816	Inner radius of inner material (m) Outer radius of outer material (m)

8.5 Output of FZK Heater Rod Model

The following output is added at a fixed frequent to the screen output (stdio).

```
At ~1000 s:
 W323x>:    1000.3    460.6 20  2 rat    57.6%  rs     15.6 rwo     9.0 rvo     6.6 pvor    77.5 pwo   265.3
        1   3   5   6    7    8    9   10   11   12   13   14   15   16   17   18   19   20   21   22   23   24   25   26   27   29   31   32
 1000. 606 701 736 764  823  866  893  912  927  941  954  967  980  993 1005 1017 1028 1039 1050 1060 1068 1073 1068 1042  975  929  847  717 K
 1000.  51  61  65  68  214  227  235  241  246  251  255  259  263  267  271  275  278  282  285  289  291  293  291  283   94   88   78   63 Q

and at ~2000 s:
 W323x>:    2000.6    760.7 20  2 rat    62.9%  rs     20.4 rwo    12.8 rvo     7.6 pvor   133.0 pwo   478.4
        1   3   5   6    7    8    9   10   11   12   13   14   15   16   17   18   19   20   21   22   23   24   25   26   27   29   31   32
 2001. 654 772 829 874  967 1033 1072 1105 1136 1166 1194 1223 1255 1295 1347 1378 1417 1461 1508 1556 1601 1632 1628 1551 1356 1226 1107  894 K
 2001.  71  87  96 103  328  355  371  384  397  409  421  433  447  463  485  499  516  535  555  576  595  609  607  574  189  164  142  106 Q
```

In the first line problem time (1000.3 s), total electric power (460.6 W), number of heater rods (20) simulated by component number (2) is given. Next the power ratio $P_{tungsten} / P_{total}$ is printed (57.6 %), the total resistance of the rod (15.6 mΩ), the tungsten resistance (9.0 mΩ), and the resistance of electrodes plus external resistance R_{static} (6.6 mΩ). A brief power balance is added including electrical power released in the electrode zones (77.5 W) and in the tungsten zone (265.3 W). The values shown above were obtained using a static resistance of 4.0 mΩ.

In the second line, the axial zone number is given (*Please note that due to line length restriction not all axial levels are printed out*). In the third line the centreline temperature of the electric heaters are given, and the fourth line shows the linear nodal power given in W/m.

Please note: only SI units are considered so far.

8.6 New SCDAP Subroutines

8.6.1 wolfht

```
subroutine wolfht(unuc,unucd,pptim)
c
c  $Id: wolfht.F,v 1.1 1998/09/23 22:43:12 ewc Exp $
c
c author : wolfgang hering kfk-irs  june 1998 mod3.2
c          FZKA-6566
c purpose: computes axial power distribution of cora heater rods
c          + no needs for copper temperatures, def. by cards 250, 251
c          + allows molybdenum in scdap volume (s. fstate.F)
c          + heater pin dimension hard wired for lwr + wwer
c          + includes thermal expansion of heater pins
c          + includes thermal feedback switched on / off
c          + includes material properties for matpro
c
c  Cognizant engineer: ewc
c
$if def,impnon,1
       implicit none
*call contrl
*call scddat
*call scdout
*call ndxara
*call cora
*call scdcom
*call ufiles
*call cons
c-----------------------------------------------------------------------
c fpt              : auxiliary printout control
c tiprt           : print frequency in counts of call wolfhe
c-----------------------------------------------------------------------
c index:
c ielec            : number of zones in bottom + top electrode
c-----------------------------------------------------------------------
c geometry:
c rtungs           : tungsten  radius
c relec            : molybdenum/copper radius      for lwr and vver
c aheiz(naz(icomp)): cross section area of wire materials          mm2
c imate(naz(icomp)): radial material sequence in heater rod        1
c-----------------------------------------------------------------------
c resistance:
c flxwid           : resistance of flexible wiring                 ohms
c rmheat           : total resitance of tungstan pin               ohms
c rmelec           : total resitance of the  electrode pin         ohms
c rax(naz(icomp))  : nodal resistance of each zone                 ohms
c vorwid           : total resistance of electrodes + wiring       ohms
c-----------------------------------------------------------------------
c power:
c pmelec           : total power released in electrode zones       w
c pmwo             : total power released in heated lenght         w
c unuc             : axial power relaesed in each zone             w/m
c pratio           : power efficiancy: power released in wo/pptim  1
c-----------------------------------------------------------------------
real unuc,unucd,pptim
      dimension unuc(*),unucd(*)
c local variables
      integer i, ic, j, k, iknt, itp, ibt, imate(ndax), io /6/
      real  fnexp, fnres, kf, pmwo, pmelec, pratio,
     + rax(ndax), rmheat, aheiz(ndax),pax,
     + vorwid,rmelec, botz, topz, stsq, fpt, tiprt
c
      data kf/1000./, tiprt /50./, fpt /0.0/
      save
c
      ic = icomp
      itp = naz(icomp)-ielec
      ibt = ielec+1
c
      do i = 1, naz(icomp)
        if (i .le. ielec .or. i .gt. itp) then
          aheiz(i)= pi * (relec * kf)**2
          imate(i)=21
        else
          aheiz(i)= pi * (rtungs * kf)**2
          imate(i)=4
        endif
```

```
      enddo
      if (icrmod .le. 2) then
        imate(1)=22
        imate(naz(icomp))=imate(1)
      endif
      rmelec   = 0.0
      rmheat   = 0.0
      do i = 1, naz(icomp)
        rax(i)=fnres(imate(i),tcond3(1,i,icomp))*dzcnd2(i,icomp)/
     +          (aheiz(i)* (1.0+fnexp(imate(i),tcond3(1,i,icomp))))
        if (i.le.ielec .or. i.gt.itp) then
          rmelec= rmelec + rax(i)
        else
          rmheat= rmheat + rax(i)
        endif
      enddo
      vorwid= flxwid + rmelec
      stsq= pptim / (vorwid + rmheat)
      pmwo= 0.0
      pmelec= 0.0
      do i=1, naz(icomp)
        pax    = stsq * rax(i)
        if (i .le. ielec .or. i .gt. itp) then
          pmelec= pmelec + pax
        else
          pmwo= pmwo + pax
        endif
        unuc(i)= pax / dzcnd2(i,icomp)
        unucd(i)= unuc(i)
      enddo
      if (pptim .le. 0.0)then
        pratio = 0.0
      else
        pratio= pmwo / pptim * 100.
      endif
      if (pratio .ge. 100.0)  then
         write  (output,1000) pratio
         fail=.true.
      else
       if (fpt .le. timehy) then
         write(io,900) timehy,pptim,nsigl(icomp),icomp,' rat',pratio,
     &  '%  rs ',(vorwid+rmheat)*kf,' rwo',rmheat*kf,
     &  ' rvo',vorwid*kf,' pvor',pmelec,' pwo',pmwo
         if (naz(icomp) .le. 16) then
           write(io,901) ' ',timehy,(tcond3(1,j,icomp),j=1,naz(icomp))
           write(io,902) ' ',timehy,(unuc(j),j=1,naz(icomp))
         else
           write(io,904) (j,j=1,ielec,2),(j,j=ielec,itp),
     &                  (j,j=itp+1,naz(ic),2),naz(ic)
           write(io,905) ' ',timehy,(int(tcond3(1,j,ic)),j=1,ielec,2),
     &         (int(tcond3(1,j,ic)),j=ielec,itp),
     &         (int(tcond3(1,j,ic)),j=itp+1,naz(ic),2),
     &          int(tcond3(1,naz(ic),ic))
           write(io,906) ' ',timehy,(int(unuc(j)),j=1,ielec,2),
     &         (int(unuc(j)),j=ielec,itp),
     &         (int(unuc(j)),j=itp+1,naz(ic),2),int(unuc(naz(ic)))

c          write(io,903) (j,j=1,naz(icomp),2)
c          write(io,901) ' ',timehy,(tcond3(1,j,icomp),j=1,naz(icomp),2)
c          write(io,902) ' ',timehy,(unuc(j),j=1,naz(icomp),2)
         endif
         fpt = timehy + tiprt
       endif
      endif
c
      return
c
 900  format(' W323x>: ',2f9.1, 2i3, 6(a,f8.1))
 901  format (a,f6.0,16f6.0,' K')
 902  format (a,f6.0,1x,16f6.1,' W/m')
 903  format (' ',4x,16i6)
 904  format (' ',5x,4i4,24i5)
 905  format (a,f5.0,4i4,24i5,' K')
 906  format (a,f5.0,4i4,24i5,' Q')
 1000 format(/,' ********* wolfhe: pratio:',1pe11.4,' > 100% ')
      end
```

8.6.2 epsmat

```
        function epsmat(im, tp)
c
c  $Id: epsmat.F,v 1.1 1998/07/29 23:17:11 whe Exp $
c
c  epsmat computes density by interpolation of user-specified
c  tables ttemp( =temperature( k )) and teps(=emissivity (1/1)).
c
c  Cognizant engineer: whe.
c
c  tables ttemp( =temperature( k ) ) and teps(=emissivity (1/1)).
c     calling subroutines:  fneps
c     engineer/programmer:  w.hering
c
c     input variables   description
c        im             material indicator
c        tp             temperature ( k )
c
$if def,impnon,1
       implicit none
*call matdat
      integer im,mark,jknt
      real tp, epsmat
c
      if(im.le.12)then
        jknt=im-8
      else
        jknt=im-45
      endif
      if( tp .ge. ttemp(markmx(jknt),jknt) ) then
        epsmat=teps(markmx(jknt),jknt)
      elseif( tp .le. ttemp(1,jknt))then
        epsmat=teps(1,jknt)
      else
        mark=1
   10   if(tp.ge.ttemp(mark,jknt) .and. tp.le.ttemp(mark+1,jknt)) then
          epsmat=teps(mark,jknt)+(teps(mark+1,jknt)-teps(mark,jknt))*
     #      (tp-ttemp(mark,jknt))/(ttemp(mark+1,jknt)-ttemp(mark,jknt))
        else
          mark=mark +1
          goto 10
        end if
      end if
      return
      end
*endif
```

8.6.3 expmat

```
        function expmat(im, tp)
c
c  $Id: expmat.F,v 1.1 1997/07/02 23:17:11 ewc Exp $
c
c  expmat computes density by interpolation of user-specified
c  tables ttemp( =temperature( k )) and texp(=thermal expansion (1/1)).
c
c  Cognizant engineer: whe.
c
c  tables ttemp( =temperature( k ) ) and texp(=thermal expansion (1/1))
c     calling subroutines:  fnexp
c     engineer/programmer:  w.hering
c
c     input variables   description
c        im             material indicator
c        tp             temperature ( k )
c
$if def,impnon,1
       implicit none
*call matdat
      integer im,mark,jknt
      real tp, expmat
c
      if(im.le.12)then
        jknt=im-8
      else
        jknt=im-45
      endif
      if( tp .ge. ttemp(markmx(jknt),jknt) ) then
        expmat=texp(markmx(jknt),jknt)
      elseif( tp .le. ttemp(1,jknt))then
        expmat=texp(1,jknt)
      else
        mark=1
   10   if(tp.ge.ttemp(mark,jknt) .and. tp.le.ttemp(mark+1,jknt)) then
          expmat=texp(mark,jknt)+(texp(mark+1,jknt)-texp(mark,jknt))*
     #      (tp-ttemp(mark,jknt))/(ttemp(mark+1,jknt)-ttemp(mark,jknt))
        else
          mark=mark +1
          goto 10
        end if
      end if
      return
      end
*endif
```

8.7 Modified SCDAP subroutines

8.7.1 cora

```
*comdeck cora
c
c
c  $Id: cora.H,v 1.2 1998/09/23 22:43:12 ewc Exp $
c
c  Simulator rod data
c
c  Cognizant engineer: ljs.
c
      common /cora/ rtungs,relec,flxwid,ibndtb(2,ndcomp),
     + icrmod,ielec,nbtcof(2,ndcomp),cora,mcme18
      real rtungs,relec,flxwid
      integer ibndtb,icrmod,ielec,nbtcof,mcme18
      logical cora

c  ibndtb is the general table number (if positive) or the
c    control variable (if negative) to the data which is
c    used to define the top (bndtab(2,icomp)) or the
c    bottom (bndtab(1,icomp)) boundary condition for the
c    simulator rod.
c
c  flxwid      = external resistance (ohm per rod) of flexible cables
c  ielec       = number of electrode zone in SCDAP
c  relec       = electrode radius (molybdenum, copper)
c  rtungs      = electrode radius (tungsten)
c  icrmod      = flag for heater model
c                0=ineel model
c                1=cora-lwr
c                2=cora-vvr
c                3=quench
```

8.7.2 scddat

```
*comdeck scddat
c
c  $Id: scddat.H,v 1.3 1997/08/27 20:36:41 ewc Exp $
*if def,selap
      integer maxpp,maxpz,ndax,ndcomp,ndgrid,ndmatr,ndrd,ndrg,ndtime,
     * nxdbrg,nmups,nmupax,nmupcn
cwh   parameter (maxpp=20,maxpz=5,ndax=20,ndcomp=16,ndgrid=11,
cwh   parameter (maxpp=36,maxpz=5,ndax=20,ndcomp=16,ndgrid=11,
     *  ndmatr=10, ndrd=20, ndrg=10, ndtime=10, nxdbrg=25, nmups=10,
cwh     *  ndmatr=10, ndrd=36, ndrg=10, ndtime=10, nxdbrg=25, nmups=10,
     #  nmupax=15, nmupcn=8)
c
       common /scddat/ icomp,ncomp,ngrid,cmpno(ndcomp),scmpnm,
     #  mcme62
c
      character scmpnm(ndcomp)*8
      integer icomp,<ncomp,ngrid,cmpno,mcme62
*endif
```

8.7.3 effht

```
+0...113
+114  c local variables:
+115  c ---------------- integer ------------------------
+116  c igs             : actual gap number
+117  c ipr             : print out pointer
+118  c igpbot          : lowest node of gap (#9)
+119  c iprmax          : print out frequency
+120  c ishrgp          : shroud identification with gapi
+121  c mgsinn          : material of inner side of gap
+122  c mgsout          : material of outer side of gap
+123  c mxgs            : maximum gap number
+124  c ---------------- real -------------------------
+125  c betta           : expansion coefficient of shroud material
+126  c fnexp           : expansion coefficient of shroud material
+127  c dss0            : distance between nodes of gap
+128  c ds0             : cold gap thickness
+129  c dsss            : actual gap thickness in case of expansion
+130  c effkgp          : heat transfer coefficient of gap
+131  c epp1            : emissivity of shroud material
+132  c fneps           : emissivity of shroud material
+133  c fkgs            : correcting factor due to gap closure
+134  c inngs           : nodes of inner gap material
+135  c lradgs          : additional heat coefficient due to radiation
+136  c outngs          : nodes of outer gap material
+137  c rep12           : radiation exchange coefficient
+138  c resitl          : heat conduction resistance of gap
+139  c routt           : outer gap radius in case of expansion
+140  c rout0           : inner radius of outer gap material
+141  c rout1           : outer radius of outer gap material
+142  c routm           : averaged radius of outer gap material
+143  c rin             : inner gap radius in case of expansion
+144  c rin0            : outer radius of inner gap material
```

```
+145  c rin1           : inner radius of inner gap material
+146  c rinm           : averaged radius of inner gap material
+147  c rshout         : outer shroud radius
+148  c zigma          : Bolzmann constant
+149  c tin0           : outer temperature of inner gap material
+150  c tinm           : averaged temperature of inner gap material
+151  c tout0          : inner temperature of outer gap material
+152  c toutm          : averaged temperature of outer gap material
+153  c
+154  c---- local FZK extentions data block --------------------------
+155        integer ih, iig, igs, mxgs /0/, ipr, iprmax, mg, istart
+156        parameter (mg=2)
+157        real dnx, rshout, rxsht, dsss(mg),ds0(mg),dss0(20),
+158     +     effkgp(mg), resitl(mg), rep12(mg), fkgs(mg), lradgs(mg),
+159     +     routt(mg), rout0(mg), rout1(mg), routm(mg),
+160     +     rin(mg), rin0(mg), rin1(mg), rinm(mg),
+161     +     tin0(mg), tinm(mg), tout0(mg), toutm(mg)
+162        real xk2c /273.15/, EE /5.0e-6/, zigma /5.67e-8/
+163        real fneps, fnexp
+164        integer igpbot /1/, ishrgp, inngs(mg,2), ipri,
+165     +        mgsinn(mg), mgsout(mg), outngs(mg,2)
+166        logical flag, flag1
+167        data flag /.true./, ipr /0/, iprmax /2000/
+168        data flag1/.true./
+169  c

+170 ... 186

+187           do 20 n=1,nmater(kx)
+188             np1=n + 1
+189             arean=pi*(radmt3(np1,inaz,icomp)**2-radmt3(n,inaz,icomp)**2)
+190             if(imatr3(n,inaz,icomp).ge.6 .and.
                imatr3(n,inaz,icomp).le.8)
+191     +     then
+192  c  layer of fuel.
+193  c  calculation of radial peaking factors fnrn=fnrn(r=rfnr).
+194               rfnr=(radmt3(n,inaz,icomp)+radmt3(np1,inaz,icomp))/2.
+195               fnrn=fnucr(rfnr,prdpr(1,icomp),xrdpr(1,icomp),
+196       #          nrdpr(icomp),zcond(kx), paxpz(1,1,icomp), naxpz(icomp),
+197       #          kshapz(icomp))
+198               sfnrn=sfnrn + fnrn * arean
+199               areaf=areaf + arean
+200               if( idcomp(icomp) .eq. 6) then
+201                 qmat3(n,inaz,icomp)=0.0
+202               else
+203                 qmat3(n,inaz,icomp)=fnrn * unuc
+204               endif
+205  cwh           else if( imatr3(n,inaz,icomp) .eq. 4) then
+206             else
+207               if(idcomp(icomp).eq.6 .and. n.eq.1) then
+208                  qmat3(n,inaz,icomp)=unuc / arean
+209               else
+210  c  non-fuel layer.
+211  c  conversion from (w/m) into (w/m3).
+212                  qmat3(n,inaz,icomp)=qmat3(n,inaz,icomp) / arean
+213               endif
+214             endif
+215     20   continue

+216 ....232

+233  c ---------------------------------------------------------------------
+234         if (idcomp(icomp).eq.2) then
+235           igs=0
+236           rshout=(slbwd(icomp)*0.159155)+xcond3(nrodes(kx),inaz,icomp)
+237           do 800 i=1,nmater(kx)
+238             if (imatr3(i,inaz,icomp).eq.9) then
+239               igs=igs+1
+240               rout0(igs)=rshout-radmt3(i,inaz,icomp)
+241               rout1(igs)=rshout-radmt3(i-1,inaz,icomp)
+242               routm(igs)=(rout0(igs)+rout1(igs))*0.5
+243               rin0(igs)=rshout-radmt3(i+1,inaz,icomp)
+244               rin1(igs)=rshout-radmt3(i+2,inaz,icomp)
+245               rinm(igs)=(rin0(igs)+rin1(igs))*0.5
+246               mgsinn(igs)=imatr3(i+1,inaz,icomp)
+247               mgsout(igs)=imatr3(i-1,inaz,icomp)
+248               mxgs=igs
+249             endif
+250   800     continue
+251           istart=1
+252            do 810 iig=1,mg
+253              do 820 ih=istart,nrodes(kx)
+254                rxsht=rshout-xcond3(ih,inaz,icomp)
+255                if (abs(rout1(iig)-rxsht) .lt. EE)  outngs(iig,1)=ih
+256                if (abs(rout0(iig)-rxsht) .lt. EE)  outngs(iig,2)=ih
+257                if (abs(rin0(iig)-rxsht) .lt. EE)   inngs(iig,2)=ih
+258                if (abs(rin1(iig)-rxsht) .lt. EE)   inngs(iig,1)=ih
+259   820     continue
+260           istart = inngs(iig,2)-1
+261   810     continue
+262  c
+263  cwh for CORA/QUENCH
+264           if (flag .and. mxgs .gt. 0) then
+265             ishrgp=icomp
+266             igpbot=inaz
+267             iprmax=iprmax*(naz(icomp)-igpbot+1)*numelm(kx)
+268             write(6,*) ' EFFHT-GAP configuration vers:04/97 FZK-IRS '
+269             write(6,903) ' GAPS        :',(j,j=1,mxgs)
```

```
+270            write(6,903) ' Comp/Typ/Ax.:',ishrgp,idcomp(ishrgp),igpbot
+271            write(6,903) '   imat_in   :',(mgsinn(j),j=1,mxgs)
+272            write(6,903) '   imat_out  :',(mgsout(j),j=1,mxgs)
+273  c
+274            write(6,903) '   inngs:  1 :',(inngs (j,1),j=1,mxgs)
+275            write(6,903) '   inngs:  2 :',(inngs (j,2),j=1,mxgs)
+276            write(6,903) '   outngs: 1 :',(outngs (j,1),j=1,mxgs)
+277            write(6,903) '   outngs: 2 :',(outngs (j,2),j=1,mxgs)
+278  c
+279            write(6,905) '   Rgap_in   :',(rin0(j),j=1,mxgs)
+280            write(6,905) '   Rgap_out  :',(rout0(j),j=1,mxgs)
+281            write(6,905) '   Rmat_in   :',(rinm(j),j=1,mxgs)
+282            write(6,905) '   Rmat_out  :',(routm(j),j=1,mxgs)
+283            flag = .false.
+284          endif
+285         do 830 i=1,mxgs
+286           tout0(i)=tcond3(outngs(i,2),inaz,icomp)
+287           toutm(i)=(tout0(i)+tcond3(outngs(i,1),inaz,icomp))*0.5
+288           tin0(i)=tcond3(inngs(i,2),inaz,icomp)
+289           tinm(i)=(tin0(i)+tcond3(inngs(i,1),inaz,icomp))*0.5
+290           effkgp(i)=0.
+291           resitl(i)=0.
+292   830    continue
+293        endif
+294        endif
+295  c -------------------------------------------------------------------

+296 ....324

+325  c calculation of gap conductivity correction factor
+326         if (icomp.eq.ishrgp .and. inaz .ge. igpbot) then
+327             do 840 i=1,mxgs
+328               rin(i)=rin0(i)+rinm(i)*
+329     +              fnexp(mgsinn(i),tinm(i))*(tinm(i)-xk2c)
+330               routt(i)=rout0(i)+
+331     +       routm(i)*fnexp(mgsout(i),toutm(i))*(toutm(i)-xk2c)
+332               if (i.eq.1) then
+333                 routt(i)=rout0(i)
+334                 rin(i)=min(routt(i),rin(i))
+335             else
+336               routt(i)=min(routt(i),rin(i-1)-rin0(i-1)+rout0(i))
+337               rin(i)=min(routt(i),rin(i))
+338             endif
+339             ds0(i)=rout0(i)-rin0(i)
+340             dsss(i)=routt(i)-rin(i)
+341             dsss(i)=max(1.e-6,dsss(i))
+342             fkgs(i)=dsss(i)/ds0(i)
+343             rep12(i)=1.0/fneps(mgsinn(i),tinm(i))+
+344     +              1.0/fneps(mgsout(i),toutm(i)) - 1.0
+345             lradgs(i)=zigma*(tin0(i)*tin0(i)+tout0(i)*tout0(i))*
+346     +               (tin0(i)+tout0(i))/rep12(i)
+347    840    continue
+348         endif
+349  c -------------------------------------------------------------------
+350         igs=1

+351 ... 380

+381  cwhs add radiation term to gap resistance for heater rod
+382             if(t1 .gt. 999.)then
+383               if(idcomp(icomp).eq.6 .and. im .eq. 9)then
+384                 kgap=zigma*(x1-x0)*(t0*t0+t1*t1)*(t0+t1)*
+385       &              fneps(imatr3(nm-1,inaz,icomp),t0)
+386  cwh
+387  c              if (ipri .le. 0) then
+388  c                write(6,903) ' H-gap  :',nm, inaz,
+389  c    &           imatr3(nm-1,inaz,icomp),im,imatr3(nm+1,inaz,icomp)
+390  c               write(6,904) '   Temp :',t0,t1,' k,eps :',
+391  c    &           fnk(im,t0,kx),kgap,fneps(imatr3(nm-1,inaz,icomp),t0)
+392  c               ipri= 19998
+393  c             else
+394  c               ipri=ipri - 1
+395  c             endif
+396                k0=1./(kgap + fnk(im, t0, kx))
+397                k1=1./(kgap + fnk(im, t1, kx))
+398              endif
+3              endif
+403  cwhe
```

8.7.4 fstate

```
...
+287          if(idcomp(icomp).eq.6)then
+288  c ------------------------------------------------ simulator
+289            nmat=nmat+1
+290  c heater system
+291            if (i.le.ielec .or. i.gt.naz(icomp)-ielec) then
+292               imatr3(nmat-1,i,icomp)=21
+293               radmt3(nmat,i,icomp)=relec
+294               imatr3(nmat-1,1,icomp)=22
+295               if (icrmod.lt.3) imatr3(nmat-1,naz(icomp),icomp)=22
+296               qmat3(nmat-1,i,icomp)=unuc(i)
+297  c electric insulation
+298              nmat = nmat + 1
+299                imatr3(nmat-1,i,icomp) = 12
```

```
+300               radmt3(nmat,i,icomp) = rci2(i,icomp)
+301            else
+302               imatr3(nmat-1,i,icomp)=4
+303               radmt3(nmat,i,icomp)=rtungs
+304               qmat3(nmat-1,i,icomp)=unuc(i)
+305  c pellet material
+306               nmat = nmat + 1
+307               if (icrmod .ge. 3) then
+308  c: QUENCH
+309                  imatr3(nmat-1,i,icomp) = 12
+310                  radmt3(nmat,i,icomp) = rpel2(i,icomp)
+311               else
+312  c: CORA (depleted / intact UO2)
+313                  imatr3(nmat-1,i,icomp) = 6
+314                  radmt3(nmat,i,icomp) = rpel2(i,icomp)
+315               endif
+316  c gap
+317               nmat = nmat + 1
+318               imatr3(nmat-1,i,icomp) = 9
+319               radmt3(nmat,i,icomp) = rci2(i,icomp)
+320            endif
+321          else
+322  c ------------------------------------------------ fuel rod
```

8.7.5 radcc2

```
….
 +35  *call intcom
 +36  *call scdcom
 +37  *call trnot1
 +38        integer nal,ndbg
 +39        real ur1,tsatrd
 +40        real qgas(ndcomp), qradi(ndcomp),
 +41     +parstm(ndax),det(2)
 +42        dimension hradg(ndcomp,ndax),hbsubi(ndcomp)
 +43        dimension hbsub1(ndcomp)
 +44        dimension frcstm(ndax)
 +45  c Local variables.
 +46        integer i,iblk,info,isteam,j,job,k,kdyni,kdynn,kk,lda,n,
 +47       # ndyni,norder, imato
 +48        real*8
           abf,abfi,abliq,abvap,alpd,amui,amuj,amun,anum1,area2,baij,
 +49       # ctmax,ddrop,denom,denom1,emf,emfi,emiui,emiuj,epsl, qconv,
 +50       # qradsm,sum,sumef,tauij, tauji,taujn,tauni,
 +51       # trm1,trm2,tmaxc,frcstm,fneps
 +52        external emissv,lsgedi,lsgefa,zoemis,fneps
 +53        real sigsb,tradth,zroxid,amurod,amushd
 +54        real hradg,hanum1,hsumef,hterm1,hterm2,hsum2,hbsubi,
           hbsub1,hsum1
 +55        real tradt1
 +56        data sigsb/ 5.6680e-8/
 +57        data tradth/500.0/, zroxid/0.3e-3/
 +58  c amurod = anisotropic radiation factor for rods.
 +59  c amushd = anisotropic radiation factor for shroud.
 +60        data amurod /0.0/, amushd/ 0.00/
 +61  cwh    tradth = 500.0
 +62        if (scntrl(12)) tradth = 4000.0
 +63  cwh loop oer axial nodes
 +64        do 210 k=1,nal
 +65  c calculate maximum component temperature.
 +66          tmaxc=0.0
 +67          iblk=0
 +68          if(idisrp(k).eq.1)iblk=1
 +69          do i=1,ncomp1
 +70            tmaxc=max(tmaxc,tsur1l((i-1)*ndax+k))
 +71          enddo
 +72          tradt1=tradth
 +73          if(iblk.eq. 1.or. tmaxc.lt.tradt1)then
 +74            do 20 i=1,ncomp1
 +75              kdyni=(i-1)*ndax+k
 +76              qoutl(kdyni)=hcnvcl(kdyni)*(tsur1l(kdyni)-tgradl(k,i))
 +77              qrdsrl(kdyni) = 0.0
 +78     20       continue
 +79            qradab(iencl,k) = 0.0
 +80            go to 210
 +81          end if
 +82  c calculate emissivities of surface of each component.
 +83          do n=1,ncomp1
 +84            imato=imatr3(nmater2(k,n),k,n)
 +85            if (imato .eq.5) then
 +86  cwh get zroxid from intcom data: equivalence (oxdeo2(1,1),oxdeo(1))
 +87                zroxid= oxdeo2(k,n)
 +88                call zoemis(tsur1l((n-1)*ndax+k),zroxid,emsubn(n))
 +89              else
 +90  cwh get emissivity from FZK generated data bank
 +91                emsubn(n)= fneps(imato,tsur1l((n-1)*ndax+k))
 +92              endif
 +93          enddo
 +94  c generate radiation matrix.
…
```

8.7.6 rusrmt

```
...
 +91  cwhb
 +92  c 4ccc2nn4 User specified Material Thermal Emissivity
 +93              l23(1)=40009004+imat*10
 +94              call inplnk(l23(1),next,where,nfield,fa(filndx(1)))
 +95              if (nfield .gt. 0) then
 +96                l23(6)=1
 +97                call inp2(fa(filndx(1)),rdatv,l23)
 +98                if (l23(6) .le. 0) then
 +99                  write (output,2001) l23(1)
+100                  fail = .true.
+101                else
+102                  do 492 knt1=1,markmx(knt)
+103                    teps(knt1,knt)=rdatv(knt1)
+104                    if(tk(knt1,knt).lt.0.0)then
+105                      write(output,2010)l23(1),'emissivity'
+106                      fail=.true.
+107                    endif
+108    492             continue
+109                endif
+110              else
+111                write(output,2020) l23(1), 'emissivity',imat
+112              endif
+113  c 4ccc2nn5 User specified Material Thermal expansion
+114              l24(1)=40009005+imat*10
+115              call inplnk(l24(1),next,where,nfield,fa(filndx(1)))
+116              if (nfield .gt. 0) then
+117                l24(6)=1
+118                call inp2(fa(filndx(1)),rdatv,l24)
+119                if (l24(6) .le. 0) then
+120                  write (output,2001) l24(1)
+121                  fail = .true.
+122                else
+123                  do 495 knt1=1,markmx(knt)
+124                    texp(knt1,knt)=rdatv(knt1)
+125                    if(tk(knt1,knt).lt.0.0)then
+126                      write(output,2010) l24(1),'thermal expansion'
+127                      fail=.true.
+128                    endif
+129    495             continue
+130                endif
+131              else
+132                write(output,2020) l24(1), 'thermal expansion',imat
+133              endif
+134            endif
+135    500   continue
+136        endif
+137        return
```

8.7.7 heatc2

```
        subroutine heatc2 (ic,ck,rocp,qss,nvirn)
c
c  $Id: heatc2.F,v 1.2 1998/09/23 22:43:05 ewc Exp $
c
c  Two dimensional heat conduction solution
c
c  Cognizant engineer: ewc.
c
$if def,impnon,1
       implicit none
*call comctl
*call contrl
*call fast
*call scddat
*call bconds
*call fpdkht
*call trnot1
*call trnot2
*call scdcom
*call ndxara
*call scdout
*call cmptim
*call cons
*call voldat
*call tblsp
*call fecom
*call nrcom
*call cora
*call gentblc
*call convarc
*call scdads
*call trpblk
*call ufiles
*call hardpn
c
c  Local variables.
       integer err,i,i0,i1,i2,ib,ib1,ib2,ibm,ic,icount,ife,ih,
     & iknt,il1,il2,il3,in1,in2,j,j1,jj,l,l0,l1,l2,m,nax,nci,nco,ndkat,
     & ndkat1,nr1,nrd,nrd2,nvirn, iip
cwh      & ndkat1,nr1,nrd,nrd2,nvirn, ito, ibo
c       real a(ndrd+1),aa((ndrd+1)*ndax+8),
c     & ab(ndrd+1,ndax),abt(ndrd+1,ndax-1),aho(2*ndrd,ndax),
c     & al(ndrd+1,ndax),alr(ndrd,ndax),ar(ndrd+1,ndax),asf(ndax),
c     & at(ndrd+1,ndax),avo(ndrd,ndax),b(ndrd+1),bb((ndrd+1)*ndax),
```

```
c     & c(ndrd+1),cc((ndrd+1)*ndax+8),ck(ndrd,ndax),d(ndrd+1),
c     & dd((ndrd+1)*ndax+8),dr(ndrd,ndax),dzav,
c     & g(ndrd+1,ndax),qss(ndrd,ndax),rocp(ndrd,ndax),
c     & sk1(ndax),sko(ndax),snk1(ndax),snko(ndax),
c     & src(ndrd+1,ndax),t1(ndrd+1,ndax),
c     & v1(2*ndrd,ndax), abtel(ndrd+1)
cwh
       real aa((ndrd+1)*ndax+8),bb((ndrd+1)*ndax+8),
     &      cc((ndrd+1)*ndax+8),dd((ndrd+1)*ndax+8),
     &      a(ndax),b(ndax),c(ndax),d(ndax)
       real ab(ndrd+1,ndax),abt(ndrd+1,ndax),aho(2*ndrd,ndax),
     & al(ndrd+1,ndax),alr(ndrd+1,ndax),ar(ndrd+1,ndax),asf(ndax),
     & at(ndrd+1,ndax),avo(ndrd,ndax),abtel(ndrd+1),
     & ck(ndrd,ndax),dr(ndrd,ndax),
     & g(ndrd+1,ndax),qss(ndrd,ndax),rocp(ndrd,ndax),
     & sk1(ndax),sko(ndax),snk1(ndax),snko(ndax),
     & src(ndrd+1,ndax), t1(ndrd+1,ndax),v1(2*ndrd,ndax)
       real delstp, dzav, trabo, trato, tiprt
c
       data icount/0/, iipr /1/
c
       nax = naz(ic)
       if (idcomp(ic).eq.5 .or. idcomp(ic).eq.7) nax = naz1(ic)
       ib = (ic - 1)*ndax
       nrd = numelm(ib+1)
       nr1 = nrd + 1
       nrd2 = 2*nrd
       trabo = 0.0
       trato = 0.0
cwh
      if (idcomp(ic).ne.6 ) then
        ndkat = 0
        ndkat1 = 0
      else
        ndkat = ibndtb(1,ic)
        ndkat1 = ibndtb(2,ic)
        if (ndkat.gt.0) then
c  Bottom Boundary temp from Relap5 general table
            iknt = filndx(11) + nbtcof(1,ic)
            call polat (gtbl(iknt-3),gtbl(iknt),timec,trabo,err)
        else
c  Bottom Temp from Relap5 control variable
            trabo = cnvarn(filndx(27) + nbtcof(1,ic))
        endif
        if (ndkat1.gt.0) then
c  Top Boundary temp from Relap5 general table
            iknt = filndx(11) + nbtcof(2,ic)
            call polat (gtbl(iknt-3),gtbl(iknt),timec,trato,err)
        else
c  Top Temp from Relap5 control variable
            trato = cnvarn(filndx(27) + nbtcof(2,ic))
        endif
      endif
cwh ----
       ibm = ib + 1
       if (ngeom(ic) .eq. 2) then
         do 15 m = 1,nax
           do 16 l = 1,nrd
             l0 = l + 1
             l2 = 2*l
             l1 = l2 - 1
             dr(l,m) = (xcond3(l0,m,ic) - xcond3(l,m,ic))*0.5
             dr(l,m) = max(1.25e-6, dr(l,m))
             avo(l,m) = 2.0*pi*(xcond3(l,m,ic)+dr(l,m))*dzcond(ibm)
             aho(l1,m) = pi*dr(l,m)*(2.0*xcond3(l,m,ic) + dr(l,m))
             aho(l2,m) = pi*dr(l,m)*(2.0*xcond3(l0,m,ic) - dr(l,m))
             v1(l1,m) = aho(l1,m)*dzcond(ibm)
             v1(l2,m) = aho(l2,m)*dzcond(ibm)
   16      continue
           ibm = ibm + 1
   15    continue
       else
         do 17 m = 1,nax
           do 18 l = 1,nrd
             l0 = l + 1
             l2 = 2*l
             l1 = l2 - 1
             dr(l,m) = (xcond3(l0,m,ic) - xcond3(l,m,ic))*0.5
             dr(l,m) = max(1.25e-6, dr(l,m))
             avo(l,m) = slbwd(ic)*dzcond(ibm)
             aho(l1,m) = slbwd(ic)*dr(l,m)
             aho(l2,m) = aho(l1,m)
             v1(l1,m) = aho(l1,m)*dzcond(ibm)
             v1(l2,m) = v1(l1,m)
   18      continue
           ibm = ibm + 1
   17    continue
       endif
cwh
       ib1 = ib + 1
       ib2 = ib + 2
       do 20 j = 1,nax-1
         j1 = j + 1
         dzav = 0.5/(dzcond(ib1) + dzcond(ib2))
         abt(1,j) = (aho(1,j) + aho(1,j1))*(ck(1,j) + ck(1,j1))*dzav
         abt(nr1,j) = (aho(nrd2,j) + aho(nrd2,j1))*(ck(nrd,j) +
     &                 ck(nrd,j1))*dzav
         if (nrd .gt. 1) then
```

```
          do 21 i = 2,nrd
            i0 = i - 1
            i1 = 2*i0
            i2 = i1 + 1
            abt(i,j) = ((aho(i1,j) + aho(i1,j1))*(ck(i0,j) +
     &      ck(i0,j1)) + (aho(i2,j) + aho(i2,j1))*(ck(i,j)+ck(i,j1)))*
     &      dzav
   21     continue
        endif
        ib1 = ib1 + 1
        ib2 = ib2 + 1
   20 continue
c
       do 24 j = 1,nax
         do  i = 1,nrd
           alr(i,j) = avo(i,j)*ck(i,j)*0.5/dr(i,j)
         enddo
   24 continue
       do 31 j = 1,nax
         al(1,j) = 0.0
         ar(nr1,j) = 0.0
         if (nrd .gt. 1) then
           do i = 2,nr1
             al(i,j) = alr(i-1,j)
           enddo
         endif
         do i = 1,nrd
           ar(i,j) = alr(i,j)
         enddo
   31 continue
       do  35 i = 1,nr1
         ab(i,1) = 0.0
             at(i,nax) = 0.0
         do j = 2,nax
           ab(i,j) = abt(i,j-1)
         enddo
         do j = 1,nax-1
           at(i,j) = abt(i,j)
         enddo
   35 continue
c
         if (ndkat.gt.0 .or. ndkat1.gt.0) then
           abtel(1)= 2.0*aho(1,1)*ck(1,1)/dzcond(1)
           do  i = 2,nrd
             i0 = i - 1
             i1 = 2*i0
             abtel(i)=2.0*(aho(i1,1)+aho(i1+1,1))*
     &                    ck(i-1,1)/dzcond(1)
           enddo
           abtel(nr1)= 2.0*aho(nrd2,1)*ck(nrd,1)/dzcond(1)
         else
           do  i = 1,nr1
             abtel(i)=0.0
           enddo
         endif
c
       do 40 j = 1,nax
         g(1,j) = v1(1,j)*rocp(1,j)
         g(nr1,j) = v1(nrd2,j)*rocp(nrd,j)
         src(1,j) = v1(1,j)*qss(1,j)
         src(nr1,j) = v1(nrd2,j)*qss(nrd,j)
         if (nrd .gt. 1) then
           do 41 i = 2,nrd
             i0 = i - 1
             i1 = 2*i0
             i2 = i1 + 1
             g(i,j) = v1(i1,j)*rocp(i0,j) + v1(i2,j)*rocp(i,j)
             src(i,j) = v1(i1,j)*qss(i0,j) + v1(i2,j)*qss(i,j)
cwh
             if (ic .eq.2 .and. i.eq.nodech(ic))
     &           src(i,j)=src(i,j)-echflx(j,ic)
   41      continue
         endif
   40 continue
cwh ------------------------------------------------------------
       il1 = ib + 1
       if (nvirn .le. 2) then
         if (ngeom(ic) .eq. 2) then
           do 42 j = 1,nax
             in1 = nvad(il1) + filndx(4)
             asf(j) = 2.0*pi*xcond3(nr1,j,ic)*dzcond(il1)
             snko(j) = asf(j)*htsht(il1)
             snk1(j) = asf(j)*(htsht(il1)*tcond3(nr1,j,ic) -
     &       htsqst(il1) - qrdsur(il1))
             il1 = il1 + 1
   42      continue
         else
           do 43 j = 1,nax
             in1 = nvad(il1) + filndx(4)
             asf(j) = avo(1,j)
             snko(j) = asf(j)*htsht(il1)
             snk1(j) = asf(j)*(htsht(il1)*tcond3(nr1,j,ic) -
     &       htsqst(il1) - qrdsur(il1))
             il1 = il1 + 1
   43      continue
           il2 = (ndcomp + nsout(ic) - 1)*ndax + 1
c  islbot(ic) = 0 = Savannah River or ATR component or shroud component
c  inside another shroud component.
```

```
          if (islbot(ic) .eq. 0) then
            do 44 j = 1,nax
              in2 = nvad(il2) + filndx(4)
              sko(j) = asf(j)*htsht(il2)
              sk1(j) = asf(j)*(htsht(il2)*tcond3(1,j,ic) -
     &        htsqst(il2))
              if (icrad(ic) .eq. ic) sk1(j) = sk1(j) - qrdsur(il2)*
     &        asf(j)
              il2 = il2 + 1
   44       continue
          else
            ih = (nsout(ic)-1)*ndax + 1
            do 45 j = 1,nax
              sko(j) = asf(j)*hout(ih)
              sk1(j) = sko(j)*tcols(ih)
              if (icrad(ic) .eq. ic) sk1(j) = sk1(j) - qrdsur(il2)*
     &        asf(j)
              il2 = il2 + 1
              ih = ih + 1
   45       continue
          endif
        endif
      else
        ife = ic
        if (ifa .ge. 2) ife = ic - idfe(nfe(ifa-1),ifa-1)
        do 142 j = 1,nax
          in1 = nvad(il1) + filndx(4)
          asf(j) = avo(1,j)
          snko(j) = asf(j)*htsht(il1)
          snk1(j) = asf(j)*(htsht(il1)*tcond3(nr1,j,ic) -
     &    htsqst(il1) - qrdsur(il1))
          il1 = il1 + 1
  142   continue
        if (ic .gt. idfe(1,ifa)) then
          do j = 1,nax
            snk1(j) = snk1(j) + qraden(ifa,j,ife-1)/nsigl(ic)
          enddo
        endif
        if (islbot(ic) .eq. 0) then
          il2 = (ndcomp + nsout(ic) - 1)*ndax + 1
          do j = 1,nax
            in2 = nvad(il2) + filndx(4)
            sko(j) = asf(j)*htsht(il2)
            sk1(j) = asf(j)*(htsht(il2)*tcond3(1,j,ic) -
     &      htsqst(il2))
            il2 = il2 + 1
          enddo
        else
          ih = (nsout(ic) - 1)*ndax + 1
          do j = 1,nax
            sko(j) = asf(j)*hout(ih)
            sk1(j) = sko(j)*tcols(ih)
            ih = ih+ 1
          enddo
        endif
        if (idcomp(ic).ge.4 .and.
     &      idcomp(ic).lt.6 .and.
     &                                        ic.lt.idfe(nfe(ifa),ifa))
         then
          do j = 1,nax
            sk1(j) = sk1(j) - qraden(ifa,j,ife)/nsigl(ic)
          enddo
        endif
      endif
cwh -----------------------------------------------------------------
      jj = 1
      do 100 i = 1,nr1
        do  j = 1,nax
         a(j)= -ab(i,j)
         b(j)= 2.0*g(i,j)/dt + ab(i,j) + at(i,j)
         c(j)= -at(i,j)
         d(j)= (2.0*g(i,j)/dt-al(i,j)-ar(i,j))*tcond3(i,j,ic)+src(i,j)
        enddo
        if (i .eq. 1) then
          do j = 1,nax
            d(j) = d(j) + ar(i,j)*tcond3(i+1,j,ic)
          enddo
          if (ngeom(ic) .ne. 2) then
            do j = 1,nax
                 d(j) = d(j) + sk1(j)
                 b(j) = b(j) + sko(j)
            enddo
          endif
        else
          if (i .eq. nr1) then
            do j = 1,nax
               d(j) = d(j) + al(i,j)*tcond3(i-1,j,ic) + snk1(j)
               b(j) = b(j) + snko(j)
            enddo
          else
            do j = 1,nax
              d(j) = d(j) + al(i,j)*tcond3(i-1,j,ic) +
     &                      ar(i,j)*tcond3(i+1,j,ic)
            enddo
          endif
        endif
        d(1) =   d(1) +   abtel(i)*trabo
        b(1) =   b(1) +   abtel(i)
```

```
          d(nax) = d(nax) + abtel(i)*trato
          b(nax) = b(nax) + abtel(i)
cwh
          do j = 1,nax
            aa(jj) = a(j)
            bb(jj) = b(j)
            cc(jj) = c(j)
            dd(jj) = d(j)
            jj = jj + 1
          enddo
  100   continue
c  Downward pass of column oriented tridiagonal solution.
        jj = 1
        j = jj
        do m = 1,nr1
          delstp = 1.0/bb(j)
          dd(j) = dd(j)*delstp
          cc(j) = cc(j)*delstp
          j = j + nax
        enddo
        jj = jj + 1
        do i = 3,nax
          j = jj
          do m = 1,nr1
            delstp = 1.0/(bb(j) - aa(j)*cc(j-1))
            dd(j) = (dd(j) - aa(j)*dd(j-1))*delstp
            cc(j) = cc(j)*delstp
            j = j + nax
          enddo
          jj = jj + 1
        enddo
        j = jj
        do m = 1,nr1
          dd(j) = (dd(j) - aa(j)*dd(j-1))/(bb(j) - aa(j)*cc(j-1))
          j = j + nax
        enddo
cwh ------------------------------------------------------------------
c  Upward pass of column oriented tridiagonal solution.
        do i = 2,nax
          jj = jj - 1
          j = jj
          do m = 1,nr1
            dd(j) = dd(j) - cc(j)*dd(j+1)
            j = j + nax
          enddo
        enddo
        jj = 1
        do 301 i = 1,nr1
          do 300 j = 1,nax
            t1(i,j) = dd(jj)
            jj = jj + 1
  300     continue
  301   continue
cwh
        jj = 1
        do 400 j = 1,nax
          do i = 1,nr1
            a(i) = -al(i,j)
            b(i) = 2.0*g(i,j)/dt + al(i,j) + ar(i,j)
            c(i) = -ar(i,j)
            d(i) = (2.0*g(i,j)/dt - ab(i,j) - at(i,j))*t1(i,j) + src(i,j)
          enddo
          if (j .eq. 1) then
            do  i = 1,nr1
cwh             d(i) = d(i) + at(i,j)*t1(i,j+1) + abtel(i)*(trabo-t1(i,j))
                b(i) = b(i) + abtel(i)
                    d(i) = d(i) + at(i,j)*t1(i,j+1) + abtel(i)*trabo
            enddo
          else
            if (j .eq. nax) then
              do i = 1,nr1
cwh             d(i) = d(i) + ab(i,j)*t1(i,j-1) + abtel(i)*(trato-t1(i,j))
                b(i) = b(i) + abtel(i)
                    d(i) = d(i) + ab(i,j)*t1(i,j-1) + abtel(i)*trato
              enddo
            else
              do i = 1,nr1
                d(i) = d(i) + ab(i,j)*t1(i,j-1) + at(i,j)*t1(i,j+1)
              enddo
            endif
          endif
          b(nr1) = b(nr1) + snko(j)
          d(nr1) = d(nr1) + snk1(j)
          if (ngeom(ic) .ne. 2) then
            b(1) = b(1) + sko(j)
            d(1) = d(1) + sk1(j)
          endif
          do i = 1,nr1
            aa(jj) = a(i)
            bb(jj) = b(i)
            cc(jj) = c(i)
            dd(jj) = d(i)
            jj = jj+1
          enddo
  400   continue
c  Downward pass of row oriented tridiagonal solution.
  910   jj = 1
        j = 1
```

```
       do m = 1,nax
         bb(j) = 1.0/bb(j)
         dd(j) = dd(j)*bb(j)
         cc(j) = cc(j)*bb(j)
         j = j + nr1
       enddo
       jj = jj + 1
       do i = 3,nr1
         j = jj
         do m = 1,nax
           bb(j) = 1.0/(bb(j) - aa(j)*cc(j-1))
           dd(j) = (dd(j) - aa(j)*dd(j-1))*bb(j)
           cc(j) = cc(j)*bb(j)
           j = j + nr1
         enddo
         jj = jj + 1
       enddo
       j = jj
       do m = 1,nax
         bb(j) = 1.0/(bb(j) - aa(j)*cc(j-1))
         dd(j) = (dd(j) - aa(j)*dd(j-1))*bb(j)
         j = j + nr1
       enddo
c  Upward pass of row oriented tridiagonal solution.
       do i = 2,nr1
         jj = jj - 1
         j = jj
         do m = 1,nax
           dd(j) = dd(j) - cc(j)*dd(j+1)
           j = j + nr1
         enddo
       enddo
       j = 1
       if (icount .ne. 1) then
cwh
         jj = 1
         do 701 j = 1,nax
           do 700 i = 1,nr1
             tcond3(i,j,ic) = dd(jj)
c  Since temperature for liquefied core material is calculated in
c  subroutine heatld, override calculated temperature in heatc2 for
c  liquefied material.
             if (lcrucb(j,ic) .ge. 1) tcond3(i,j,ic) = tupool
             jj = jj + 1
  700      continue
  701    continue
cwh
c  Process arrays for implicit connection between Scdap components and
c  hydrodynamics.
       if (iand(print,64) .ne. 0) then
c  Left boundary.
         if (islbot(ic) .eq. 0) then
           il2 = (ndcomp + nsout(ic) - 1)*ndax + 1
           jj = 1
           j = jj
           do m = 1,nax
             delstp = -asf(m)*bb(j)
             dfx(j,1,ic) = htshff(il2)*delstp
             dfx(j,2,ic) = htshgg(il2)*delstp
             dfx(j,3,ic) = (htshft(il2) + htshgt(il2))*delstp
             dfx(j,4,ic) = htshgp(il2)*delstp
             il2 = il2 + 1
             j = j + nr1
           enddo
c  Apply foward and backward parts of tridiagonal solution.
           jj = jj + 1
           do i = 2,nr1
             j = jj
             do m = 1,nax
               delstp = -aa(j)*bb(j)
               dfx(j,1,ic) = delstp*dfx(j-1,1,ic)
               dfx(j,2,ic) = delstp*dfx(j-1,2,ic)
               dfx(j,3,ic) = delstp*dfx(j-1,3,ic)
               dfx(j,4,ic) = delstp*dfx(j-1,4,ic)
               j = j + nr1
             enddo
             jj = jj + 1
           enddo
c
           do i = 2,nr1
             jj = jj - 1
             j = jj
             do m = 1,nax
               dfx(j,1,ic) = dfx(j,1,ic) - cc(j)*dfx(j+1,1,ic)
               dfx(j,2,ic) = dfx(j,2,ic) - cc(j)*dfx(j+1,2,ic)
               dfx(j,3,ic) = dfx(j,3,ic) - cc(j)*dfx(j+1,3,ic)
               dfx(j,4,ic) = dfx(j,4,ic) - cc(j)*dfx(j+1,4,ic)
               j = j + nr1
             enddo
           enddo
         endif
c  Right boundary.
         il1 = ib + 1
         jj = nr1
         j = jj
         do m = 1,nax
           delstp = -asf(m)*bb(j)
           dfx(j,5,ic) = htshff(il1)*delstp
```

```
          dfx(j,6,ic) = htshgg(il1)*delstp
          dfx(j,7,ic) = (htshft(il1) + htshgt(il1))*delstp
          dfx(j,8,ic) = htshgp(il1)*delstp
          il1 = il1 + 1
          j = j + nr1
        enddo
c  Apply backward part of tridiagonal solution.
        do i = 2,nr1
          jj = jj - 1
          j = jj
          do m = 1,nax
            dfx(j,5,ic) = -cc(j)*dfx(j+1,5,ic)
            dfx(j,6,ic) = -cc(j)*dfx(j+1,6,ic)
            dfx(j,7,ic) = -cc(j)*dfx(j+1,7,ic)
            dfx(j,8,ic) = -cc(j)*dfx(j+1,8,ic)
            j = j + nr1
          enddo
        enddo
      endif
        if (nvirn.ne.3 .and. nvirn.ne.4 .and. nvirn.ne.6) then
          if (chngno(30)) then
            jj = 1
            do 800 j = 1,nax
              do 801 i = 1,nr1
                a(i) = -al(i,j)
                b(i) = 2.0*g(i,j)/dt + al(i,j) + ar(i,j)
                c(i) = -ar(i,j)
                d(i) = 0.
  801           continue
              if (j .eq. 1) then
                do i = 1,nr1
                  d(i) = 0.
                enddo
              else
                if (j .eq. nax) then
                  do i = 1,nr1
                    d(i) = 0.
                  enddo
                else
                  do i = 1,nr1
                    d(i) = 0.
                  enddo
                endif
              endif
              b(nr1) = b(nr1) + snko(j)
              if (ngeom(ic) .eq. 2) then
                d(nr1) = d(nr1) + 1.0
              else
                b(1) = b(1) + sko(j)
                d(1) = d(1) + 1.0
              endif
              do 903 i = 1,nr1
                aa(jj) = a(i)
                bb(jj) = b(i)
                cc(jj) = c(i)
                dd(jj) = d(i)
                jj = jj+1
  903           continue
  800         continue
              icount = icount + 1
              if (icount .eq. 1) goto 910
            endif
          endif
        else
          jj = 1
          do 901 j = 1,nax
            do 900 i = 1,nr1
              dtgrad(i,j,ic) = asf(j)*dd(jj)
              jj = jj + 1
  900       continue
  901     continue
        endif
        icount = 0
        if (idcomp(ic).ne.5 .and. idcomp(ic).ne.7) then
          il1 = ib + 1
          do 234 j = 1,nax
            nci = nrcldi(il1)
            nco = numelm(il1) + 1
            in1 = nvad(il1) + filndx(4)
            if (numelm(il1) .eq. 1) then
              qclad(il1) = -ck(1,j)*(tcond3(2,j,ic) - tcond3(1,j,ic))/
     &        (2.0*dr(1,j))
            else
              qclad(il1) = -(ck(nci-1,j)*(tcond3(nci,j,ic) -
     &        tcond3(nci-1,j,ic))/dr(nci-1,j) + ck(nci,j)*
     &        (tcond3(nci+1,j,ic) - tcond3(nci,j,ic))/
     &        dr(nci,j))*0.25
            endif
            delstp = tcond3(nco,j,ic) - tcnd03(nco,j,ic)
            qout(il1) = htsht(il1)*delstp + htsqst(il1)
            qscd(il1) = qout(il1)*htsasv(il1)
            qwgscd(il1) = ((htshgg(il1) + htshgt(il1) + htshgp(il1))*
     &      delstp + htsqsg(il1))*htsasv(il1)
            il1 = il1 + 1
            in1 = in1 + 1
  234     continue
        else
          il1 = ib + 1
```

```
        il2 = nsout(ic)*ndax + 1
        il3 = (ndcomp + nsout(ic) - 1)*ndax + 1
        do 235 i=1,nax
          nci = numelm(il1) + 1
          delstp = tcond3(nci,i,ic) - tcnd03(nci,i,ic)
          qout(il1) = htsht(il1)*delstp + htsqst(il1)
          qscd(il1) = qout(il1)*htsasv(il1)
          qwgscd(il1) = ((htshgg(il1) + htshgt(il1) + htshgp(il1))*
     &     delstp + htsqsg(il1))*htsasv(il1)
          delstp = tcond3(1,i,ic) - tcnd03(1,i,ic)
          qouts(il2) = htsht(il3)*delstp + htsqst(il3)
          qscd(il3) = qouts(il2)*htsasv(il3)
          qwgscd(il3) = ((htshgg(il3) + htshgt(il3) + htshgp(il3))*
     &     delstp + htsqsg(il3))*htsasv(il3)
          il1 = il1 + 1
          il2 = il2 + 1
          il3 = il3 + 1
  235    continue
       endif
cwh
c 1900  format (A,2i9,2f10.1)
c 1901  format (' Matr: ', 2i4, 4e12.4 )
c 1902  format (' Tc3: ', 2I4, 90f6.0)
c 1903  format (i4, 20e9.3)
cwh
       return
       end
```

8.7.8 scdad4

```
+... +168  cwhs
+169            if(tcond3(nrods2(i,j),i,j).lt.tdtmin) timcnt(i,j)=timehy
+170  cwh
+171     60   continue
+172     70 continue
+173  cwh
+174          if (bgmct .gt. tdtmin .and. bgmct .le. 2500.) then
+175            do j = 1,ncomp
+176              if (idcomp(j).eq.0 .or. idcomp(j).eq.6) then
+177                do i = 1,naz(1)
+178                  if (tcond3(nrods2(i,j),i,j) .gt. tdtmin) then
+179                    dtiwh=max(timehy-timcnt(i,j), 1.0)
+180                    dtr=(tcond3(nrods2(i,j),i,j)-tdtmin)/dtiwh
+181  c ---- polynom derived from Alex. Miassoedovs data
+182                    tcfail(i,j)= ((6.*dtr-41.*dtr)-12.)*dtr + 2507.
+183                    tcfail(i,j)= max(tcfail(i,j), 2230.)
+184                    if (tpri - timehy .le. 0.)  write (6,1111) i,j,
+185       #              idcomp(j),dtr, timcnt(i,j),tcfail(i,j)
+186                  endif
+187                enddo
+188              endif
+189            enddo
+190            if (tpri - timehy .le. 0.) tpri = timehy+100.
+191          endif
+192   1111   format(' DBG-scdad4: ', 3i4, f10.3, 3f10.1)
+193  cwhe

+194 ....
```

8.8 New MATPRO Subroutines

8.8.1 fnres

```
function fnres(im,tp)
c--------------------------------
c     fnres : ohms * mm2 / m
c  $Id: fnres.F,v 1.1 1998/09/23 22:43:04 ewc Exp $
c--------------------------------
cwh:  data stored here are extracted from: IKE 2-100,1993 (8/98)
c
c     calling routine: wolfhe
c     called         : none
c
      real fnres, tp
      integer im
c     tc = tp - tref
c-1 zry
c-2 Zr-UO liq
c-3 Zr-UO solif
c
c-4 tungsten
      if (im .eq. 4) then
        fnres = -2.61e-2 + tp * ( 2.63e-4 + 2.20e-8 * tp)
c
c-5 ZrO2
c
c-6...7 UO2 (org: INEEL wolfhe)
      elseif (im .ge. 6 .and. im .le.8) then
        fnres = max((6.548e-7*exp(28600.0/tp)),0.75)
c
c-9...12 User-mat
```

```
c-13 U metallic
c-14 ????
c-15 Al
c-16 Al2O3
c-17 Li
c-18 SS304
c-19 SSOxid
c-20 Ag/In/Cd
c
c-21 molybdenum
      elseif (im .eq. 21 ) then
        fnres = 2.249e-2 + 5.36e-5*tp + 1.38e-7*tp**2 - 2.22e-11*tp**3
c-22 copper
      elseif (im .eq. 22 ) then
        fnres = -7.89e-3 + 9.90e-5*tp - 5.49e-8*tp**2 + 3.16e-11*tp**3
      else
        write(6,*) ' fnres: Material # ',im,' not defined. T=',tp
        stop ' fnres '
      endif
      return
      end
```

8.8.2 fneps

```
function fneps(im,tp)
c
c  $Id: fneps.F,v 1.1 1998/09/23 22:43:01 ewc Exp $
c
c  fneps computes thermal expansion based on MATPRO or
c                 user defined Materials
c
c  calling subroutines:  effht
c  subroutines called:   epsmat
c
c  input variables                  description
c        im             material indicator
c        tp             temperature ( k )
c
cwh:  data stored here are extracted from: kfk-15/77-2 (8/98)
c
$if def,impnon,1
      implicit none
c  Local variables.
      integer im
      real fneps,tp, tc, tref/273.15/, alpha
      real femiss, epsmat
c
      tc = tp - tref
c-1 zry
       if (im .eq. 1) then
         fneps=0.325
c-2 Zr-UO liq
c-3 Zr-UO solif
       elseif (im .ge. 2 .and. im .le.3) then
         fneps=femiss(tp)
c-4 tungsten
       elseif (im .eq. 4) then
         fneps=0.4
c-5 ZrO2
       elseif (im .eq. 5) then
        fneps= 8.08642e-01 - 5.00e01 * 1.e-4
c-6...7 UO2
       elseif (im.eq.6 .or. im.eq.7)then
c
c-9...12 User-mat
       elseif (im .ge. 10 .and. im .le. 12) then
        fneps= epsmat(im, tp)
       elseif (im.eq.13)then
c-13 U metallic
c-15 Al
       elseif (im .eq. 15) then
         fneps = 0.8 - 3.615e-4 * tc
c-16 Al2O3
c-16 Al2O3
       elseif (im .eq. 16) then
         fneps = 0.8 - 3.615e-4 * tc
c-17 Li
       elseif (im .eq. 17) then
c-18 SS304
       elseif (im .eq. 18) then
        fneps=0.69
c-19 SSOxid
       elseif (im .eq. 19) then
        fneps=0.8
c-20 Ag/In/Cd
       elseif (im .eq. 20) then
c-22 copper
      elseif (im .eq. 22 ) then
        fneps=0.3
c-21 molybdenum
      elseif (im .eq. 21 ) then
        fneps= 0.25
c-50...12 User-mat
      elseif (im .ge. 50 .and. im .le. 59) then
        fneps=epsmat(im, tp)
      else
        write(6,*) ' fneps: Material # ',im,' not defined. T=',tp
```

```
        stop ' fneps '
      endif
      return
      end
```

8.8.3 fnexp

```
function fnexp(im,tp)
c
c  $Id: fnexp.F,v 1.1 1998/09/23 22:43:02 ewc Exp $
c
c  fnexp computes thermal expansion based on MATPRO or
c                 user defined Materials
c
c  calling subroutines:  effht
c  subroutines called:   expmat
c
c  input variables                  description
c        im             material indicator
c        tp             temperature ( k )
c
cwh:  data stored here are extracted from: kfk-15/77-2 (8/98)
cwh:  transformation dehn/tc = fnexp
c
$if def,impnon,1
      implicit none
c
c  Local variables.
      integer im
      real fnexp,tp, tc, tref /273./
      real expmat,alfa
c
      tc = tp - tref
c-----------
c-1 zry
      if (im .eq.1 ) then
        if (tp .le. 1098) then
          fnexp=(8.207e-4 + tp*(-7.856e-6 + tp*
 +          (1.9236e-8 - tp*6.1409e-12)))/tc
        else
          fnexp=7.3e-3/tc
        endif
c-2 Zr-UO liq
c-3 Zr-UO solif
c
c-4 tungsten
      elseif (im .eq. 4) then
        fnexp= 4.428e-6 + 7.775e-11*tc + 6.6408e-13*tc**2
c
c-5 ZrO2
c
c-6...7 UO2
c
c-9...12 User-mat
       elseif (im .ge. 10 .and. im .le. 12) then
        fnexp= expmat(im, tp)
c-13 U metallic
c-14 ????
c-15 Al
c-16 Al2O3
      elseif (im .eq. 16 ) then
        if (tc .gt. 1000.) tc = 1200.
        fnexp=-2.931e-4/tc + (6.91e-6 + 1.814e-9*tc)
c
c-17 Li
c-18 SS304
      elseif (im .eq. 18 ) then
        fnexp=-3.248e-4/tc + (1.316e-5 + 4.789e-9*tc)
c-19 SSOxid
c-20 Ag/In/Cd
c
c-22 copper
      elseif (im .eq. 22 ) then
        if (tc .gt. 1000.) tc = 1000.
          fnexp= -4.1977e-4/tc +
     &          (1.673e-5 + (2.528e-9 + 8.037e-13*tc)*tc)
c
c-21 molybdenum
      elseif (im .eq. 21 ) then
        fnexp=-1.648e-3/tc+6.511e-6 -1.278e-9*tc +6.396e-13*tc*tc
c
c-50...55 User-mat
      elseif (im .ge. 50 .and. im .le. 55) then
        fnexp= expmat(im, tp)
      else
c
        write(6,*) ' fnexp: Material # ',im,' not defined. T=',tp
        stop ' fnexp '
      endif
      return
      end
```

8.9 Modified MATPRO Subroutines

8.9.1 matdat

```
*comdeck matdat
c
c  $Id: matdat.H,v 1.1 1997/07/02 23:18:26 ewc Exp $
c  $Id: matdat.H,v 1.1 1998/07/29 23:18:26 whe Exp $
c
c   matdat contains fuel rod and shroud material data.
c
c  Cognizant engineer: ewc.
c
*if def,selap
      integer imax,mxmatd
c imax = maximum number of user defined materials
c mxmatd - maximum number of data points for materials
       parameter (imax=10,mxmatd=10)
       common /matdat/ ttemp,tcp,tro,tk,teps,texp,
     * epsz,facmot,fotmtl,fraden,flux,coldw,
     & tfshrd,fmshrd,markmx,imshrd,ifshrd,mcme44
       real ttemp(mxmatd,imax),tcp(mxmatd,imax),
     & tro(mxmatd,imax),tk(mxmatd,imax),
     & teps(mxmatd,imax),texp(mxmatd,imax),
     & epsz,facmot,fotmtl,fraden,flux,coldw,tfshrd,fmshrd
       integer markmx(imax),imshrd,ifshrd,mcme44
c  ttemp - temperature array for thermal properties of user
c          defined materials
c  tcp   - specific heat for user defined material
c  tro   - density for user defined material
c  tk    - conductivity for user defined material
c  teps  - material emissivity
c  texp  - material thermal expansion
c  markmx- number of data points for user defined material
c
c      imshrd = material indicator for shroud insulation.
c      tfshrd = time at which shroud fails (s)
c      fmshrd = multiplier on conductivity of failed shroud
c      ifshrd = switch indicating whether shroud has failed or not
c             = 0 = no, 1 = yes.
*endif
```

8.9.2 fnk

```
...
+117  cwhb
+118  c molybdenum
+119          fnk = 154.188-tp*(4.2528e-3+tp*(3.443e-6-2.713e-10*tp))
+120          return
+121        elseif (im.eq.22) then
+122  c copper
+123          tc= tp - 273.15
+124          fnk = 3.991e-2 - (4.484e-2 - 1.779e-5*tc)*tc
+125          return
+126  c
+127  cwhe
+128        elseif (im.ge.50. and. im .le.59)then
+129          fnk = conmat(im,tp)
+130        endif
+131        return
+132        end
+133  *endif
```

8.9.3 fncp

```
...
+102  cwhb
+103  c molybdenum
+104          fncp = 237.48 + tp*(3.846e-2 + 1.453e-5*tp)
+105          return
+106        elseif (im .eq. 22) then
+107  c copper
+108          fncp = 378.2 + tp*(0.1473 - 2.968e-5*tp)
+109          return
+110  cwhe
+111        elseif (im.ge.50. and. im .le.59)then
+112          fncp = cpmat(im,tp)
+113        endif
+114        return
+115  c
+116        end
+117  *endif
```

8.9.4 fnro

```
...
+103  cwhb
+104  c molybdenum
+105           fnro=8930.
+106  cwh:  data stored here are extracted from: kfk-15/77-2 (8/98)
+107           return
+108         elseif (im .eq. 22) then
+109  c copper
+110           fnro=10200.
+111           return
+112  cwhe
+113         elseif (im.ge.50. and. im .le.59)then
+114  c user defined
+115           fnro = denmat(im,tp)
+116         endif
+117         return
+118         end
+119  *endif
```

8.9.5 coxthk

```
*deck coxthk
      function coxthk(ctemp,kpick)
c
c  function coxthk returns the growth rate constant for oxide thickness,
c  oxygen-stabilized alpha layer thickness (inner and outer),and
c  thickness of the oxygen-stabilized alpha layer between the outer and
c  inner alpha layers. for temperatures of 1273k-1853k data and analyses
c  from j.v. cathcart of ornl are used to compute the zro2 and oxygen-
c  stabilized alpha thicknesses on the outer surface and similar
c  equations from p. hofmann of the kernforschungszentrum karlsruhe
c  (kfk) for oxygen-stabilized alpha layers on the cladding inner
c  surface when there is pellet-cladding mechanical inter-action (pcmi).
c  for temperatures of 1853k-2100k,data and analyses from v.f urbanic
c  and t.h. heidrick , "high temperature oxidation of zircaloy-2 and
c  zircaloy-4 in steam," journal of nuclear materials 75,(1978) pp.
c  251-261, are used to compute zro2 layer thickness.
c
c     coded by n. hampton november 1981
c     last updated by d. l. hagrman july 1982
c
c     coxthk= output growth rate constant (m**2/s)
c     ctemp = input cladding temperature (k)
c     kpick = input integer 1-4, where:
c     kpick=1 is growth rate constant for oxide thickness.
c     kpick=2 is growth rate constant for oxygen-stabilized
c              alpha layer nearest outer cladding surface.
c     kpick=3 is growth rate constant for oxygen-stabilized
c              alpha layer nearest uo2 fuel.
c     kpick=4 is growth rate constant for oxygen-stabilized
c              alpha layer between outer and inner alpha layers.
c
c NOTE by e.w. coryell
c  kpick=3 or 4 are NOT used by SCDAP/RELAP5
c  design report is "CLADDING OXIDATION" n.l. hampton, d.l. hagrman
c    Nov. 1981, EGG-CDD-5647
c
$if def,impnon,1
      implicit none
      real ctemp,coxthk
      integer kpick
c growth rate constant for oxide thickness.
      if(kpick.eq.1.) then
        if(ctemp.gt.1853) then
          coxthk=2.0*1.035e-06*exp(-16014./ctemp)
        else
          coxthk=2.0*1.12569e-06*exp(-18063./ctemp)
        endif
      elseif(kpick.eq.2) then
c growth rate constant for oxygen-stabilized alpha layer nearest
c  outer cladding surface.
        coxthk=2.0*0.76149e-04*exp(-24228./ctemp)
      elseif(kpick.eq.3) then
c growth rate constant for oxygen-stabilized alpha layer nearest uo2.
        coxthk=0.32e-04*exp(-4.9e04/(1.987*ctemp))
      elseif(kpick.eq.4) then
c growth rate constant for oxygen-stabilized alpha layer between
c  outer and inner alpha layers
        coxthk=0.70e-04*exp(-4.4e04/(1.987*ctemp))
      endif
      return
      end
```

8.9.6 coxthk

```
      function coxwtk(ctemp)
c
c  function coxthk returns the parabolic oxidation constant for zircaloy
c  oxidation.  for temperatures of 1273k-1853k data and analyses from
c  j.v. cathcart of ornl are used.  for temperatures in the range of
```

```
c  1853k-2100k, data and analyses from v.f. urbanic and t.h. heidrick,
c  "high temperature oxidation of zircaloy-2 and zircaloy-4 in steam",
c  journal of nuclear materials 75,(1978) are used.
c
c     coxwtk = output parabolic oxidation constant (kg**2/m**4*s)
c     ctemp  = input cladding temperature (k)
c
c     coded by n. hampton november 1981
c     last updated by d. l. hagrman july 1982
cwh    h:    coxwtk=2.0*54.26*exp(-16610./ctemp)
cwh    l:    coxwtk=2.0*16.8*exp(-20065.0/ctemp
c
c- 22.10.02 Schanz proposal
c     l:     coxwtk=2.0*52.46 * exp(-20962/ctemp)
c     t:     coxwtk=2.0*1.25e12* exp(-63974/ctemp)
c     h:     coxwtk=2.0*3.295e3 * exp(-26440/ctemp)
$if def,impnon,1
      implicit none
      real ctemp,coxwtk
c
      if(ctemp .le.1800.) then
        coxwtk=33.6*exp(-20065.0/ctemp)
cwh         coxwtk=2.0*52.46 * exp(-20962/ctemp)
      elseif (ctemp .le. 1900) then
         coxwtk=2.0*1.25e12* exp(-63974/ctemp)
c        if(ctemp .lt.1873.) then
c          coxwtk=(33.6*exp(-20065.0/ctemp) +
c     &       10.852*exp(-16610./ctemp))*0.5
           else
c            coxwtk=10.852*exp(-16610./ctemp)
          coxwtk=2.0*3.295e3 * exp(-26440/ctemp)
c          endif
      endif
      return
      end
```